Conformational transformations induced by temperature and pressure in molecular crystals and coordination polymers

Zmiany konformacyjne wywołane temperaturą i ciśnieniem w kryształach molekularnych i polimerach koordynacyjnych

Aleksandra Półrolniczak

A thesis submitted to
the Faculty of Chemistry, Adam Mickiewicz University, Poznań
in fulfilment of requirements for the degree of
Doctor of Philosophy in Chemistry

supervised by Prof. dr. hab. Andrzej Katrusiak

Poznań, 2023

Acknowledgements

Niniejsza praca stanowi podsumowanie sześciu lat mojego życia – okresu pełnego wzlotów i upadków. Dotarcie do tego momentu nie byłoby możliwe bez wsparcia wielu osób, którym pragnę serdecznie podziękować.

Chciałbym wyrazić ogromne uznanie i wdzięczność za przekazaną wiedzę, rady oraz nieustanną motywację, którą otrzymałem od promotora mojej pracy – Pana Profesora Andrzeja Katrusiaka. Jest Pan Profesor dla mnie mentorem i wzorem naukowca, godnym naśladowania. Dziękuję serdecznie za możliwość pracy w Pańskiej grupie badawczej.

Moja przygoda nie byłaby możliwa, gdyby nie Ty, Szymonie Sobczak. Twoja przyjaźń, która tak wiele razy została okazana, pomogła mi stać się lepszym naukowcem, ale przede wszystkim lepszym człowiekiem. Twoja obecność i wsparcie są nieocenione, a moja wdzięczność jest niemożliwa do wyrażenia słowami. Jesteś niepodważalnie współtwórcą mojego sukcesu i najwspanialszym przyjacielem.

Chciałbym także serdecznie podziękować całemu Zakładowi Chemii Materiałów za tworzenie miłej i pomocnej atmosfery pracy. Szczególne słowa wdzięczności kieruję w stronę Kingi Roszak, Ani Olejniczak oraz Pauliny Ratajczyk. To dzięki Waszej obecności i często ogromnemu wsparciu będę wspominać ten rozdział mojego życia z uśmiechem i wiarą w ludzi. Choć naszą więź początkowo zapoczątkowała praca, to teraz jesteście dla mnie niezwykle bliskimi osobami.

Pragnę także wyrazić wdzięczność moim wspaniałym przyjaciołom.

Kaju, znamy się już wiele lat, ale nigdy nie będzie ich za dużo. Dziękuję Ci za to, że zawsze jesteś przy mnie, gdy tego potrzebuję.

Dominiko, Twoja odwaga dodaje mi sił i poszerza horyzonty. Dziękuję Ci za to, kim jesteś i za to, kim ja się stałam dzięki Tobie.

Mateuszu, dziękuję Ci za to, że zawsze mogę na Ciebie liczyć. Twoje wsparcie jest bezcenne.

Mojej rodzinie — siostrom Kasi i Ani oraz bratu Pawłowi. Wiem, że zawsze mogę na Was liczyć i że będziecie mnie wspierać, cokolwiek się nie dzieje. Takie rodzeństwo to największy skarb.

Moim wspaniałym rodzicom — Wandzie i Stefanowi, dziękuję za to, kim jestem. Za to, że zawsze we mnie wierzyliście, wspieraliście i robicie wszystko, żebym była szczęśliwa. Za cały trud włożony w moje wychowanie i umożliwienie mi dotarcia do tego miejsca. Nie ma lepszego wsparcia niż to, które dostałam od Was. Dziękuję.

Kevin, sabes lo importante que eres para mí y cuánto te debo.

The research presented in this thesis was funded by the National Science Center as part of projects:

OPUS 10 (2015/19/B/ST5/00262) and PRELUDIUM 18 (2019/35/N/ST5/01838).

NATIONAL SCIENCE CENTRE
POLAND

This research was also supported by the ChemInter project (POWR.03.02.00-00-I026/16)

co-financed by the European Union from the European Social Fund under

the Operational Program Knowledge Education Development

European
Funds
Knowledge Education Development

European Union
European Social Fund

“A thesis has to be presentable... but don't attach too much importance to it.
If you do succeed in the sciences, you will do later on better things and then it will be of little moment.
If you don't succeed in the sciences, it doesn't matter at all.”

Paul Ehrenfest

Table of Contents

1. Introduction

Materials Chemistry focuses on the synthesis, structure, properties and applications of compounds primarily designed and prepared for practical uses, in devices, textiles, constructions and others. The main purpose of Materials Chemistry is aims to understand the relations between the composition and structure at the atomic scale, with the macroscopic properties of materials. The understanding of the structure-property relations is used to design and develop new materials with specific desired features.[1] Elasticity is a fundamental characteristic essentially important for all practical applications of materials.[2] The elasticity parameters are vital for identifying suitability of materials for their envisaged applications, predicting their response to external forces, assessing the limits of elastic strain, and comparing the functionality of different materials. All materials are exposed to some stress and temperature changes, resulting in certain deformation. By testing the elastic properties, scientists can choose suitable materials and optimize their design, which is crucial for preventing damage, ensuring the safety and reliability of structures, components, and durability of devices.[1,2] Materials exhibiting excellent and desirable conductive/optical/magnetic properties may turn out to be useless without appropriate elasticity, fully described by a tensor of anisotropic dependence of strain and stress. Taking into account all the factors discussed above, the primary focus of my research was to examine the conformational changes induced by temperature and pressure in order to gain valuable insights into the interplay between the elastic properties of a material and their microstructure. Through the study of how variations in the arrangement and interactions between atoms influence the elastic response, it becomes possible to develop fundamental mechanisms that determine the material's response to stress. My research is aimed at establishing structure-property relations involving conformational changes induced by pressure and temperature in molecular crystals and coordination polymers. I have focused on understanding how molecular conformation changes affect the macroscopic properties and compressibility of the crystals. My goal was to identify the compounds with flexible structural components and to explore various effects, such as the kinetics of applying stress and temperature variations, crystal-environment versus pore-size correlation, self-assembly behaviour, and linker-conformation conversions for the elastic properties of these materials.

1.1. Elastic properties

Elastic properties of materials can be determined by subjecting the samples to external stress and by measuring their deformation. Elasticity refers to the reversible property of a material, which is strained when subjected to external stress and returns to its original dimensions once the stress is removed.[2] An elastic material can be stretched, compressed, or bent under stress, but it will regain its original dimensions when the stress is released. Elasticity is quantified by parameters such as Young's modulus, which measures the stiffness of a material, Poisson's ratio, which describes the transverse contraction or expansion of a material when subjected to axial stress, bulk modulus, which describes the resistance to uniform volume reduction under applied pressure, and shear modulus, that describes a material's resistance to shear deformation (Figure 1, Table 1).[1,2] These parameters are often used for characterizing isotropic materials, which exhibit the same physical properties in all directions when subjected to uniaxial stress. Of the above-mentioned parameters, only the bulk modulus is suitable for describing the effects of hydrostatic pressure, which can be used in very high pressure ranges.

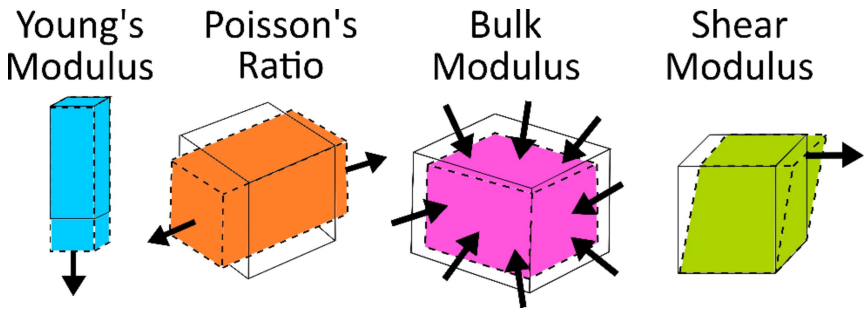

Figure 1. Schematic representations of the stress arrows used for measuring elasticity parameters of materials. Full lines indicate the shape of samples before applying the stress.

The properties described above apply to materials in the macroscopic scale. Macroscopic properties and microstructure are inherently interconnected. Macroscopic properties reflect the overall contribution of atoms and their interactions in the microstructure. By introducing structural changes, we can adjust macroscopic properties. Atomic-scale distortions occur during the compression of any material, accommodating the effects of macroscopic strain within the microscopic structure. The specific chemical components, the overall architecture of their interactions, and potential structural distortions significantly influence the macroscopic elastic properties of these materials. Therefore, in my work, I focused on determining relations between the elastic properties and the microscale and specifically on describing the deformation of the molecular conformation under pressure.

Table 1. Elastic parameters of selected materials.[3]

Material	Young modulus (GPa)	Poisson's ratio	Bulk modulus (GPa)	Shear modulus (GPa)
Diamond	1050-1210	0.18-0.22	530-548	440-470
Cooper	121-133	0.34-0.35	130-145	44-49
Silicone	140-180	0.265-0.275	95-105	60-63
Silver	69-74	0.365-0.395	84-118	24-28
Gold	76-81	0.415-0.425	148-180	26-30
Aluminium	69-72	0.32-0.36	63-83	25-27
Rubber	0.001- 0.05	0.47- 0.49	1.5-2	0.0003-0.02

Elasticity, concerning the deformation of microstructure, is generally associated with the "softest" parameters of structures, such as voids, intra- and intermolecular interactions, cohesion forces, and conformations of molecules. In the group of molecular crystals, where the molecules interact through relatively weak dispersion forces and hydrogen or halogen bonds, the conformational properties of molecules and voids, which in most cases are too small to accommodate solvent molecules during the process of crystallization, are often neglected.[4,5] For the group of coordination polymers (CPs) and metal-organic frameworks (MOFs) the elastic properties are inevitably connected with the distortions of the frameworks, where the linkers are usually considered as rigid elements and their coordination bonds to the metallic centres act as the hinges yielding under the external stimuli.[6] In MOFs, the crucial role is played by the voids, which can either shrink and collapse or accept guest molecules from the environment. Such a sorption can result in the counterintuitive increase of the crystal volume, due to the transport of the guest molecules and the increased molecular volume of the crystals.[7] All these properties of molecular crystals, CPs, and MOFs can be affected by the conformational properties of molecules and linkers in CPs and MOFs, as well as by the modifications in coordination schemes. The understanding of elasticity of materials is crucial in various fields of engineering, materials design, thin layers coatings and wherever the performance and integrity of materials under various conditions are of utmost importance.[2] Therefore, the main aim of this thesis is to investigate the contributions of conformational and coordination-scheme transformations to the elastic properties of molecular crystals, CPs and MOFs.

1.2. Materials investigated

Systematic studies on the deformation of molecular structures were initially concerned with compounds in which deformations were associated with weak intermolecular forces.[8–10] Gradually, there are increasingly more studies on the conformational transformations of molecules and linkers in polymers.[11–13] Presently, the role of conformational transformations for the elasticity of materials is still far from full understanding. In my thesis, I focused on materials generally regarded as the most soft ones, *i.e.* the molecular crystals, CPs and MOFs, particularly those with conformational flexibility in their structures (Figure 2).

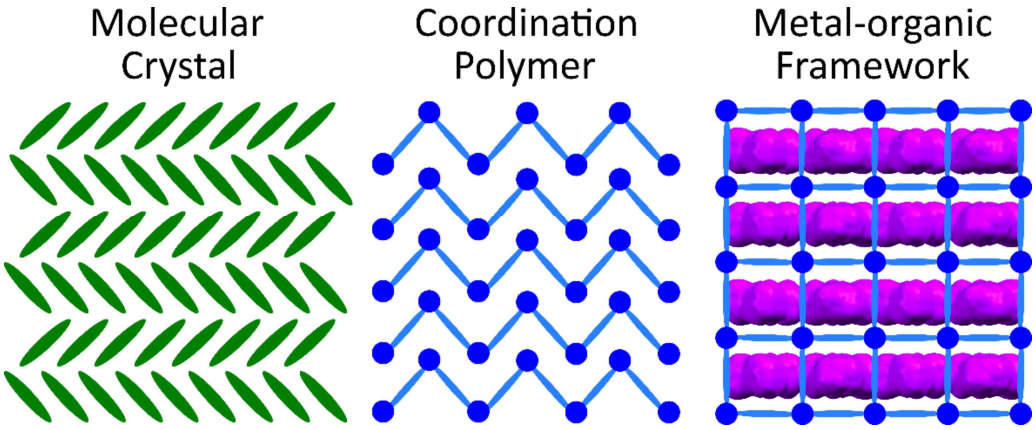

Figure 2. Schematic representation of investigated materials. Green colour depicts molecules, blue circles - metal nodes, blue lines – ligands, violet tunnels - pores.

Molecular crystals are composed of discrete molecules held together by weak intermolecular forces. These crystals are distinct from other types of solids, such as metallic or ionic crystals, where cohesion forces are dominated by metallic and electrostatic forces.[5] Molecular crystals comprise molecules with a definite shape and size, packed together in an organized arrangement in a solid state. The intermolecular forces, such as van der Waals forces, dipole-dipole interactions, or hydrogen bonds, are of similar strength.[1,4] The properties of molecular crystals are determined by the molecular shape and the molecular arrangement symmetry. Molecular crystals have versatile applications, from pharmaceuticals[14] to construction elements,[15] and electronic devices.[16] Their properties can be tailored by modifying the molecular structure or by introducing impurities,[17] optimizing their properties for different purposes.[14,18] When a molecular crystal is subjected to stress, the bonds and contacts accommodate the strain in the structure by shortening, stretching, or bending the contacts, rotating the molecules and changing their conformation.[16,19] In this way the crystal deform in response to the external stress.[20] Also other mechanisms of compression were reported, for example those involving the intercalation of the molecules from the crystal environment.[21]

Coordination polymers are classified as the compounds consisting of metal ions or clusters coordinated to organic ligands.[22] These compounds form 1-D, 2-D or 3-dimensional

networks or frameworks through coordination bonds between the metal ions and the ligands. In coordination polymers, the metal ions act as "nodes", while the organic ligands serve as "linkers" connecting the nodes.[22,23] The coordination bonds between the metal ions and ligands are typically formed through the donation of electron pairs from the ligands to the metal ions, resulting in the formation of coordination complexes.[24] The specific arrangement of metal ions and ligands in coordination polymers can vary, leading to a diverse range of structures and properties. The choice of metal ion and ligand determines the overall composition and properties of the coordination polymer.[22] Some common metal ions used in coordination polymers include transition metals such as cadmium, copper, zinc, and nickel.[24] CPs have attracted significant attention in recent years due to their unique properties and potential applications. They often exhibit porosity, large surface areas, and tuneable structures, making them useful for applications in catalysis, sensing, and electronic devices.[22,25] For coordination polymers with charged central atom, it is common that voids contain counter-ions, which stabilize the structure. The field of CPs is still actively researched, and scientists continue to explore new metal-ligand combinations and synthetic strategies to design and develop CPs with tailored properties for various applications. Elastic properties of CPs are connected with ligands strain, as well as deformation of coordination to the metal centre. The flexibility of polymers is more predictable than for molecular crystals, so it is easier to design a polymer with the required elastic properties.[22,26,27]

Metal-organic frameworks are a type of CP that consists of metal ions or clusters coordinated to organic ligands.[28,29] MOFs are formed through the self-assembly of metal ions or clusters with ligands. The metal ions act as the central coordination sites, while the organic ligands serve as linkers between the metal ions, forming a three-dimensional framework.[28,29] The coordination bonds between the metal ions and ligands give rise to the MOF structure.[30] One of the defining features of MOFs is their high porosity. The framework structure of MOFs contains empty spaces or pores that can be used for various applications, which can be tuned by selecting different combinations of metal ions and organic ligands.[30] This flexibility enables the design and synthesis of MOFs with specific functionalities for desired applications.[30,31] The porosity of MOFs allows for the adsorption and storage of gases, including hydrogen, carbon dioxide, and methane, which have attracted significant attention due to their potential to solve challenges in areas such as clean energy, environmental remediation, and drug delivery.[32–35] The elastic properties of MOFs are complex, because the distinction between intermolecular and intramolecular interactions is not easily defined. While intermolecular interactions appearing in the pores undergo some changes, significant modifications can also occur within the structure itself. These modifications involve alterations in distances between the metal and ligands, variations in angles involving bridging ligands, shifts in spin states, and increasing coordination numbers.[28,36,37]

The terms "coordination polymers" and "metal-organic frameworks" are often used interchangeably, but some nuanced differences can be listed.[38,39] First focuses on terminology: term CP is broader and encompasses a range of compounds consisting of metal ions or clusters coordinated to organic ligands. This includes MOFs as a specific subclass of coordination polymers. The next major divergence is porosity. While many coordination polymers exhibit porosity, not all coordination polymers are classified as MOFs due to the absence of interconnected channels and cavities. This feature in turn affects the application focus. While coordination polymers have a wide range of potential applications, MOFs attract the particular attention owing to their exceptional porosity and large surface area. Term MOF often have a more pronounced emphasis on these specific applications compared to coordination polymers in general.[38,39]

1.3. Extreme conditions

Most often the properties of chemical compounds are described at ambient conditions. The term “extreme conditions” usually refers to the situations when temperature or pressure are well outside the range of typical room temperature and atmospheric pressure.[40] The common effect of temperature changes is thermal expansion.[2,41] When heated, the energy of molecules and lattice vibrations in the crystal increases, which affects the lattice dimensions. Usually it leads to the expansion of the crystal, as a result of increased interatomic or intermolecular distances.[42] The temperature reduction leads to the opposite behaviour. The molecular vibrations become less pronounced, usually causing the contraction. Lower vibrational energy, often eliminates various types of structural disorder.[43] Temperature can induce phase transitions, *i.e.* anomalous changes in the structure or symmetry of the crystal.[4,15,44] Well known are examples of counter-intuitive negative thermal expansion (NTE), when materials contract with increasing temperature or expand upon cooling.[45,46] Although it is a relatively rare phenomenon, materials possessing this property are highly desirable, because of the wide range of their potential applications.[45,47]

The significance of pressure changes is often diminished, despite their prominent effects and connections with elastic, mechanic and other properties of materials.[36,48–50] High pressure has proven to be a highly effective tool for inducing structural changes in various chemical compounds, finding applications in multiple industrial sectors. The use of high pressure has yielded significant advancements, including the pioneering method of producing synthetic diamonds;[51] facilitating chemical synthesis,[52] catalysis,[53,54] and extraction processes.[55,56] It has also played a crucial role in the production of polymers,[57] such as polyethylene[58] and polypropylene,[59] as well as in the petroleum industry for hydrocracking,[60] hydrotreating,[61] and reforming.[62] Moreover, high pressure has found applications in pharmaceutical manufacturing,[63,64] the Haber-Bosch synthesis of ammonia,[65] high-pressure

food pasteurization,[66] such as in the production of guacamole.[67] These examples illustrate the wide-scale industrial application of high-pressure techniques, underscoring the importance of exploring and using high-pressure methods to modify and synthesize materials.

High-pressure conditions are becoming increasingly important in materials research and development or in geology and geophysics.[36,48,50] The synthesis of novel materials, such as superconductors,[68] superhard materials[69] and high-energy-density materials[70] often requires the application of high-pressure conditions. The specific effect of pressure on a material depends on its composition, structure, and the magnitude and duration of the applied pressure. However, there are some general effects on materials, such as compression, where the interatomic distances within the structure decrease (Figure 3).[71] The compression results in a reduction in lattice parameters, altering the size of the unit cell. The application of high pressure induces modifications in bond lengths, angles, and intermolecular forces. These gradual changes in the atomic arrangement can result in a phase transition from a low-pressure phase to a high-pressure phase, characterized by a denser packing of atoms and the formation of a new polymorph (Figure 3). The resulting polymorph may have different physical and chemical properties compared to the original phase.[17,44] High pressure can also enhance the reactivity of chemical compounds, leading to accelerated or modified chemical reactions.[72] Furthermore, high pressure promotes increased overlap of electron clouds between neighbouring atoms, influencing the strength and nature of chemical bonds in the crystal. However, there are examples of anomalies in response to pressure, such as negative linear or area compressibility, where a system expands in one or two directions when uniformly compressed.[73–75] Even the effect of a less-dense high-pressure polymorph was evidenced recently.[76] Thus, it is important to note that each material has its own, unique characteristics that may be particularly affected by high pressure. The following sections discuss the specific pressure-induced effects in the groups of compounds studied in my thesis.

Starting with molecular crystals, high pressure can cause diverse changes in molecular packing, intermolecular interactions, and crystal symmetry, which are schematically illustrated in Figure 3.[20,77,78] The crystal may undergo compression, structural transformations, and phase transitions.[4,79] As the molecular distances decrease, van der Waals forces, hydrogen bonding, and other intermolecular interactions may become stronger.[80] This can affect the physical properties of the crystal, such as its mechanical strength, melting point, and thermal expansion.[81] Changes in crystal structure and molecular arrangements can impact the absorption and emission spectra,[82] energy transfer,[71] and charge transport properties.[83] This is of interest for applications in sensors, optoelectronics, and photovoltaics.[71]

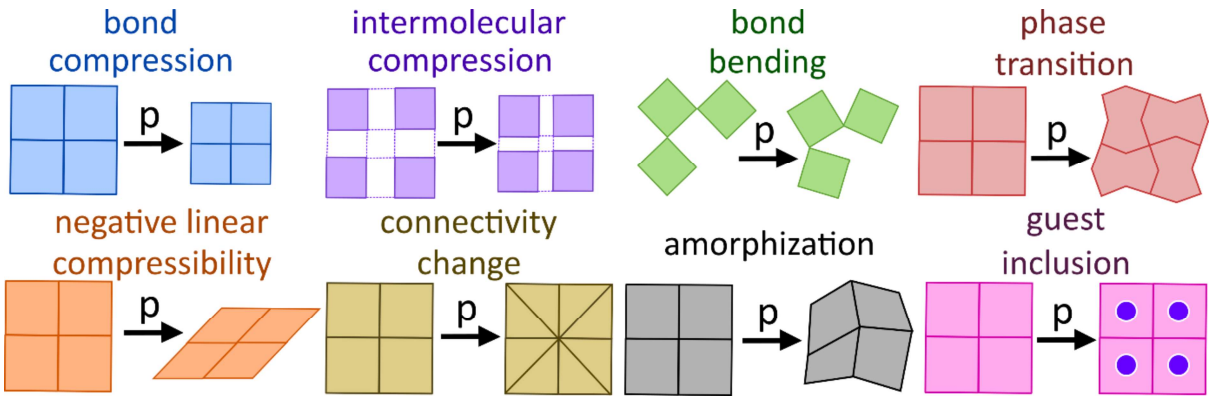

Figure 3. Schematic representation of selected pressure-induced effects on crystals.

Several specific effects can be listed for compressed coordination polymers and MOFs.[84] As pressure increases the intermolecular distances and angles in the crystal structure are changed. The arrangement of linkers or metal centres in the framework, as well as the packing scheme of the polymer chains, also changes and can lead to a reduction in pores or even amorphization.[85,86] Pressure can also influence the stability of polymeric crystals. Some materials may increase their stability under high pressure, while others may undergo phase transitions or their framework may collapse.[85] The compression of the crystal affects the elasticity, stiffness, and strength.[36,87] In the group of coordination polymers and MOFs, the response to pressure is highly dependent on their specific composition, structure, and the type of guest molecules. Given the wide range of practical applications for porous crystals, particularly MOFs, it is of utmost importance to investigate these modifications.[88–90] High pressure can influence the adsorption capacity, selectivity, and uptake of guest molecules in the pores of material, as well as trigger the release of adsorbed molecules. The compression of the crystal influences the size, shape and volume of the pores, thereby changing the interaction between the porous material and the adsorbate molecules. These pressure-induced guest uptake and release capabilities have the potential for applications in gas storage, separation, and sensing.[91]

High pressure and temperature can induce phase transitions, affect the properties of materials and lead to changes in the dimensions of crystals, but their effects are based on different mechanisms.[88,92] Temperature affects kinetic energy, while pressure impacts potential energy between atoms and molecules. It is worth noting that the effects of temperature or pressure on compounds depend on its specific composition, its molecular or crystal structure, and the applied temperature/pressure conditions.[93] The search for new materials with the desired properties are often supported by computational methods.[94] In the coming years, the combination of high-pressure and temperature experiments with theoretical and computational tools is expected to bring multiple discoveries and breakthroughs.[4,95]

1.4. Conformational changes

Chemical conformation refers to the spatial arrangement or shape of a molecule resulting from the rotation of its atoms around bonds. It describes the different ways in which a molecule can adopt different three-dimensional arrangements, while maintaining the same connectivity of atoms.[96,97] Conformational changes refer to the different spatial arrangements or shapes that a molecule can take without breaking any covalent bonds. Molecules can have multiple conformations due to the rotation of bonds, which allows for different spatial orientations of the constituent atoms (Figure 4).

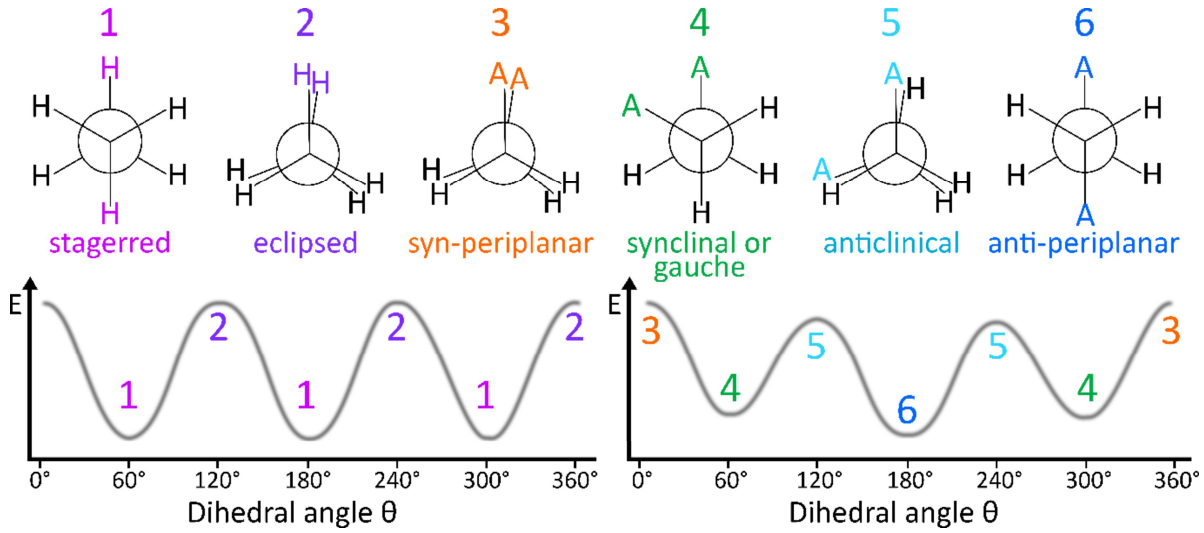

Figure 4. Multiple types of molecular conformations, together with relative conformation energies plot.

The conformation is closely related to the flexibility of molecules, and their ability to assume different shapes. The conformational changes are associated with rotations of groups or atoms about single bonds.[96,97] Consequently, the molecules containing many atoms in sp^3 hybridization, usually have a wide range of conformations. For ethane-like structures, with one type of substituent, two extreme conformations, staggered and eclipsed, are possible (Figure 4). In the staggered conformation, all the carbon-hydrogen bonds are positioned as far as possible, while in the eclipsed conformation, they are located in the closest position. For compounds with more substituents, there are additional conformational possibilities, such as synperiplanar conformation, where the substituents are positioned at torsion angle range from -30° to 30°, or antiperiplanar conformation, for the -150° to 150°. The inclination of substituents by 60°, is known as the synclinal (or gauche) conformation, and inclination by 120° is described as the anticlinal conformation (Figure 4).[96,97] Conformations can be represented using Newman projections, three-dimensional models, or sawhorse projections. Conformations differ in their potential energies, the most stable one, i.e. with the lowest energy, is known as the ground-state conformation.[96,97]

The conformation of a molecule has a significant impact on its interactions with other molecules, and therefore on the material properties.[98–100] Various techniques, such as X-ray crystallography, nuclear magnetic resonance (NMR) spectroscopy, infrared (IR) spectroscopy, and computational modelling, are commonly used to determine conformational changes in materials. These techniques provide valuable experimental and computational tools for studying and analysing the conformational behaviour of materials.[98–102]

1.5. Aims and objectives

Determining the structure-property relationships of materials was one of the key objectives of my research. Since even a small change in the structure of a compound can results in a significant change in properties, I decided to investigate conformational changes induced by pressure and temperature on molecular crystals and coordination polymers. The conformation of molecules/linkers determines the crystal structure and can increase the compressibility and resistance of the crystal by increasing the number of deformable structural elements. The larger range of possible elastic deformations increases the magnitude of compressibility, which can be sought for new applications. Hence, my aim was to investigate a group of compounds with conformationally flexible structural components (molecules or linkers), and to study the following aspects: (i) the impact of low temperature, (ii) the influence of compression speed on the behaviour of the crystal, (iii) the influence of the crystal environment on its pressure-induced effects, (iv) the correlation between the pore size and their accessibility under high-pressure conditions, (v) the relation between the properties of the linker itself and the metal-organic framework containing such a linker, and (vi) the interplay between the porous crystal structure and the its environment , as well as the guest molecules in its pores under high pressure. I also planned to characterize the common properties of such conformationally flexible materials and outline their possible applications. With these aims in mind, for my thesis I have chosen the compounds with flexible molecules or linkers, presented in Figure 5.

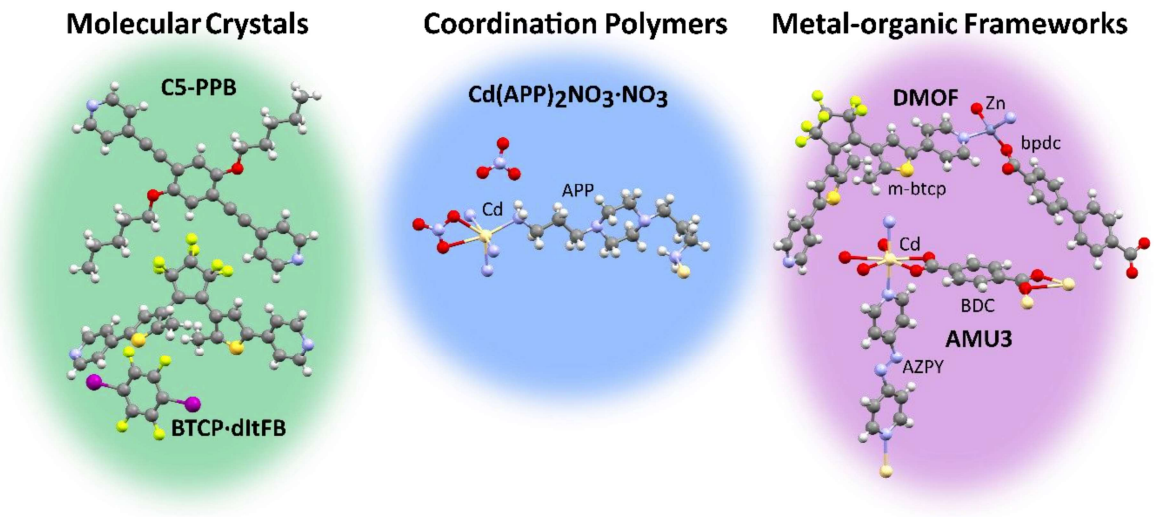

Figure 5. Compounds investigated in this thesis: molecular crystals (green background): C5-PPB = 1,4-bis(pentyloxy)-2,5-bis(2-pyridineethynyl)-benzene; BTCP·dItFB = co-crystal of 1,2-bis[2'-methyl-5'-(pyrid-4"-yl)-thien-3'-yl]perfluoro-cyclopentene with 1,4-diiodotetrafluorobenzene; coordination polymer (blue): $Cd(APP)_2NO_3{\cdot}NO_3$ [APP = 1,4-bis(3-aminopropyl)-piperazine]; metal-organic frameworks (violet): DMOF = $[Zn(m\text{-}btcp)_2(bpdc)_2]{\cdot}2DMF{\cdot}H_2O$ [btcp = 1,2-bis[2'-methyl-5'-(pyrid-4"-yl)-thien-3'-yl]perfluoro-cyclopentene; H_2bpdc = 4,4'-biphenyldicarboxylic acid]; and AMU3 = Cd(BDC)(AZPY) [H_2BDC = terephthalic acid; AZPY = 4,4'-azopyridine]. The content of voids is omitted for clarity.

The results of the research described in my thesis have been published in a series of 5 papers. The details of these papers are listed below, and their copies are included in the Appendices section:

A1 *Dynamic Resolution of Piezosensitivity in Single Crystals of π-Conjugated Molecules*
S. Bhattacharyya*, S. Sobczak*, **A. Półrolniczak***, S. Roy, D. Samanta, A. Katrusiak, T. K.Maji.
Chemistry–A European Journal 25 (24), 6092-6097, **2019.**

A2 *Large negative linear compressibility of a porous molecular co-crystal*
S. Sobczak, **A. Półrolniczak**, P. Ratajczyk, W. Cai, A. Gładysiak, V. I Nikolayenko, D. C Castell, L. J Barbour, A. Katrusiak.
Chemical Communications 56 (31), 4324-4327, **2020.**

A3 *Solvent-controlled elongation and mechanochemical strain in a metal-organic framework*
A. Półrolniczak, S. Sobczak, V. Nikolayenko, L. Barbour, A. Katrusiak.
Dalton Transactions 50 (47), 17478-17481, **2021.**

A4 *Self-healing ferroelastic metal-organic framework sensing guests, pressure and chemical environment*
A. Półrolniczak, A. Katrusiak.
Materials Advances 2 (14), 4677-4684, **2021.**

A5 *Solid-state associative reactions and the coordination compression mechanism*
A. Półrolniczak*, S. Sobczak*, A. Katrusiak.
Inorganic Chemistry 57 (15), 8942-8950, **2018.**

** These authors contributed equally.*

2. Experimental Methods

All articles constituting my thesis, include an experimental section that outlines the employed syntheses of the samples and measurement techniques (articles A1 and A3 in the Supporting Information). Therefore, in this section, I broadly overview the experimental methods and equipment used in my research.

2.1. Syntheses

I have synthesized compounds related to articles A4-A6 using the slow diffusion technique, which is one of the methods used for obtaining single crystals of CPs and MOFs. The compound described in article A1 was synthesized by the group of Prof. Dr. T. K. Maji (see the Supporting Information of article A1). The compounds investigated in Articles A2-A3 were synthesized by the group of Prof. L. J. Barbour (see the Supporting Information of article ref. 37).

The slow diffusion technique involves dissolving substrates in solvents with different densities and placing both solutions in a test tube. The higher-density solution is placed in the test tube; then an intermediate layer of the mixture of two solvents (1:1 vol.) is gently placed to form a second layer; and finally the lowest-density solution is added to form the third layer. The system is then tightly sealed, and crystals of the compounds form over a period of several days or weeks (Figure 6). The slow diffusion technique is often chosen when the reactants have different solubilities, or when the formation of metal-organic frameworks requires a specific diffusion rate. By controlling the rate of diffusion, it is possible to achieve the desired

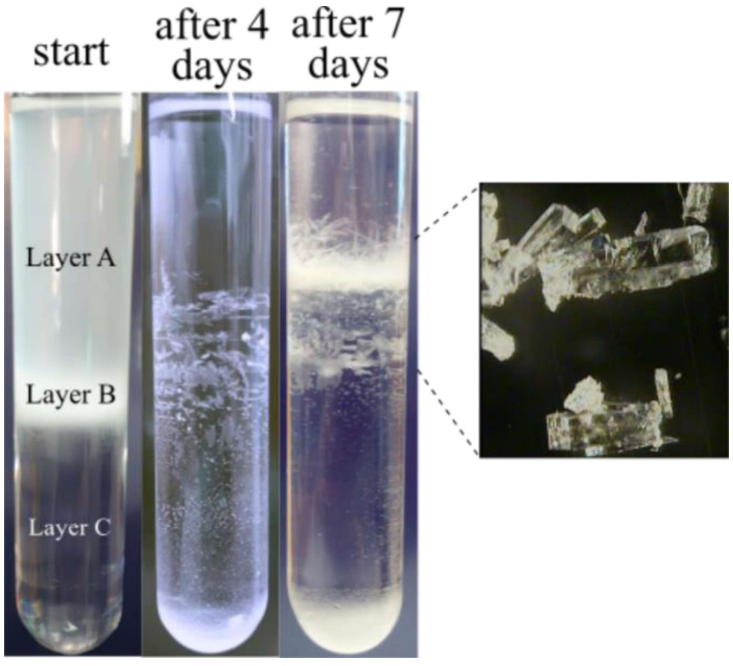

Figure 6. Slow diffusion of reagent layers in a test tube results in a desired reaction to occur and the product to crystallise in the form of single crystals.

crystallinity, morphology, and size of the resulting MOFs. Slow diffusion techniques can be conducted under ambient conditions or various temperature conditions to further regulate the crystallization process.

This method offers several advantages, including its ease of implementation, no need of advanced devices, and the single-crystal form of the obtained products. However, there are some drawbacks, such as the possibility of obtaining co-crystals or complexes instead of metal-organic polymers, the potential for non-homogeneous product formation, and challenges when dealing with substrates of low solubility. Despite these limitations, I found the slow diffusion technique more favourable than the widely used solvothermal synthesis method.

2.2. Single-crystal X-ray diffraction

X-Ray diffraction measurements were conducted on the as-synthesized compounds at ambient pressure. The measurements were carried out using either a 4-circle SuperNova CCD diffractometer equipped with an X-ray micro-source (Cu Kα=1.54178 Å) or an Oxford Diffraction Xcalibur CCD Eos diffractometer with a graphite-monochromated Mo Kα (λ=0.71073 Å) radiation source. For low-temperature measurements, a CryoStream attachment was employed to cool the sample using a stream of gaseous nitrogen, reaching temperatures as low as 100 K.

Data collection, measurement control, and initial data reduction were performed with the CrysAlisPro software.[103] The crystal structures were solved and refined using programs SHELXS and SHELXL[104] incorporated in the OLEX2 interface.[105] Structural analyses of interactions in crystals were performed in the Mercury.[106] The morphological features of crystals were observed with microscope Olympus MVX10. The detailed experimental and crystallographic data have been deposited in the Cambridge Structural Database via www.ccdc.cam.ac.uk/structures.

2.3. High-pressure crystallography

High-pressure studies were carried out using a diamond-anvil cell (DAC). The DAC is a simple device comprising two diamond anvils positioned opposite one to the other on two supporting discs. In an experiment using a DAC, the sample is mounted in a hole, drilled in a metal gasket, which is then sealed from both sides by diamonds to prevent their direct contact (Figure 7). The gasket, typically made of stainless steel or tungsten, is a thin metal foil measuring 0.3 mm in thickness, with a spark-eroded hole of 0.40 – 0.50 mm. Pressure is generated by transferring forces between the large upper surface of a brilliant-cut diamond and the studied sample. To ensure uniform pressure distribution on the sample, a liquid hydrostatic medium is employed to surround it. In our laboratory, the pressure is calibrated using a ruby fluorescence method

with a Photon Control spectrometer.[107] Our research group has developed specific procedures for sample centring and the measurement process.[108]

For high-pressure structural analyses, the 4-circle diffractometers KM-4 CCD or an Oxford Diffraction Xcalibur CCD Eos was used. Both diffractometers used a graphite-monochromated MoKα (λ=0.71073 Å) radiation sources. Diffraction data collections and processing followed the same procedures as those used under ambient conditions, except that corrections of reflection intensities for the DAC absorption and gasket shadowing of the sample were calculated.[109]

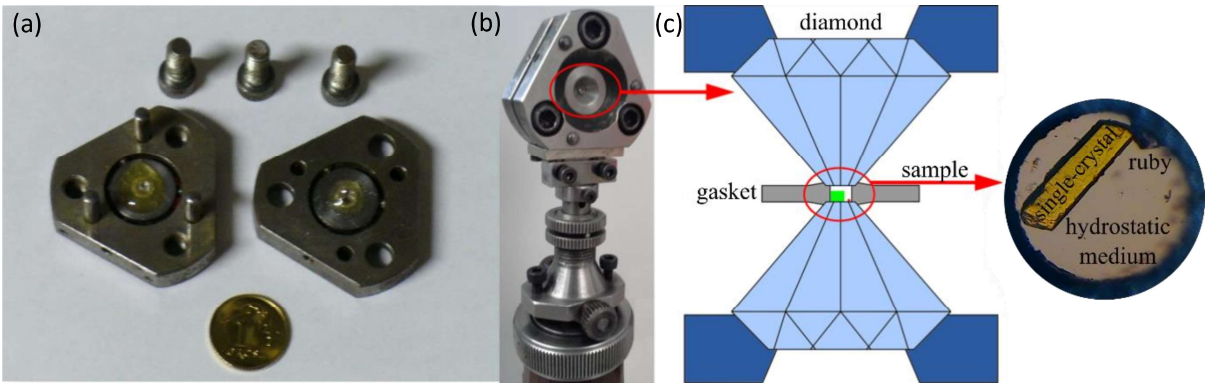

Figure 7. (a) Disassembled parts of a diamond-anvil cell. (b) The DAC mounted on the goniometer. (c) A schematic diagram illustrating the construction of the DAC, as well as a photograph of the DAC inside.

3. Results

Communication

A1 Dynamic Resolution of Piezosensitivity in Single Crystals of π-Conjugated Molecules

Sohini Bhattacharyya, Szymon Sobczak, Aleksandra Półrolniczak, Dr. Syamantak Roy, Dr. Debabrata Samanta, Prof. Andrzej Katrusiak ✉, Prof. Dr. Tapas Kumar Maji ✉

The results presented in **article A1** focused on investigating the impact of high pressure on a crystal of 1,4-bis(pentyloxy)-2,5-bis(2-pyridineethynyl)-benzene (C5-PPB). In the C5-PPB molecule, there are flexible substituents. Consequently, this molecular crystal is likely to display a conformational polymorphism. To examine these properties, we carried out high-pressure experiments using a DAC. We monitored the crystal structure by single-crystal X-ray diffraction (SCXRD) at various compression rates.

We established that the pressure-induced effects on the C5-PPB crystal depend on the compression rate. The fast compression leads to the formation of an amorphous phase, and slow compression leads to a new crystalline phase β. The amorphous transition involved a strong compression, resulting in irregular "wrinkles" appearing on the crystal faces. The single-crystal to single-crystal transition proceeds with a clearly visible transition front between two phases. The transition is associated with an abrupt change of the crystal shape. Initially, during the compression of phase α, the sample monotonically shrinks until 0.8 GPa. The rapid compression of C5-PPB from 0.8 to approximately 1.2 GPa maintains the stability of phase α. However, upon further slow compression to around 1.5 GPa, irregular wrinkles appear, indicating the occurrence of the sample amorphization. When phase α is slowly compressed beyond 0.8 GPa, a discontinuous phase transition occurs at 0.9 GPa, resulting in the formation of phase β. This isostructural transition involves a reduction in volume, significant conformational changes in the molecules, and a visible giant negative-linear strain. The compression induces remarkable conformational changes in two independent molecules, while maintaining the crystal symmetry of the triclinic space group $P\bar{1}$. The phase transition from α to β phase reduces distances between the central aromatic rings of neighbouring molecules and elongates the two n-pentyloxy chains. Torsion angles of the pentyloxy chains change by approximately 150°. In the β phase, the terminal pyridines exhibit only slight rotations of the central benzene rings, whereas the rigid ethynyl bridge bends with increasing pressure. At higher temperatures, the critical pressure for the α-to-β transition slightly decreases, while the amorphization pressure somewhat increases. The crucial role in α-to-β

phase transition is played by voids, which are present in the α-phase structure. Although these voids are too small to accommodate guest molecules, they play a pivotal role, by enabling the molecules to adapt their conformation by effectively occupying the available empty spaces. The observed conformational changes between neighbouring molecules required sufficient time, and fast compression effectively "froze" the conformers of phase α, due to rapid intermolecular interactions. This study provides insights into the interplay of molecular and crystal structural transformations of the C5-PPB, revealing the time-dependent phenomena potentially applicable in smart devices.

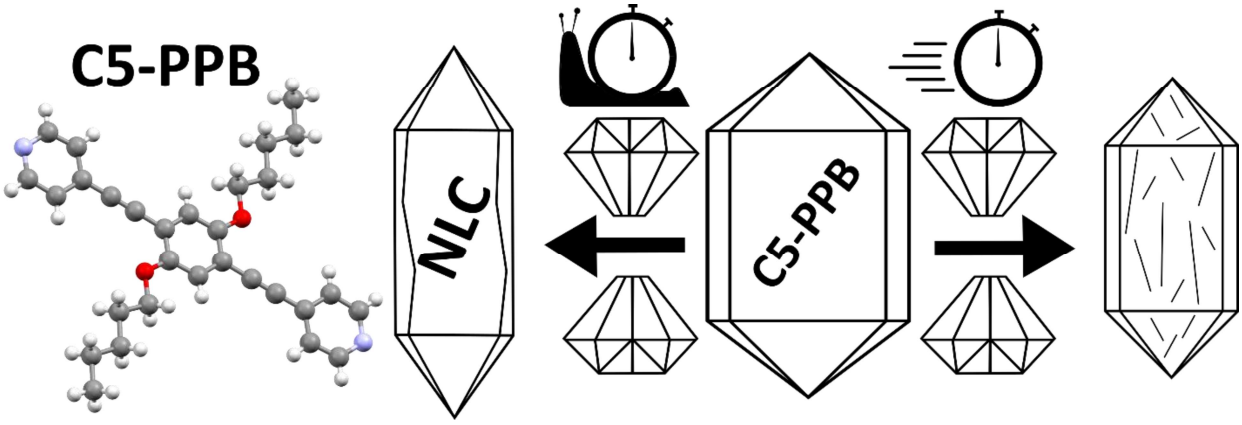

Figure 8. C5-PPB crystal undergo a unique time-dependent changes either to isostructural phase β or to over compressed α phase.

A2

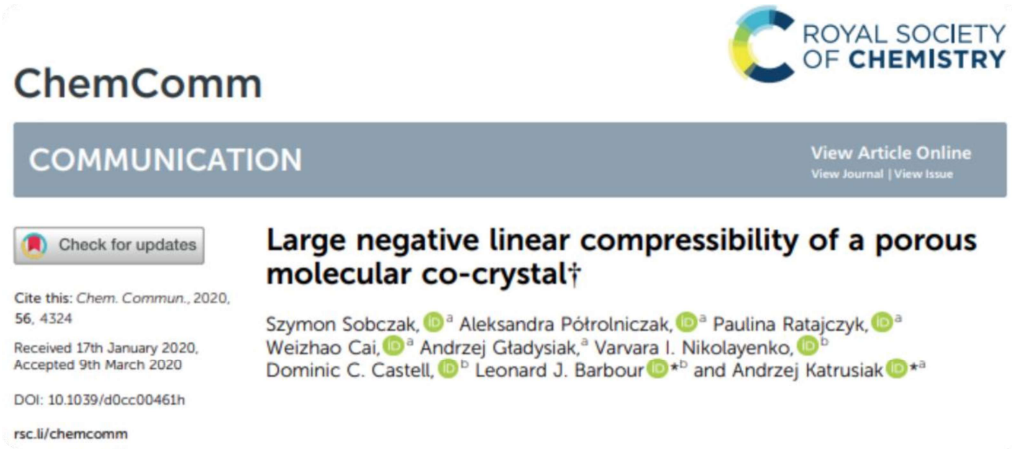

Article A2 reports the high-pressure effects on the acetone (Ac) solvate of co-crystal of 1,2-bis[2'-methyl-5'-(pyrid-4"-yl)-thien-3'-yl]perfluoro-cyclopentene (BTCP) with 1,4-diiodotetrafluorobenzene (dItFB). The aim of this study was to investigate the effects of pressure on the flexible molecule BTCP. BTCP was found by Nikolayenko *et al.* to undergo solid-state photocyclization, switching between a closed-ring isomeric form under ultraviolet light and an open-ring form under visible light.[37] Due to its flexible nature, it was hypothesized that BTCP could exhibit unique elastic properties under high pressure, including negative linear and area compressibility, involving chemical reaction.

The study focuses on the isothermal compression of the molecular co-crystal solvate. The crystals were synthesized from acetone under ambient conditions. The acetone molecules become trapped in guest-accessible pockets in the crystal structure. It was observed that the co-crystals lost some of their solvent content when exposed to air, which resulted in opaque faces and visible cracks. The single-crystal quality could be recovered by adding a few drops of water. The sorption of water in the crystal results in an anisotropic strain including both: elongation and shortening of crystal dimensions. Despite this apparent water uptake, no water molecules could be located in the crystal structure, suggesting the non-stoichiometric sorption in disordered positions in the pores.

In high-pressure experiments, performed with a diamond-anvil cell (DAC), a single crystal of BTCP·dItFB·Ac, previously stored in dry environment, was compressed in glycerol. Although disordered water molecules could not be located at pressures up to 1.95 GPa, one water molecule per asymmetric unit could be modelled at 2.5 GPa. It indicates that starting from about 2.5 GPa, the water molecules start to become ordered. The presence of water in the glycerol (less than 2% wt), which could be the origin of the water molecules located in the pores of the compressed sample, was confirmed by Karl Fischer titration. The compression of the BTCP·dItFB·Ac in glycerol induced the negative linear compressibility (NLC) along direction [100], which is perpendicular to the pore channels. Remarkably, the magnitude of NLC observed in this co-crystal was unprecedented for the organic molecular crystals, reaching 30 TPa^{-1} between 0.1 MPa and 0.4 GPa, the largest NLC value so far reported for any organic molecular crystal. The compression significantly changes the conformation of BTCP molecules and their arrangement. The initial compression up to 0.4 GPa primarily affected the conformation of BTCP, causing elongation between terminal pyridine rings. At higher pressures, up to 2.5 GPa, the distance between carbon atoms in the thienyl groups considerably increases, indicating that high pressure is unfavourable for closing the ring. Thus, no pressure-induced transformations involving this chemical reaction were observed.

The unique elastic properties, including its record-breaking NLC, observed in this organic molecular crystal, illustrate the behaviour of flexible molecules and their significant role for absorbing the external stress.

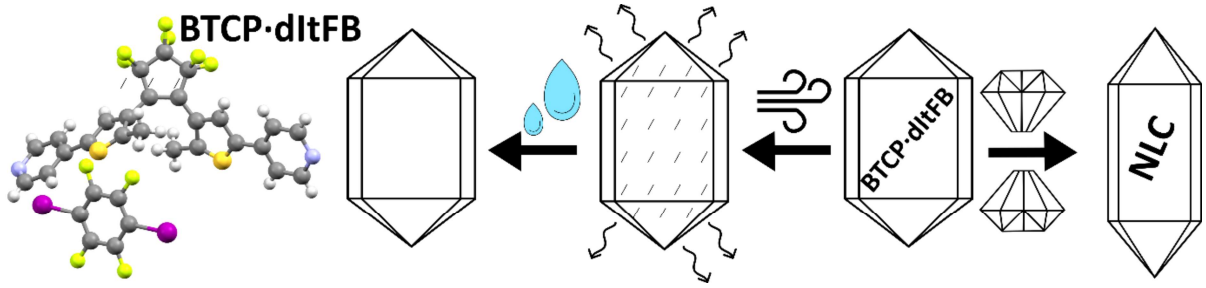

Figure 9. Photo-switchable porous 1,2-bis[2-methyl-5-(pyridyl)-3thienyl] cyclopentene cocrystal with 1,4-diiodotetrafluorobenzene exhibits large NLC under hydrostatic pressure.

A3

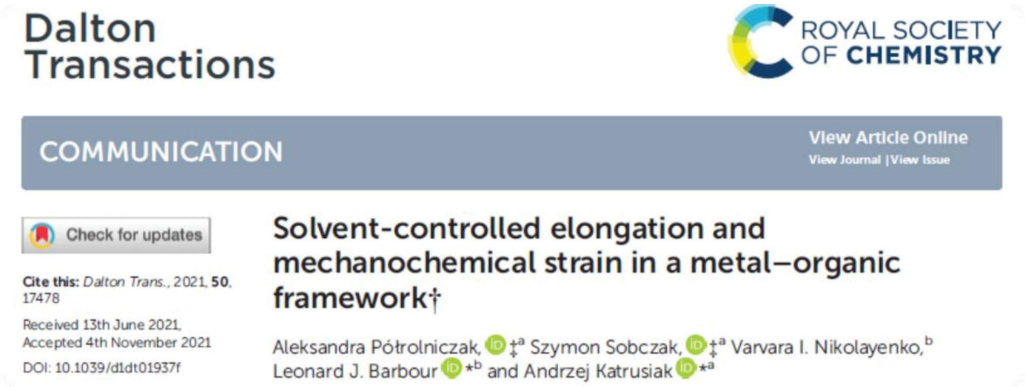

Article A3 reports the structural effects of hydrostatic pressure on single crystals of a 3D-host framework called DMOF ($[Zn(m\text{-}btcp)_2(bpdc)_2]\cdot 2DMF\cdot H_2O$; m-btcp = 1,2-bis[2'-methyl-5'-(pyrid-4"-yl)-thien-3'-yl]perfluoro-cyclopentene; H_2bpdc = 4,4'-biphenyldicarboxylic acid). In DMOF the central zinc cation is 4-fold coordinated by two bpdc anions and two m-btcp molecules, in a honeycomb-like structure. The as-synthesized crystals of DMOF contain guest molecules, such as DMF and water in their large accessible channels, extending along the *b*-axis. The compression effects on the DMOF crystals were studied in DAC filled with non-penetrating hydrostatic fluids (glycerol and Daphne 7474) or a penetrating mixture of methanol: ethanol: water (MEW). The results show that DMOF is most compressed along the *c*-axis in non-penetrating media, accompanied by the negative linear compression (NLC) along the *b*-axis. The elliptical shape of the pores contributes to changes in the crystal dimensions by lengthening the *b* and shortening the *c* axes. When compressed in penetrating media (MEW), DMOF exhibits reversed (compared to non-penetrating media) mechanochemical strains: shortening of the unit-cell parameter *b* and lengthening of parameter *c*. This reversal is attributed to the intake of new guest molecules, causing elongation along the *c*-axis and shortening along the *b*-axis. During compression, superfilling is observed, resulting in an increased unit-cell volume by approximately 100 $Å^3$ at 0.25 GPa. This corresponds to the intake of about 5 non-hydrogen atoms per unit cell, equivalent to approximately 74 additional electrons in the pores. Further compression in MEW enhances the sorption, enabling additional molecules to penetrate the structure. However, the compression continued till about 1.2 GPa leads to the destruction of the DMOF crystal structure, either the collapse of its pores or their expansion breaking the framework, resulting in the amorphous state. This amorphization can be either due to the pressure-induced framework destabilization or transport of guest molecules. The conformational changes of DMOF in both penetrating and non-penetrating hydrostatic media are associated with the rotations about single bonds. Owing to this conformational flexibility, the crystal structure adopts to different contents of the pores and consequently, the crystal directions shrinking and expanding under pressure can interchange in different environments.

The unique mechanochemical properties of DMOF make it a promising candidate for molecular sensing applications, capable of detecting the size of molecules in compressed environments. The NLC exhibited in non-penetrating media and the elongation in penetrating media offer potential applications in the pressure sensors discriminating fluids and micro-mechanisms controlled by a hydraulic system. This study emphasizes the importance of conducting experiments under various thermodynamic conditions, which include the chemical composition of the pressure-transmitting environment.

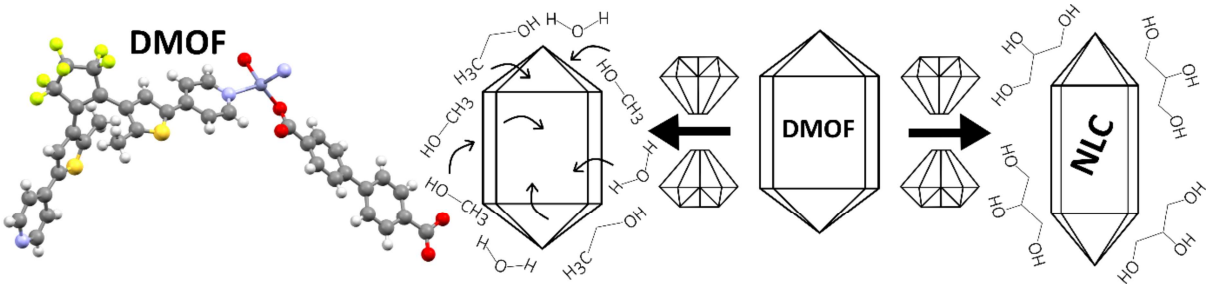

Figure 10. The DMOF crystal shows different negative linear compressibility depending on the chemical composition of compression environment.

A4


Materials Advances
ROYAL SOCIETY OF CHEMISTRY
PAPER
View Article Online
View Journal | View Issue
Check for updates
Cite this: Mater. Adv., 2021, 2, 4677

Self-healing ferroelastic metal–organic framework sensing guests, pressure and chemical environment†

Aleksandra Półrolniczak and Andrzej Katrusiak*

One of the key findings of **article A4** is that the crystals of AMU3 [Cd(BDC)(AZPY); H_2BDC = terephthalic acid, AZPY = 4,4'-azopyridine] exhibits ferroelastic properties, which depend on the type of guest molecules present in the framework. This means that the ferroelastic properties of the MOF can be effectively tuned by exchanging the guest molecules. In AMU3 the presence of rigid Cd(II)-BDC sheets contrasts with the AZPY linkers disordered in two orientations, which reflects the flexibility of the framework. The AZPY disorder is influenced by the lattice strain, guest types, and the crystal environment. Under ambient conditions, AMU3 crystallizes in an orthorhombic space group *Cmce*, due to disordered AZPY molecules: the symmetry of averaged two sites is higher than that of one ordered molecule. The AZPY molecules, in their energetically optimized conformation, exhibit a skewed configuration, as the diazo-bridge shifts in the axes of the pyridyls by approximately 2.8 Å. To investigate the effects of pressure, the AMU3 crystals were placed in a DAC. As the pressure increased, the phase transition occurs, when the AZPY linkers order and change their conformation from planar to twisted. No such a ferroelastic strain or ordering of the AZPY linkers was observed

when the crystals were cooled down to 100 K. This pressure-induced effect of eliminating the disorder in the crystal structure is caused by its volume reduction, rather than by temperature-controlled energy of vibrations. The inclination of the pyridine rings in the AZPY molecules increased with pressure, causing shear displacement of the CdBDC sheets along the *b*-axis, leading to ferroelastic strain in the crystal lattice. The compression of phase α-AMU3 with DMF molecules filling its pores (AMU3·DMF) in a methanol: ethanol: water mixture (MEW) is more than three times higher compared to its compression in glycerine. Surprisingly, the largest volume change is observed when AMU3·DMF is compressed in the MEW, while its small molecules of methanol, ethanol and water are able to penetrate the pores of the crystal. In contrast, the compression of AMU3·DMF in glycerine is less affected by pressure, due to the viscous nature of glycerine, the larger size of its molecules and its high viscosity, slowing down the kinetics of the molecular motion in the ligand and along the pores. The differences in compressibility can be attributed to the presence of voids in the AMU3 structure and the ability of the crystal to extrude DMF molecules, when compressed with suitable hydrostatic fluids. The substitution of DMF with smaller water and methanol molecules from the crystal environment is easier compared to such an exchange with glycerine molecules. The stronger volume reduction of α-AMU3·DMF in compressed MEW is likely due to the altered pores contents, as evidenced by the lower transition pressure compared to that of α-AMU3·DMF compressed in glycerine. Additionally, the volume reduction of α-AMU3 with acetonitrile molecules filling its pores (AMU3·MeCN) compressed in MEW is between those of α-AMU3·DMF in glycerine and MEW, which further suggests a reduction in the pores contents in α-AMU3·DMF in MEW.

Our research revealed the interplay between the flexibility of the linkers and structural transformations in MOFs. Besides, we observed that, the crystals demonstrate remarkable self-healing properties, allowing them to repair damage caused by the phase transition to ferroelastic orientational states. As AMU3 is a promising candidate for chemo-mechanical transducers in sensor applications, this restorative ability is particularly significant as it overcomes a common limitation faced by many ferroelastic materials in practical applications.

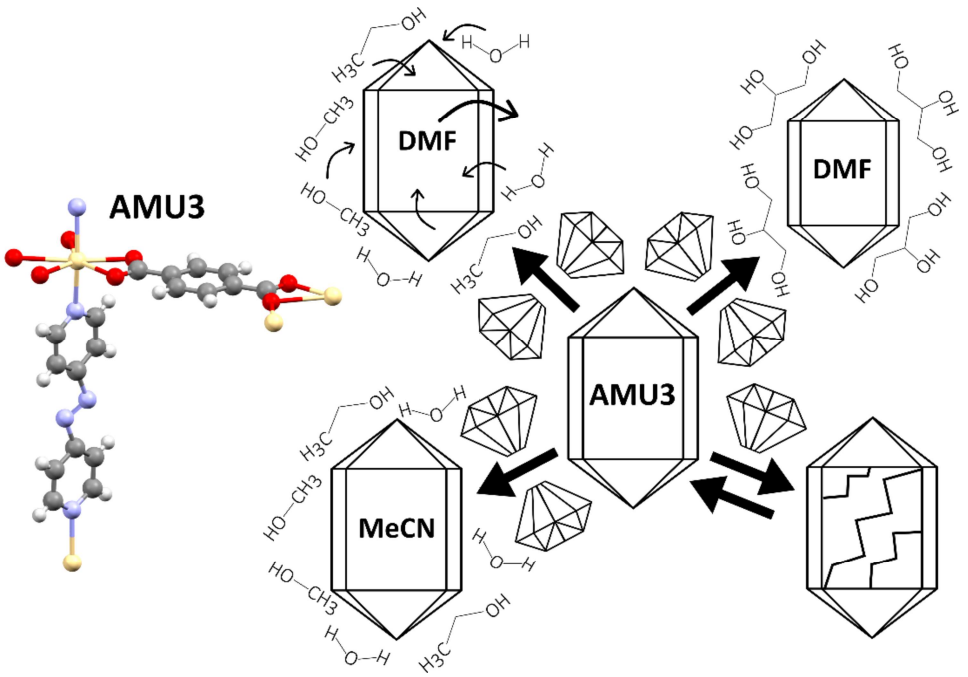

Figure 11. Photochromic AMU3 is ferroelastic under high pressure, but it is not affected by temperature changes. The transition pressure depends on the guest and environment. The crystals are capable of self-healing at normal conditions.

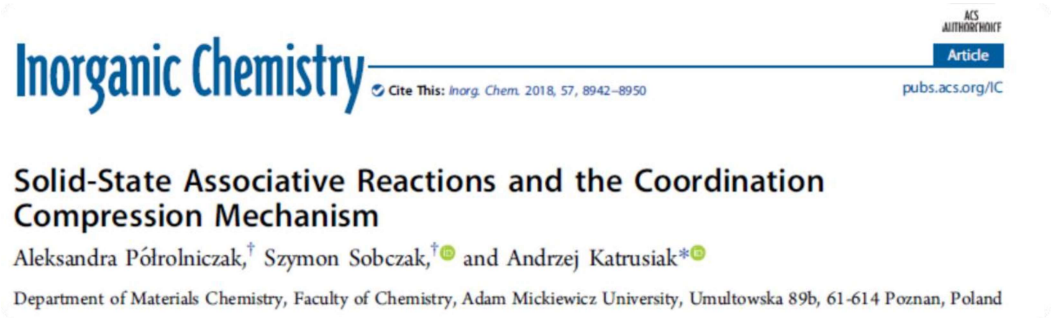
Inorganic Chemistry
Article
Cite This: Inorg. Chem. 2018, 57, 8942−8950
pubs.acs.org/IC

A5

Solid-State Associative Reactions and the Coordination Compression Mechanism

Aleksandra Półrolniczak,† Szymon Sobczak,† and Andrzej Katrusiak*

Department of Materials Chemistry, Faculty of Chemistry, Adam Mickiewicz University, Umultowska 89b, 61-614 Poznan, Poland

In **article A5**, a pressure-controlled reaction of a CP is reported. It was found that high pressure increases the coordination number of the Cd cation by shifting the NO_3^- anions. This is the first known pressure-induced topochemical reaction of a CP, where the metal cation becomes coordinated by a NO_3^- anion, unbonded under ambient pressure. The reaction was explained by the compression of the ionic radii of ligands coordinating Cd^{2+}. At ambient conditions, the crystal structure of hydrated $Cd(APP)_2NO_3{\cdot}NO_3$, abbreviated CdAPP, consisted of polymeric sheets separated by water molecules. The Cd^{2+} cation is 6-fold-coordinated by four APP linkers and one bidentate nitrate anion, and the voids comprise another NO_3^- anion and two water molecules per formula unit. The compression of $Cd(APP)_2NO_3{\cdot}NO_3$ performed in DAC, triggers an associative reaction, resulting in the formation of $Cd(APP)_2(NO_3)_2$. This reaction increases the coordination number of the central Cd cation from 6 to 7. The strain in the crystal environment is absorbed by a flexible APP linker, changing its two torsion angles by 20°. This solid-state reaction resembles an isostructural phase transition. At 0.4 GPa the crystal consist of coexisting parts of $Cd(APP)_2NO_3{\cdot}NO_3$ and $Cd(APP)_2(NO_3)_2$ compounds: the diffraction patterns showed split reflections due to the strain between those two phases. The unit-cell

dimensions and structural model obtained at this pressure were average of both compounds. The pressure-induced reaction involved the formation of a new Cd–O bond, between the Cd^{2+} cation and the nitrate NO_3^- anion. This reaction increased the coordination number by pushing the NO_3^- anion closer to the Cd^{2+} cation. The changes induced by pressure can be rationalized based on three rules: the stronger compression of anionic or neutral ligands compared to the central cations, the radii-coordination scheme relation, and the proximity of potential ligands. These rules explained the structural changes and associative reaction under pressure. Analogous transformations, but induced by temperature, have been found in literature. The study provided insights into the effects of pressure on the structure and properties of coordination compound, and the rules governing pressure-induced associative reaction.

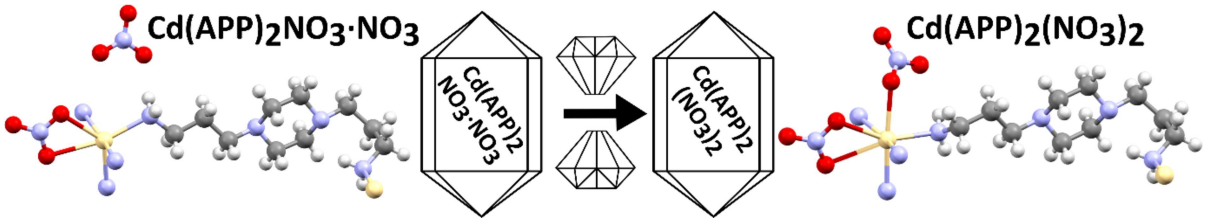

Figure 12. Solid-state associative reaction in $Cd(APP)_2NO_3{\cdot}NO_3$ at 0.4 GPa. The compression results in a new Cd-O bond and the coordination number increases from 6 to 7.

4. Discussion

The structure-property relations between the structure and elastic properties of molecular crystals, CPs, and MOFs involve such structural features as voids, intermolecular interactions, molecular shape and conformation. The role of these factors can be studied in varied temperature and pressure conditions. My interest was focused on the materials containing potentially flexible molecules or linkers. The objective was to analyse their effects, identify structural transformations, and find the mechanisms underlying their responses.

4.1 Temperature-induced effects

The effect of temperature on the crystal structures with conformationally flexible components were investigated for compounds described in articles A1, A4 and A5. Generally, it is expected that heated crystal would expand its volume and its linear directions; in crystal structure the increased thermal vibrations of atoms can lead to different types of disorder and to phase transitions, which usually would increase the crystal symmetry. These usually observed trends have exceptions. For example, there are crystals which reduce their volume when temperature increases (so called negative thermal expansion – NTE, or negative volume expansions – NVE); or the crystals which reduce their symmetry in the high-temperature phases.

In most materials the temperature and pressure effects are inverse: the higher temperature results in larger volume, stronger atomic vibrations and higher symmetry of phases, whereas the higher pressure decreases the volume, reduces the amplitude of vibrations and induce transitions to phases of lower symmetry. Hence, the rule of inverse temperature and pressure effects was formulated.[110] However, there are exceptions from this rule.[77,92,111,112] For example, for the solid-state reaction of coordination polymer CdAPP (article A5), we observed an increase in the coordination number with increasing pressure. This reaction occurred at the pressure of 0.4 GPa, so one would expect a similar reaction to occur at low temperature based on the rule of the inverse relationship of temperature and pressure, which suggests that the effects observed at 0.4 GPa correspond to those observed at 100 K. However, such a reaction does not take place at low temperature. The phenomenon of increasing the coordination number is more commonly associated with the temperature variations rather than application of high pressure, as it is described in detail in article A5, where we provide examples of increasing the coordination number induced by temperature, illustrated in Figure 5 of article A5. Also, it is generally expected that low temperatures promote ordering in disordered structures. In the case of AMU3 (Article A4), we observed that the conformational disorder persist at low temperature, whereas the structure orders under high pressure.

Moreover, when we consider the pressure and temperature changes applied simultaneously, we can observe that temperature can influence the critical point of pressure-induced transformation. In article A1, we have shown that high temperature shifts the boundary between the α and β phases towards lower pressures, in contrast to the amorphization of C5-PPB. This observation aligns with the hypothesis that significant atomic rearrangement is necessary for the α-β phase transition, so as the vibrational energy of atoms increases with temperature, the transformation occurs at lower pressure. For the over-compressed α-phase of C5-PPB, the amorphization occurs at higher pressure with increasing temperature, which indicates that the amorphization process is connected with the vibrational energy of atoms. The increased temperature intensify their thermal vibrations, making the crystal structure more resistant to amorphization. Consequently, higher pressures are required to induce amorphization. Thus, an increase in temperature enhances the stability of C5-PPB. Similar effects were previously reported for MnAs,[113] $LiAlO_2$,[114] or $BiFeO_3$.[115] However, also examples with the opposite relation between temperature and the pressure of transformation were described.[116,117] Therefore, the interplay of temperature and pressure effects on the phase transition or amorphization requires case-by-case study.

4.2 Compression of crystals with flexible molecules and linkers

Pressure is a one of the fundamental thermodynamic variable affecting the properties of materials, as a consequence of the changes in their crystal structure. The most deformable structural elements can be arranged as following: (I) voids in the structure; (II) weakest intermolecular interactions (e.g. van der Waals forces); (iii) stronger cohesion forces (electrostatic, hydrogen bonds, halogen bonds); and (iv) deformations of molecules. There are specific types of pressure effects depending on the presence of voids/pores in crystals and on the molecules size of the hydrostatic fluid. Other types of pressure effects can be connected to the conformational changes of flexible molecules or linkers and to the transformable conformations of ligands around metal centres. Such specific types of pressure effects are the main subject of my thesis.

Article A1 describes the significant conformational changes of C5-PPB induced by pressure, which depend on the compression rate. In Article A2, compound BTCP·dItFB·Ac shows the NLC effect and sensitivity to different PTM. A similar observation was reported in Article A3 for DMOF, a metal-organic framework, where previously reported BTCP molecule serve as a linker. Article A4 describes another MOF compound, AMU3, exhibiting the dependence of the phase-transition pressure on the PTM and the guest molecule filling the voids. The AMU3 crystal samples cracked under pressure, however the rare phenomenon of self-healing was observed when the pressure was released. Article A5 focuses on a coordination polymer, where a pressure-induced reaction leads to an increase in the coordination number of the central atom. All these articles provide in-depth discussions on

pressure-induced changes in the crystal structures, thus in this section of my thesis, I present the relative changes of unit-cell volume and available intermolecular spaces as a function of pressure for all the compounds studied in this work (Figure 13), together with description of conformational changes in compounds displaying the most prominent transformations (Figure 15).

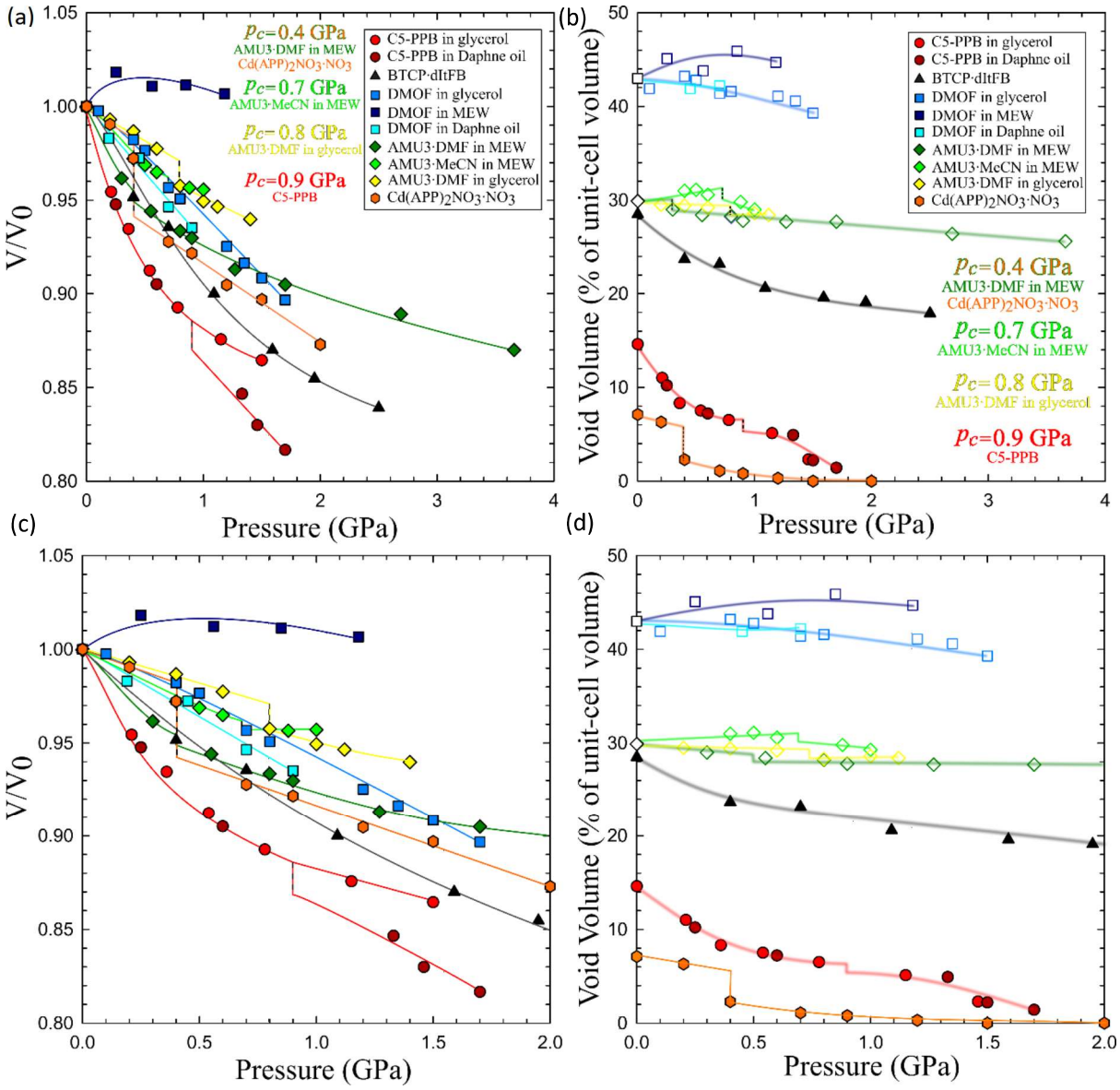

Figure 13. (a) Relative volume changes of the compounds studied under hydrostatic pressure in this thesis, listed in the legend and (b) the voids volume changes related to the crystal volume. The vertical lines correspond to the phase transitions at critical pressures, p_c, listed in the drawings.(c)(d) The bottom plots magnify the range of pressure limited to 2 GPa.

It is remarkable that compound DMOF exhibits an expansion of the crystal volume under increased pressure. This is a consequence of compressing a porous crystal in penetrating PTM, where small molecules of the MEW mixture penetrate the voids. In the non-penetrating Daphne oil, the crystal volume was compressed at a rate of -6% GPa^{-1}, somewhat higher than in glycerine of -5% GPa^{-1}. This result suggests that the glycerine sample used in

the experiment contained a small amount of water absorbed from the air, and these water molecules penetrated the voids. Moreover, the DMOF crystal, with its larger voids, was expected to exhibit the most significant change in unit-cell volume. Therefore, the rule that voids are the most compressible parts in crystal structures does not apply in this case. The explanation is that the voids are filled by guest molecules which were masked in the refinements. When voids are filled with unbonded guest molecules, the determination of their structural arrangement by XRD is not possible. Therefore, for refining the host structure, the pore content is omitted. Such a mask was applied for both DMOF and AMU3. In the plots in Figure 13, the void volume refers to "cleared" voids, which in fact are filled with guest molecules. For example, in the case of DMOF, the pore-to-crystal volume ratio with the guest molecules included is 27% (out of 43% with the applied mask), and for AMU3, it is 11% (out of 30% with the mask). The voids volume for compounds DMOF and AMU3 with guest molecules inside the pores was estimated for the structures refined with the mask, i.e. by omitting the guest molecules.

The strongest compression was observed in the molecular crystal C5-PPB, which contains relatively small voids and highly flexible molecules. The pressure-induced transition is connected to both: conformational rearrangement and void compression. The conformational changes occur due to the availability of space, and the reduction of voids is a result of tighter packing of conformationally transformed molecules. Furthermore, a crucial role is played by the speed of this transformation: when compressed quickly, the structure "freezes" in the α phase and then the sample becomes amorphous and visible cracks appear on its surface. The slow compression leads to an isostructural phase transition, strongly changing the conformation of pentoxy chains (Figure 14), which causes clear differentiation of molecules A and B in the high-pressure β-phase. The angle between benzene rings in two molecules A and B varies from 1.44° to 2.38°, and from 11.01° to 16.41° for pyridine rings between phases α and β, respectively. The largest compressibility of C5-PPB is accompanied by the strongest changes of torsion angles, exceeding 120° (Figure 15).

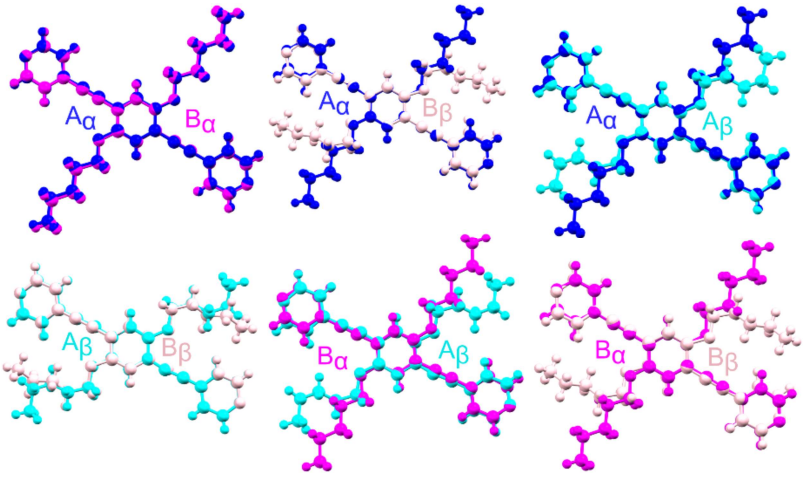

Figure 14. Interpolation of two independent molecules in C5-PPB phases α and β.

The porous molecular co-crystal solvate abbreviated as BTCP·dItFB·Ac undergoes no phase transition in the investigated pressure range, but a strong volume compression is observed. Because in this crystals there are relatively big voids, a strong compression of the crystal volume can be expected. On the other hand, the voids can absorb guest molecules from the environment, for example from the PTM. Hence the conclusion that the significant compression of the crystal volume results from the compression of voids accompanied by conformational changes in the structure.

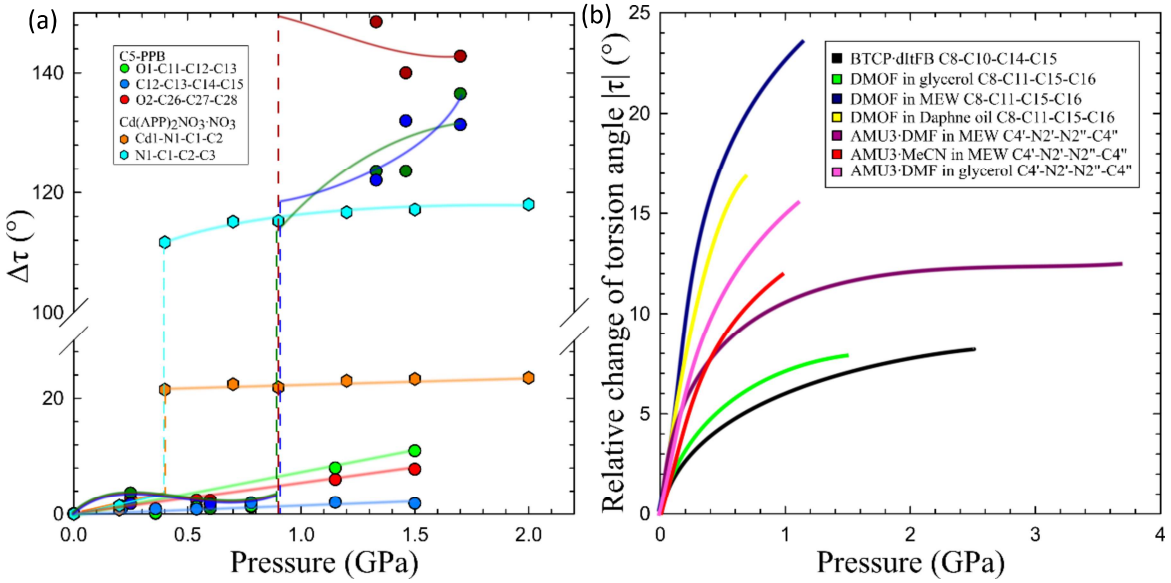

Figure 15. (a) Monotonic and anomalous changes in the torsion angles (Δτ) in crystals: C5-PPB (circles) and CdAPP (hexagonals). Different torsion angles are distinguished by colours indicated in the legend. (b) Average change in selected torsion angles in crystals: BTCP·dItFB (black), DMOF (green, blue and yellow) and AMU3 (violet, red and pink).

A nearly complete reduction of voids is observed in the coordination polymer CdAPP. This reduction occurs due to the solid-state reaction involving the connection of the NO_3 group to the central atom, resulting in its increased coordination number. Additionally, significant changes in torsion angles are observed (Figure 15). The conformation of linkers adjusts to the pressure-induced tightening of the crystal packing, facilitating the connection of the new ligand with the cadmium cation. Thus the compression of CdAPP results of the combination of several structural effects. However, the compressibility of coordination polymer CdAPP is still smaller than that of molecular crystal C5-PPB.

The remaining compounds studied in my thesis illustrate various aspects of the compressibility of crystals with flexible structural elements. Their conformational changes may be, or may be not induced by high pressure, depending on a myriad of other structural properties. However, undoubtedly the flexible structural elements provide efficient means to crystal engineers for designing new materials with high compressibility and desired interactions with the pressure transmitting media.

Conclusions

The comprehensive study presented in the discussed articles show the intricate interplay between the structure and elastic properties of molecular crystals, coordination polymers (CPs), and metal-organic frameworks (MOFs) under the various temperature and pressure conditions. The research was based on materials containing potentially flexible molecules or linkers, and focused on analysing their effects, identify structural transformations, and understand the underlying mechanisms of their responses.

In my thesis I extensively studied the compression of crystals with flexible molecules and linkers, which shown various, interesting effects. In C5-PPB, the rapid compression effectively "froze" the conformers of phase α due to rapid intermolecular interactions, leading to amorphization. Slow compression, resulted in an isostructural phase transition to a new high-pressure phase β, showing the complex interplay of conformational changes and void reduction. The co-crystal solvate BTCP·dItFB·Ac (Article A2) exhibited negative linear compressibility under high pressure, highlighting its unique elastic properties. The significant volume compression was attributed to the compression of voids accompanied by conformational changes. The porous MOF compound - DMOF (Article A3) showed high sensitivity to the type of pressure-transmitting media (PTM). Compression in PTM with large molecules lead to negative linear compressibility (NLC), while a use of the PTM with small molecules resulted in increasing the crystal dimensions in the directions perpendicular to that of the NLC. This effect is caused by hyperfilling the pores with small PTM molecules, which eventually lead to pressure-induced amorphization. Both these analogous host and inclusion compounds are described in the same reference crystal axes, which prove its high flexibility. The study underscored the importance of type of PTM when analysing the compressibility of porous materials. The second MOF crystal, called AMU3 (Article A4) showed ferroelastic properties tuneable by exchanging guest molecules or crystal environment. The crystals have self-healing property, overcoming a common limitation faced by many ferroelastic materials. These unique characteristic make AMU3 as a promising candidate for chemo-mechanical transducers in sensor applications. For the coordination polymer CdAPP (Article A5), a pressure-induced topochemical reaction of a coordination polymer was observed. The increase in coordination number through a solid-state associative reaction revealed is the first-known case of such an effect of pressure on the structure and properties of coordination compounds.

Of all the compounds studied in my thesis, C5-PPB and CdAPP showed the most significant pressure-induced structural changes, highlighting the interplay of volume changes, conformational adjustments and voids. Framework materials, DMOF and AMU3, capable of guest intrusion/exclusion, showed a smaller volume reduction. In these crystals guest molecules filled the voids, preventing their compression.

This study on a series of crystals with flexible structural units highlights the complex interplay between crystal structure, crystal environment, temperature, and pressure, providing the comprehensive insights into the behaviour of molecular crystals, CPs, and MOFs under varying conditions. The results not only contribute to fundamental knowledge in materials science but also offer crucial implications for the design and understanding of diverse materials for practical applications. In recent years, the investigation of temperature and pressure effects on versatile materials has become more available and is often performed with standard laboratory diffractometers, without the need for very high X-ray beam intensity provided by synchrotrons or advanced experimental setups for extremely high pressure and temperature. This area of moderate pressure changes to about 10 GPa and temperature between 100 - 500 K shows significant potential and offers intriguing paths for future research. With the potential of in-house pressure equipment, there are several pivotal challenges ahead. First, the perspective of temperature and pressure-induced changes helps to understand the complex relationship between intramolecular and intermolecular distortions and finding their contribution to structural strain anisotropy within the limits of phase stability, as well as their role in structural rearrangements leading to phase transitions and chemical reactions. In addition, it is an efficient method to use high pressure as a tool to identify specific structural elements in materials capable of improving their physicochemical properties. Instead of synthesizing new analogous compounds, it is possible to follow the structural changes as a function of pressure, which can suggest the optimal structure with required properties. The pressure-supported determination of structure–property relation has significant potential, especially when flexible substrates are involved. It has been demonstrated in my thesis, that such materials are highly susceptible to various factors and particularly to high pressure, inducing phase transitions, chemical reactions, different behaviour in the penetrating and non-penetrating fluids, as well as to the types of guest molecules filling the structural voids. Owing to their conformational flexibility and stepwise transformations, the properties of materials with elastic linkers or molecules differ from the ones with the rigid components only. Therefore the application of crystals with elastic elements offers new avenues for controlling and manipulating properties of materials. I hope that my work will stimulate further investigations on elastic properties in molecular crystals, coordination polymers and MOFs, their transitions and amorphization, and that it will be useful for the design and optimization of materials for a variety of new applications.

References

(1) Fahlman, B. D. *Materials Chemistry*, 1st ed.; Springer Netherlands: Dordrecht, **2007**. https://doi.org/10.1007/978-1-4020-6120-2.

(2) Barber, J. R. *Elasticity*, 3rd ed.; Springer New York, NY, **2010**. https://doi.org/10.4324/9781003239857-4.

(3) https://www.azom.com/. Access date 05/05/2023

(4) Hoja, J.; Reilly, A. M.; Tkatchenko, A. First-Principles Modeling of Molecular Crystals: Structures and Stabilities, Temperature and Pressure. *Wiley Interdiscip. Rev. Comput. Mol. Sci.* **2017**, *7* (1). https://doi.org/10.1002/wcms.1294.

(5) Wright, J. D. *Molecular Crystals*, 1st ed.; Molecular Crystals; Cambridge University Press: Cambridge, **1995**.

(6) Zhou, H. C. J.; Kitagawa, S. Metal-Organic Frameworks (MOFs). *Chem. Soc. Rev.* **2014**, *43* (16), 5415–5418. https://doi.org/10.1039/c4cs90059f.

(7) McKellar, S. C.; Sotelo, J.; Greenaway, A.; Mowat, J. P. S.; Kvam, O.; Morrison, C. A.; Wright, P. A.; Moggach, S. A. Pore Shape Modification of a Microporous Metal-Organic Framework Using High Pressure: Accessing a New Phase with Oversized Guest Molecules. *Chem. Mater.* **2016**, *28* (2), 466–473. https://doi.org/10.1021/acs.chemmater.5b02891.

(8) Williams J. E., Stand P.J., Schleyer, P. R. Quantitative Conformational Analysis; *Annu. Rev. Phys. Chem.* **1968**, *19*, 531–558. https://doi.org/https://doi.org/10.1146/annurev.pc.19.100168.002531.

(9) Müller, F. H. CHAPTER 8 - THERMODYNAMICS OF DEFORMATION; CALORIMETRIC INVESTIGATIONS OF DEFORMATION PROCESSES. In *Rheology*; EIRICH, F. R., Ed.; Academic Press: Cambridge, Massachusetts, **1969**; pp 417–489. https://doi.org/https://doi.org/10.1016/B978-1-4832-2942-3.50014-4.

(10) Braude, E. A.; Nachod, F. C. Contributors. In *Determination of Organic Structures by Physical Methods*; Elsevier: Cambridge, Massachusetts, **1955**; https://doi.org/10.1016/B978-1-4832-3166-2.50004-4.

(11) Slonimsky, G. L. Laws of Mechanical Relaxation Processes in Polymers. *J. Polym. Sci. Part C Polym. Symp.* **1967**, *16* (3), 1667–1672. https://doi.org/10.1002/polc.5070160342.

(12) Vinogradova, S. V; Vinogradova, O. V. Coordination Polymers with Inorganic Main Chains. *Russ. Chem. Rev.* **1975**, *44* (6), 510–521. https://doi.org/10.1070/rc1975v044n06abeh002357.

(13) Rubinstein, M.; Panyukov, S. Elasticity of Polymer Networks. *Macromolecules* **2002**, *35* (17), 6670–6686. https://doi.org/10.1021/ma0203849.

(14) Shefter, E.; Higuchi, T. Dissolution Behavior of Crystalline Solvated and Nonsolvated Forms of Some Pharmaceuticals. *J. Pharm. Sci.* **1963**, *52* (8), 781–791. https://doi.org/10.1002/jps.2600520815.

(15) Naumov, P.; Chizhik, S.; Panda, M. K.; Nath, N. K.; Boldyreva, E. Mechanically Responsive Molecular Crystals. *Chem. Rev.* **2015**, *115* (22), 12440–12490. https://doi.org/10.1021/acs.chemrev.5b00398.

(16) Awad, W. M.; Davies, D. W.; Kitagawa, D.; Mahmoud Halabi, J.; Al-Handawi, M. B.; Tahir, I.; Tong, F.; Campillo-Alvarado, G.; Shtukenberg, A. G.; Alkhidir, T.; et al. Mechanical Properties and Peculiarities of Molecular Crystals. *Chem. Soc. Rev.* **2023**, 3098–3169. https://doi.org/10.1039/d2cs00481j.

(17) Safari, F.; Katrusiak, A. High-Pressure Polymorphs Nucleated and Stabilized by Rational Doping under Ambient Conditions. *J. Phys. Chem. C* **2021**, *125* (42), 23501–23509. https://doi.org/10.1021/acs.jpcc.1c07297.

(18) Kaupp, G. Solid-State Reactions, Dynamics in Molecular Crystals. *Curr. Opin. Solid State Mater. Sci.* **2002**, *6* (2), 131–138. https://doi.org/10.1016/S1359-0286(02)00041-4.

(19) Thompson, A. J.; Chamorro Orué, A. I.; Nair, A. J.; Price, J. R.; McMurtrie, J.; Clegg, J. K. Elastically

Flexible Molecular Crystals. *Chem. Soc. Rev.* **2021**, *50* (21), 11725–11740. https://doi.org/10.1039/d1cs00469g.

(20) Ahmed, E.; Karothu, D. P.; Naumov, P. Crystal Adaptronics: Mechanically Reconfigurable Elastic and Superelastic Molecular Crystals. *Angew. Chemie - Int. Ed.* **2018**, *57* (29), 8837–8846. https://doi.org/10.1002/anie.201800137.

(21) Guńka, P. A.; Dranka, M.; Hanfland, M.; Dziubek, K. F.; Katrusiak, A.; Zachara, J. Cascade of High-Pressure Transitions of Claudetite II and the First Polar Phase of Arsenic(III) Oxide. *Cryst. Growth Des.* **2015**, *15* (8), 3950–3954. https://doi.org/10.1021/acs.cgd.5b00567.

(22) Kitagawa, S.; Kitaura, R.; Noro, S. I. Functional Porous Coordination Polymers. *Angew. Chemie - Int. Ed.* **2004**, *43* (18), 2334–2375. https://doi.org/10.1002/anie.200300610.

(23) Liu, X.; Xie, L.; Lin, J.; Lin, R.; Zhang, J.; Chen, X. Flexible Porous Coordination Polymers Constructed from 1,2-Bis(4-Pyridyl)Hydrazine. **2011**, 8549–8554. https://doi.org/10.1039/c1dt10682a.

(24) Du, M.; Li, C. P.; Liu, C. Sen; Fang, S. M. Design and Construction of Coordination Polymers with Mixed-Ligand Synthetic Strategy. *Coord. Chem. Rev.* **2013**, *257* (7–8), 1282–1305. https://doi.org/10.1016/j.ccr.2012.10.002.

(25) Chen, C. T.; Suslick, K. S. One-Dimensional Coordination Polymers: Applications to Material Science. *Coord. Chem. Rev.* **1993**, *128* (1–2), 293–322. https://doi.org/10.1016/0010-8545(93)80036-5.

(26) Zheng, Y.; Sato, H.; Wu, P.; Jeon, H. J.; Matsuda, R.; Kitagawa, S. Flexible Interlocked Porous Frameworks Allow Quantitative Photoisomerization in a Crystalline Solid. *Nat. Commun.* **2017**, *8* (1), 100. https://doi.org/10.1038/s41467-017-00122-5.

(27) Liu, X.; Xie, L.; Lin, J.; Lin, R.; Zhang, J.; Chen, X. Flexible Porous Coordination Polymers Constructed from 1,2-Bis(4-Pyridyl)Hydrazine via Solvothermal in Situ Reduction of 4,4¢-Azopyridine. *Dalt. Trans.*, **2011**, *40*, 8549–8554. https://doi.org/10.1039/c1dt10682a.

(28) Zhou, H. C.; Long, J. R.; Yaghi, O. M. Introduction to Metal-Organic Frameworks. *Chem. Rev.* **2012**, *112* (2), 673–674. https://doi.org/10.1021/cr300014x.

(29) Lee, Y. R.; Kim, J.; Ahn, W. S. Synthesis of Metal-Organic Frameworks: A Mini Review. *Korean Journal of Chemical Engineering*. **2013**, pp 1667–1680. https://doi.org/10.1007/s11814-013-0140-6.

(30) Safaei, M.; Foroughi, M. M.; Ebrahimpoor, N.; Jahani, S.; Omidi, A.; Khatami, M. A Review on Metal-Organic Frameworks: Synthesis and Applications. *TrAC - Trends Anal. Chem.* **2019**, *118*, 401–425. https://doi.org/10.1016/j.trac.2019.06.007.

(31) Li, J. R.; Sculley, J.; Zhou, H. C. Metal-Organic Frameworks for Separations. *Chemical Reviews*. **2012**, 869–932. https://doi.org/10.1021/cr200190s.

(32) Murray, L. J.; Dincă, M.; Long, J. R. Hydrogen Storage in Metal–Organic Frameworks. *Chem. Soc. Rev.* **2009**, *38* (5), 1294. https://doi.org/10.1039/b802256a.

(33) Li, J. R.; Ma, Y.; McCarthy, M. C.; Sculley, J.; Yu, J.; Jeong, H. K.; Balbuena, P. B.; Zhou, H. C. Carbon Dioxide Capture-Related Gas Adsorption and Separation in Metal-Organic Frameworks. *Coord. Chem. Rev.* **2011**, *255* (15–16), 1791–1823. https://doi.org/10.1016/j.ccr.2011.02.012.

(34) Chaemchuen, S.; Kabir, N. A.; Zhou, K.; Verpoort, F. Metal-Organic Frameworks for Upgrading Biogas via CO2 Adsorption to Biogas Green Energy. *Chem. Soc. Rev.* **2013**, *42* (24), 9304–9332. https://doi.org/10.1039/c3cs60244c.

(35) Horcajada, P.; Serre, C.; Maurin, G.; Ramsahye, N. A.; Balas, F.; Vallet-Regí, M.; Sebban, M.; Taulelle, F.; Férey, G. Flexible Porous Metal-Organic Frameworks for a Controlled Drug Delivery. *J. Am. Chem. Soc.* **2008**, *130* (21), 6774–6780. https://doi.org/10.1021/ja710973k.

(36) Collings, I. E.; Goodwin, A. L. Metal-Organic Frameworks under Pressure. *J. Appl. Phys.* **2019**, *126* (18), 181101. https://doi.org/10.1063/1.5126911.

(37) Nikolayenko, V. I.; Herbert, S. A.; Barbour, L. J. Reversible Structural Switching of a Metal-Organic Framework by Photoirradiation. *Chem. Commun.* **2017**, *53* (81), 11142–11145. https://doi.org/10.1039/c7cc06074b.

(38) Batten, S. R.; Champness, N. R.; Chen, X.-M.; Garcia-Martinez, J.; Kitagawa, S.; Öhrström, L.; O'Keeffe, M.; Paik Suh, M.; Reedijk, J. Terminology of Metal–Organic Frameworks and Coordination Polymers (IUPAC Recommendations 2013). *Pure Appl. Chem.* **2013**, *85* (8). https://doi.org/10.1351/PAC-REC-12-11-20.

(39) Batten, S. R.; Champness, N. R.; Chen, X.-M.; Garcia-Martinez, J.; Kitagawa, S.; Öhrström, L.; O'Keeffe, M.; Suh, M. P.; Reedijk, J. Coordination Polymers, Metal–Organic Frameworks and the Need for Terminology Guidelines. *CrystEngComm* **2012**, *14* (9), 3001. https://doi.org/10.1039/c2ce06488j.

(40) Zurek, E.; Grochala, W. Predicting Crystal Structures and Properties of Matter under Extreme Conditions via Quantum Mechanics: The Pressure Is On. *Phys. Chem. Chem. Phys.* **2015**, *17* (5), 2917–2934. https://doi.org/10.1039/c4cp04445b.

(41) Drebushchak, V. A. Thermal Expansion of Solids: Review on Theories. *J. Therm. Anal. Calorim.* **2020**, *142* (2), 1097–1113. https://doi.org/10.1007/s10973-020-09370-y.

(42) George, J.; Deringer, V. L.; Wang, A.; Müller, P.; Englert, U.; Dronskowski, R. Lattice Thermal Expansion and Anisotropic Displacements in α-Sulfur from Diffraction Experiments and First-Principles Theory. *J. Chem. Phys.* **2016**, *145* (23). https://doi.org/10.1063/1.4972068.

(43) Chiang, C. C.; Lai, C. H.; Wu, Y. C. Low-Temperature Ordering of L10 FePt by PtMn Underlayer. *Appl. Phys. Lett.* **2006**, *88* (15), 0–3. https://doi.org/10.1063/1.2191422.

(44) Bond, A. D. Polymorphism in Molecular Crystals. *Curr. Opin. Solid State Mater. Sci.* **2009**, *13* (3–4), 91–97. https://doi.org/10.1016/j.cossms.2009.06.004.

(45) Miller, W.; Smith, C. W.; MacKenzie, D. S.; Evans, K. E. Negative Thermal Expansion: A Review. *J. Mater. Sci.* **2009**, *44* (20), 5441–5451. https://doi.org/10.1007/s10853-009-3692-4.

(46) Lind, C. Two Decades of Negative Thermal Expansion Research: Where Do We Stand? *Materials (Basel).* **2012**, *5* (6), 1125–1154. https://doi.org/10.3390/ma5061125.

(47) Barrera, G. D.; Bruno, J. A. O.; Barron, T. H. K.; Allan, N. L. Negative Thermal Expansion. *J. Phys. Condens. Matter* **2005**, *17* (4). https://doi.org/10.1088/0953-8984/17/4/R03.

(48) Zakharov, B. A.; Boldyreva, E. V. High Pressure: A Complementary Tool for Probing Solid-State Processes. *CrystEngComm* **2019**, *21* (1), 10–22. https://doi.org/10.1039/c8ce01391h.

(49) Katrusiak, A. Lab in a DAC - High-Pressure Crystal Chemistry in a Diamond-Anvil Cell. *Acta Crystallogr. Sect. B Struct. Sci. Cryst. Eng. Mater.* **2019**, *75*, 918–926. https://doi.org/10.1107/S2052520619013246.

(50) Zhang, L.; Wang, Y.; Lv, J.; Ma, Y. Materials Discovery at High Pressures. *Nat. Rev. Mater.* **2017**, *2* (4). https://doi.org/10.1038/natrevmats.2017.5.

(51) Angus, J. C. Diamond Synthesis by Chemical Vapor Deposition: The Early Years. *Diam. Relat. Mater.* **2014**, *49*, 77–86. https://doi.org/10.1016/j.diamond.2014.08.004.

(52) Graham, R. A.; Morosin, B.; Venturini, E. L.; Carr, M. J. Materials Modification and Synthesis Under High Pressure Shock Compression. *Annu. Rev. Mater. Sci.* **1986**, *16*, 315–341. https://doi.org/10.1146/annurev.ms.16.080186.001531.

(53) Lesage, C.; Devers, E.; Legens, C.; Fernandes, G.; Roudenko, O.; Briois, V. High Pressure Cell for Edge Jumping X-Ray Absorption Spectroscopy: Applications to Industrial Liquid Sulfidation of Hydrotreatment Catalysts. *Catal. Today* **2019**, *336*, 63–73. https://doi.org/10.1016/j.cattod.2019.01.081.

(54) Falbe, J.; Bahrmann, H.; Gilde, H. G. Homogeneous Catalysis - Industrial Applications. *J. Chem. Educ.* **1984**, *61* (11), 961–967. https://doi.org/10.1021/ed061p961.

(55) Khan, S. A.; Aslam, R.; Makroo, H. A. High Pressure Extraction and Its Application in the Extraction of Bio-Active Compounds: A Review. *J. Food Process Eng.* **2019**, *42* (1), 1–15. https://doi.org/10.1111/jfpe.12896.

(56) Prasad, K. N.; Yang, E.; Yi, C.; Zhao, M.; Jiang, Y. Innovative Food Sci. *Emerg. Technol* **2009**, *10* (2), 155–159. https://doi.org/10.1016/j.ifset.2008.11.007.

(57) Das, T. K.; Ghosh, P.; Das, N. C. Preparation, Development, Outcomes, and Application Versatility of Carbon Fiber-Based Polymer Composites: A Review. *Adv. Compos. Hybrid Mater.* **2019**, *2* (2), 214–233. https://doi.org/10.1007/s42114-018-0072-z.

(58) Nisticò, R. Polyethylene Terephthalate (PET) in the Packaging Industry. *Polym. Test.* **2020**, *90* (July). https://doi.org/10.1016/j.polymertesting.2020.106707.

(59) Yan, W.-C.; Dong, T.; Zhou, Y.-N.; Luo, Z.-H. Computational Modeling toward Full Chain of Polypropylene Production: From Molecular to Industrial Scale. *Chem. Eng. Sci.* **2023**, *269*, 118448. https://doi.org/https://doi.org/10.1016/j.ces.2023.118448.

(60) Liu, C.; Wang, K.; Ye, L.; Wang, Y.; Yuan, X. Deep Learning with Neighborhood Preserving Embedding Regularization and Its Application for Soft Sensor in an Industrial Hydrocracking Process. *Inf. Sci. (Ny).* **2021**, *567*, 42–57. https://doi.org/10.1016/j.ins.2021.03.026.

(61) Grange, P.; Vanhaeren, X. Hydrotreating Catalysts, an Old Story with New Challenges. *Catal. Today* **1997**, *36* (4), 375–391. https://doi.org/10.1016/S0920-5861(96)00232-5.

(62) Wittich, K.; Krämer, M.; Bottke, N.; Schunk, S. A. Catalytic Dry Reforming of Methane: Insights from Model Systems. *ChemCatChem* **2020**, *12* (8), 2130–2147. https://doi.org/10.1002/cctc.201902142.

(63) Dong, M. W.; Guillarme, D. Newer Developments in HPLC Impacting Pharmaceutical Analysis: A Brief Review. *Am. Pharm. Rev.* **2013**, *16* (4).

(64) Yadav, K. S.; Kale, K. High Pressure Homogenizer in Pharmaceuticals: Understanding Its Critical Processing Parameters and Applications. *J. Pharm. Innov.* **2020**, *15* (4), 690–701. https://doi.org/10.1007/s12247-019-09413-4.

(65) Liu, H. Ammonia Synthesis Catalyst 100 Years: Practice, Enlightenment and Challenge. *Cuihua Xuebao/Chinese J. Catal.* **2014**, *35* (10), 1619–1640. https://doi.org/10.1016/S1872-2067(14)60118-2.

(66) NAIK, L.; SHARMA, R.; GAARE, R. Application of High Pressure Processing Technology for Dairy Food Preservation - Future Perspective: A Review. *J. Anim. Prod. Adv.* **2013**, *3* (8), 232. https://doi.org/10.5455/japa.20120512104313.

(67) Alañón, M. E.; Cádiz-Gurrea, M. L.; Oliver-Simancas, R.; Leyva-Jiménez, F. J.; Arráez-Román, D.; Segura-Carretero, A. Quality Assurance of Commercial Guacamoles Preserved by High Pressure Processing versus Conventional Thermal Processing. *Food Control* **2022**, *135*, 108791. https://doi.org/https://doi.org/10.1016/j.foodcont.2021.108791.

(68) Flores-Livas, J. A.; Boeri, L.; Sanna, A.; Profeta, G.; Arita, R.; Eremets, M. A Perspective on Conventional High-Temperature Superconductors at High Pressure: Methods and Materials. *Phys. Rep.* **2020**, *856*, 1–78. https://doi.org/10.1016/j.physrep.2020.02.003.

(69) Le Godec, Y.; Courac, A.; Solozhenko, V. L. High-Pressure Synthesis of Superhard and Ultrahard Materials. *J. Appl. Phys.* **2019**, *126* (15). https://doi.org/10.1063/1.5111321.

(70) Yongjin, C.; Shuhong, B. High Energy Density Material (HEDM) – Progress in Research Azine Energetic Compounds. *Johnson Matthey Technol. Rev.* **2019**, *63* (1), 51–72. https://doi.org/10.1595/205651319X15421043166627.

(71) Hemley, R. J.; Dera, P. Molecular Crystals. *Rev. Mineral. Geochemistry* **2000**, *41* (1), 335–419. https://doi.org/10.2138/rmg.2000.41.12.

(72) Półrolniczak, A.; Sobczak, S.; Katrusiak, A. Solid-State Associative Reactions and the Coordination Compression Mechanism. *Inorg. Chem.* **2018**, *57* (15), 8942–8950.

https://doi.org/10.1021/acs.inorgchem.8b00913.

(73) Cairns, A. B.; Goodwin, A. L. Negative Linear Compressibility. *Phys. Chem. Chem. Phys.* **2015**, *17* (32), 20449–20465. https://doi.org/10.1039/c5cp00442j.

(74) Cai, W.; Gładysiak, A.; Anioła, M.; Smith, V. J.; Barbour, L. J.; Katrusiak, A. Giant Negative Area Compressibility Tunable in a Soft Porous Framework Material. *J. Am. Chem. Soc.* **2015**, *137* (29), 9296–9301. https://doi.org/10.1021/jacs.5b03280.

(75) Cai, W.; Katrusiak, A. Giant Negative Linear Compression Positively Coupled to Massive Thermal Expansion in a Metal-Organic Framework. *Nat. Commun.* **2014**, *5*, 1–8. https://doi.org/10.1038/ncomms5337.

(76) Roszak, K.; Katrusiak, A. Low-Density Preference of the Ambient and High-Pressure Polymorphs of DL-Menthol. *IUCrJ* **2023**, *10* (Pt 3), 341–351. https://doi.org/10.1107/S2052252523002452.

(77) Montisci, F.; Lanza, A.; Casati, N.; Macchi, P. NO2···NO2 Contacts under Compression: Testing the Forces in Soft Donor-Acceptor Interactions. *Cryst. Growth Des.* **2018**, *18* (12), 7579–7589. https://doi.org/10.1021/acs.cgd.8b01392.

(78) Tomkowiak, H.; Katrusiak, A. Compression of Hydrogen-Bonded Layers in Imidazolidine-2-Thione. *Cryst. Growth Des.* **2018**, *19*, 285–290. https://doi.org/10.1021/acs.cgd.8b01363.

(79) Sobczak, S.; Katrusiak, A. Colossal Strain Release by Conformational Energy Up-Conversion in a Compressed Molecular Crystal. *J. Phys. Chem. C* **2017**, *121* (5), 2539–2545. https://doi.org/10.1021/acs.jpcc.6b11030.

(80) Cai, W.; He, J.; Li, W.; Katrusiak, A. Anomalous Compression of a Weakly CH···O Bonded Nonlinear Optical Molecular Crystal. *J. Mater. Chem. C* **2014**, *2* (32), 6471–6476. https://doi.org/10.1039/c4tc00654b.

(81) Zieliński, W.; Katrusiak, A. Colossal Monotonic Response to Hydrostatic Pressure in Molecular Crystal Induced by a Chemical Modification. *Cryst. Growth Des.* **2014**, *14* (9), 4247–4253. https://doi.org/10.1021/cg5008457.

(82) Runowski, M.; Woźny, P.; Stopikowska, N.; Guo, Q.; Lis, S. Optical Pressure Sensor Based on the Emission and Excitation Band Width (Fwhm) and Luminescence Shift of Ce3+-Doped Fluorapatite - High-Pressure Sensing. *ACS Appl. Mater. Interfaces* **2019**, *11* (4), 4131–4138. https://doi.org/10.1021/acsami.8b19500.

(83) Lin, J.; Zhao, Z.; Liu, C.; Zhang, J.; Du, X.; Yang, G.; Ma, Y. IrF 8 Molecular Crystal under High Pressure. *J. Am. Chem. Soc.* **2019**, *141* (13), 5409–5414. https://doi.org/10.1021/jacs.9b00069.

(84) Andrzejewski, M.; Katrusiak, A. Piezochromic Topology Switch in a Coordination Polymer. *J. Phys. Chem. Lett.* **2017**, *8* (5), 929–935. https://doi.org/10.1021/acs.jpclett.7b00019.

(85) Sobczak, S.; Katrusiak, A. Zone-Collapse Amorphization Mimicking the Negative Compressibility of a Porous Compound. *Cryst. Growth Des.* **2018**, *18* (2), 1082–1089. https://doi.org/10.1021/acs.cgd.7b01535.

(86) Andrzejewski, M.; Casati, N.; Katrusiak, A. Reversible Pressure Pre-Amorphization of a Piezochromic Metal-Organic Framework. *Dalt. Trans.* **2017**, *46* (43), 14795–14803. https://doi.org/10.1039/c7dt02511d.

(87) Coudert, F.-X. Responsive Metal–Organic Frameworks and Framework Materials: Under Pressure, Taking the Heat, in the Spotlight, with Friends. *Chem. Mater.* **2015**, *27* (6), 1905–1916. https://doi.org/10.1021/acs.chemmater.5b00046.

(88) Sobczak, S.; Katrusiak, A. Environment-Controlled Postsynthetic Modifications of Iron Formate Frameworks. *Inorg. Chem.* **2019**, *58* (17), 11773–11781. https://doi.org/10.1021/acs.inorgchem.9b01817.

(89) Liu, D.; Lu, K.; Poon, C.; Lin, W. Metal-Organic Frameworks as Sensory Materials and Imaging Agents.

Inorg. Chem. **2014**, *53* (4), 1916–1924. https://doi.org/10.1021/ic402194c.

(90) McKellar, S. C.; Graham, A. J.; Allan, D. R.; Mohideen, M. I. H.; Morris, R. E.; Moggach, S. A. The Effect of Pressure on the Post-Synthetic Modification of a Nanoporous Metal-Organic Framework. *Nanoscale* **2014**, *6* (8), 4163–4173. https://doi.org/10.1039/c3nr04161a.

(91) Li, J.-R.; Kuppler, R. J.; Zhou, H.-C. Selective Gas Adsorption and Separation in Metal–Organic Frameworks. *Chem. Soc. Rev.* **2009**, *38* (5), 1477. https://doi.org/10.1039/b802426j.

(92) Kaźmierczak, M.; Patyk-Kaźmierczak, E.; Katrusiak, A. Compression and Thermal Expansion in Organic and Metal-Organic Crystals: The Pressure-Temperature Correspondence Rule. *Cryst. Growth Des.* **2021**, *21* (4), 2196–2204. https://doi.org/10.1021/acs.cgd.0c01636.

(93) Marciniak, J.; Katrusiak, A. Direct and Inverse Relations between Temperature and Pressure Effects in Crystals: A Case Study on o-Xylene. *J. Phys. Chem. C* **2017**, *121* (40), 22303–22309. https://doi.org/10.1021/acs.jpcc.7b03543.

(94) Gavezzotti, A. Structure and Intermolecular Potentials in Molecular Crystals. *Model. Simul. Mater. Sci. Eng.* **2002**, *10* (3). https://doi.org/10.1088/0965-0393/10/3/201.

(95) Rychkov, D. A. A Short Review of Current Computational Concepts for High-Pressure Phase Transition Studies in Molecular Crystals. *Crystals* **2020**, *10* (2). https://doi.org/10.3390/cryst10020081.

(96) Clayden, J.; Greeves, N.; Warren, S. *Organic Chemistry*; OUP Oxford, **2012**.

(97) McMurry, J. *Organic Chemistry*, 7e ed.; Brooks/Cole: Belmont, CA SE -, **2008**. https://doi.org/LK - https://worldcat.org/title/126224144.

(98) Savir, Y.; Tiusty, T. Conformational Proofreading: The Impact of Conformational Changes on the Specificity of Molecular Recognition. *PLoS One* **2007**, *2* (5). https://doi.org/10.1371/journal.pone.0000468.

(99) Plazinski, W.; Drach, M. Kinetic Characteristics of Conformational Changes in the Hexopyranose Rings. *Carbohydr. Res.* **2015**, *416*, 41–50. https://doi.org/10.1016/j.carres.2015.08.010.

(100) Qiu, X. H.; Nazin, G. V.; Ho, W. Mechanisms of Reversible Conformational Transitions in a Single Molecule. *Phys. Rev. Lett.* **2004**, *93* (19), 1–4. https://doi.org/10.1103/PhysRevLett.93.196806.

(101) Donhauser, Z. J.; Mantooth, B. A.; Kelly, K. F.; Bumm, L. A.; Monnell, J. D.; Stapleton, J. J.; Price, J.; Rawlett, A. M.; Allara, D. L.; Tour, J. M.; et al. Conductance Switching in Single Molecules through Conformational Changes. *Science (80-.).* **2001**, *292* (5525), 2303–2307. https://doi.org/10.1126/science.1060294.

(102) Wu, Y.; Potempa, L. A.; El Kebir, D.; Filep, J. G. C-Reactive Protein and Inflammation: Conformational Changes Affect Function. *Biol. Chem.* **2015**, *396* (11), 1181–1197. https://doi.org/10.1515/hsz-2015-0149.

(103) Agilent. CrysAlisPro Software System. *Technol. UK Ltd, Yarnton, Oxford, UK* **2014**, *44* (0).

(104) Sheldrick, G. M. Crystal Structure Refinement with SHELXL. *Acta Crystallogr. Sect. C Struct. Chem.* **2015**, *71*, 3–8. https://doi.org/10.1107/S2053229614024218.

(105) Dolomanov, O. V.; Bourhis, L. J.; Gildea, R. J.; Howard, J. A. K.; Puschmann, H. OLEX2: A Complete Structure Solution, Refinement and Analysis Program. *J. Appl. Crystallogr.* **2009**, *42* (2), 339–341. https://doi.org/10.1107/S0021889808042726.

(106) Macrae, C. F.; Bruno, I. J.; Chisholm, J. A.; Edgington, P. R.; Mccabe, P.; Pidcock, E.; Rodriguez-monge, L.; Taylor, R.; Streek, J. Van De; Wood, P. A. Mercury CSD 2 . 0 – New Features for the Visualization and Investigation of Crystal Structures. *J. Appl. Cryst.* **2008**, *41*, 466–470. https://doi.org/10.1107/S0021889807067908.

(107) Piermarini, G. J.; Block, S.; Barnett, J. D.; Forman, R. A. Calibration of the Pressure Dependence of the R1 Ruby Fluorescence Line to 195 Kbar. *J. Appl. Phys.* **1975**, *46* (6), 2774–2780.

https://doi.org/10.1063/1.321957.

(108) Budzianowski, A. .; Katrusiak, A. A. High-Pressure Crystallographic Experiments with a CCD Detector. In High-Pressure Crystallography; Katrusiak, A., McMillan, P. F., Eds. *Kluwer Acad. Publ. Dordrecht, Netherlands* **2004**, 101–113. https://doi.org/10.1007/978-1-4020-2102-2_7

(109) Katrusiak, A. REDSHABS- Program for Correcting Reflections Intensities for DAC Absorption, Gasket Shadowing and Sample Crystal Absorption. *Adam Mickiewicz Univ. Poznań* **2003**.

(110) Hazen, R. M.; Finger, L. W. *Comparative Crystal Chemistry: Temperature, Pressure, Composition and the Variation of Crystal Structure*; Wiley: New York, **1982**.

(111) Katrusiak, A. High-pressure X-ray Diffraction Study on the Structure and Phase Transition of 1,3-cyclohexanedione Crystals. *Acta Crystallogr. Sect. B* **1990**, *46* (2), 246–256. https://doi.org/10.1107/S0108768189012310.

(112) Patyk, E.; Podsiadło, M.; Katrusiak, A. CH···N Bonds and Dynamics in Isostructural Pyrimidine Polymorphs. *Cryst. Growth Des.* **2015**, *15* (8), 4039–4044. https://doi.org/10.1021/acs.cgd.5b00657.

(113) Goodenough, J. B.; Kafalas, J. A. High-Pressure Study of the First-Order Phase Transition in MnAs. *Phys. Rev.* **1967**, *157* (2), 389–395. https://doi.org/10.1103/PhysRev.157.389.

(114) Lei, L.; He, D.; Zou, Y.; Zhang, W.; Wang, Z.; Jiang, M.; Du, M. Phase Transitions of LiAlO2 at High Pressure and High Temperature. *J. Solid State Chem.* **2008**, *181* (8), 1810–1815. https://doi.org/10.1016/j.jssc.2008.04.006.

(115) Guennou, M.; Bouvier, P.; Chen, G. S.; Dkhil, B.; Haumont, R.; Garbarino, G.; Kreisel, J. Multiple High-Pressure Phase Transitions in BiFeO3. *Phys. Rev. B - Condens. Matter Mater. Phys.* **2011**, *84* (17), 1–10. https://doi.org/10.1103/PhysRevB.84.174107.

(116) Rastogi, S.; Newman, M.; Keller, A. Unusual Pressure-induced Phase Behavior in Crystalline Poly-4-methyl-pentene-1. *J. Polym. Sci. Part B Polym. Phys.* **1993**, *31* (2), 125–139. https://doi.org/10.1002/polb.1993.090310202.

(117) Bouchet, J.; Bottin, F. High-Temperature and High-Pressure Phase Transitions in Uranium. *Phys. Rev. B* **2017**, *95* (5), 1–6. https://doi.org/10.1103/PhysRevB.95.054113.

Summary

Physical properties of chemical compounds are generally associated with their 'softest' parameters, such as the cohesion forces, conformations, intra- and intermolecular interactions, inversions, or tautomeric forms. However, the elastic and thermal properties of most compounds are connected to the cohesion forces and intermolecular voids. In the group of molecular crystals, where the molecules interact through relatively weak dispersion forces and hydrogen or halogen bonds, the conformational properties of molecules and intermolecular voids, which in most cases are too small to accommodate solvent molecules during the process of crystallization, are often neglected. For the group of coordination polymers (CPs) and metal-organic frameworks (MOFs) the properties are connected with the distortions of the frameworks, where the linkers are usually considered as rigid elements and their coordination bonds to the metallic centres as the hinges bending under the external stimuli. In MOFs, the crucial role is played by the voids, which can either shrink and collapse or accept guest molecules from the environment. Such sorption can result in the

counterintuitive increase of the crystal volume, due to the transport of the guest molecules and the increased molecular volume of the compounds. All these properties of molecular crystals, CPs, and MOFs can be affected by the conformational properties of molecules and linkers in CPs and MOFs, as well as by the coordination schemes. Hence, the main aim of my PhD thesis: the investigation of the contribution of the conformational and coordination-scheme transformations to the properties of molecular crystals, CPs and MOFs, under various temperature and pressure conditions.

In a series of 5 articles, we have shown how high pressure affects the structure and properties of materials that differ in pore size, type of central atom, and ligand used. The pressure-induced effects described in this work show that the use of high-pressure conditions is an extremely effective thermodynamic parameter affecting the structure of compounds and modifying their properties. Some of the most important results described within this work are summarized below.

An interesting phenomenon was observed in the molecular crystal build of 1,4-bis(pentyloxy)-2,5-bis(2-pyridineethynyl)-benzene. This study demonstrates a new perspective on the compression rate in creating the phase diagrams of solids. Under high hydrostatic pressure, depending on the speed of compression, two phases of the same crystal could be observed. During compression, the two different sets of effects were visually observed: (i) the strong monotonic compression followed by the appearance of irregular "wrinkles" on the face upon rapid compression; and (ii) a transition front traveling along the crystal plane followed by abrupt shape change upon slow compression. These initially inconsistent observations were detected for the same crystal sample on subsequent experiments.

We have also investigated a porous and polar co-crystal solvate BTCP·dItFB·Ac (BTCP= 1,2-bis[2-methyl-5-(pyridyl)-3thienyl]cyclopentene, dItFB= 1,4-diiodotetrafluorobenzene). At ambient conditions, it absorbs or releases water depending on the surrounding moisture. Under pressure, the crystal displays a strongly anisotropic compression coupled to the conformation of BTCP molecules. To our knowledge, the negative linear compressibility of over 30 TPa^{-1} is the strongest ever reported for an organic molecular crystal; similarly, we have observed that BTCP·dItFB·Ac displays an impressive positive linear compression of about 90 TPa^{-1}.

Flexible and transformable molecules, particularly those responding to external stimuli, are needed for designing sensors and porous compounds capable of storing or separating gases and liquids. We have established that crystals of the porous metal-organic framework, referred as DMOF, exhibits interesting mechanochemical behaviour when compressed in non-penetrating and penetrating pressure transmitting media (PTM). Under

high pressure, DMOF is sensitive to the type of PTM used: large PTM molecules can not be absorbed into the pores, so DMOF is compressed as a closed system, which leads to the negative linear compressibility (NLC) in the direction of axis *y*. Under compression in penetrating liquid, small PTM molecules are pushed into the pores, thus changing the stoichiometry of DMOF, which strongly increase the dimensions of DMOF in the directions perpendicular to that of the NLC of the crystal, when compressed in non-penetrating PTM (both these analogous host and inclusion compounds are described in the same reference crystal axes). Owing to the strong and inverse elastic responses, DMOF can be considered as a molecular sensor capable of detecting molecules of different sizes in its compressed environment.

We have also synthesized and investigated a porous MOF, capable of self-repairing its single crystal after high pressure damage. The compression is compensated by tilts and conformational changes of the linkers, leading to ferroelastic transition to the high-pressure phase β. Further compression leads to clearly visible scratches and fractures, along the domain boundaries. When the pressure is released, the traces of damage disappear after each of the repeated cycles of increased and decreased pressure. In addition to the self-healing property, the material showed high sensitivity to the compression conditions. The observed effects depend on both the guest molecules fulfilling the voids and the hydrostatic fluid. This sensitivity to the type of guest molecules and to the crystal environment can be applied in sensors.

The pressure-induced changes in the structure of compounds and related chemical reactions in coordination polymers can be predicted using three rules. The first is related to the change in the ratio of radii of metal cations and ligands, with increasing pressure, leading to an increased coordination number. The ligands around the central atom should be elastic, to modify or change their conformation. Also the close location of the potential new ligand to the coordination centre is necessary for such transformations.

In conclusion, there are many factors, such as the coordination scheme, topology of connections, the size and shape of voids, the chemical character of linkers, their capability to form intermolecular interactions, the type of pressure-transmitting medium (PTM), or the speed of compression, which have an impact on pressure-induced transformations of crystals. The compression of such a crystalline compound can proceed as a one-component or multi-component system, within the pressure ranges of monotonic changes and through phase transitions. In the one-component structure, high pressure reduces the void spaces and distances between molecules. The compressed volume increases the energy of interactions and thermal collisions, which, for specific components can trigger a chemical reaction. On the other hand, the compression of porous crystals in small-molecule liquids can cause a significantly different response compared to the compression in oils and large-molecule PTMs.

Apart from the molecular size, also other properties of the PTMs, such as their density, viscosity, and their freezing pressure can promote or prohibit the formation of new polymer–PTM interactions. A variety of possible structural responses of materials to external stimuli often leads to strongly anisotropic and anomalous effects, such as negative linear and area compressibility, phase transitions, amorphization, guest inclusions, and even topochemical reactions.

Streszczenie

Właściwości fizyczne związków chemicznych są zwykle związane z ich podstawowymi parametrami, takimi jak siły spójności, konformacje, oddziaływania międzycząsteczkowe, inwersje czy formy tautomeryczne. Elastyczność i właściwości termiczne większości związków są determinowane przez siły spójności i wielkość luk. W grupie kryształów molekularnych, gdzie cząsteczki oddziałują poprzez stosunkowo słabe siły dyspersyjne i wiązania wodorowe lub halogenowe, właściwości konformacyjne cząsteczek i luk, które w większości przypadków są zbyt małe, aby pomieścić cząsteczki rozpuszczalnika podczas procesu krystalizacji, są często zaniedbywane. W przypadku grupy polimerów koordynacyjnych (CP) i sieci metaloorganicznych (MOF) właściwości te są związane z odkształceniami struktur, w których ligandy są zwykle uważane za elementy sztywne, a ich wiązania koordynacyjne z centrami metalicznymi za przeguby zginające się pod wpływem bodźców zewnętrznych. W MOF-ach kluczową rolę odgrywają puste przestrzenie – pory, które mogą albo kurczyć się i zapadać, albo przyjmować cząsteczki gości z otoczenia. Taka sorpcja może skutkować sprzecznym z intuicją wzrostem objętości kryształu, ze względu na transport cząsteczek gości i zwiększoną objętość molekularną związków. Na wszystkie te właściwości kryształów molekularnych, CP i MOF mogą wpływać właściwości konformacyjne cząsteczek i ligandów w CP i MOF, a także schematy koordynacji. Stąd główny cel mojej pracy doktorskiej: zbadanie wpływu przemian konformacyjnych na właściwości kryształów molekularnych, CP i MOF, w różnych warunkach temperatury i ciśnienia.

W serii 5 artykułów pokazaliśmy, jak wysokie ciśnienie wpływa na strukturę i właściwości materiałów różniących się wielkością porów, rodzajem atomu centralnego i zastosowanym ligandem. Efekty wywołane ciśnieniem opisane w tej pracy pokazują, że zastosowanie warunków wysokiego ciśnienia jest niezwykle skutecznym parametrem termodynamicznym wpływającym na strukturę związków i modyfikującym ich właściwości. Poniżej podsumowano niektóre z najważniejszych wyników opisanych w tej pracy.

Interesujące zjawisko zaobserwowano w krysztale molekularnym zbudowanym z 1,4-bis(pentyloksy)-2,5-bis(2-pirydynoetynylo)-benzenu. Badanie to udowadnia wpływ szybkości kompresji na tworzenie diagramów fazowych ciał stałych. Pod wysokim ciśnieniem hydrostatycznym, w zależności od prędkości ściskania, można zaobserwować dwie fazy tego

samego kryształu. Podczas ściskania zaobserwowano dwa różne zestawy efektów: (i) silne monotoniczne ściskanie, po którym następowało pojawienie się nieregularnych "zmarszczek" na powierzchni przy szybkim ściskaniu; oraz (ii) przemieszczający się wzdłuż płaszczyzny kryształu front przejściowy, po którym następowała gwałtowna zmiana kształtu przy powolnym ściskaniu. Te początkowo niespójne obserwacje zostały uchwycone dla tej samej próbki kryształu w jednej serii eksperymentów.

Zbadaliśmy również porowaty i polarny solwat kokryształu BTCP·dItFB·Ac (BTCP= 1,2-bis[2-metylo-5-(pirydylo)-3-tienylo]cyklopenten, dItFB= 1,4-dijodotetrafluorobenzen). W warunkach otoczenia absorbuje lub uwalnia wodę w zależności od otaczającej wilgoci. Pod ciśnieniem kryształ wykazuje silnie anizotropową kompresję powiązaną z konformacją cząsteczek BTCP. Zgodnie z naszą wiedzą, ujemna ściśliwość liniowa wynosząca ponad 30 TPa^{-1} jest najsilniejszą, jaką kiedykolwiek odnotowano dla organicznego kryształu molekularnego; podobnie zaobserwowaliśmy, że BTCP·dItFB·Ac wykazuje imponującą dodatnią ściśliwość liniową wynoszącą około 90 TPa^{-1}.

Elastyczne i zdolne do przekształceń cząsteczki, szczególnie te reagujące na bodźce zewnętrzne, są potrzebne do projektowania czujników i porowatych związków zdolnych do przechowywania lub oddzielania gazów i cieczy. Ustaliliśmy, że kryształy porowatego szkieletu metaloorganicznego, określanego jako DMOF, wykazują interesujące zachowanie mechanochemiczne, gdy są ściskane w niepenetrujących i penetrujących mediach przenoszących ciśnienie (PTM). Pod wysokim ciśnieniem DMOF jest wrażliwy na rodzaj zastosowanego PTM: duże cząsteczki PTM nie mogą zostać wchłonięte przez pory, więc DMOF jest ściskany jako układ zamknięty, co prowadzi do ujemnej ściśliwości liniowej (NLC) w kierunku osi *y*. Podczas ściskania w penetrującej cieczy, małe cząsteczki PTM są wpychane do porów, zmieniając w ten sposób stechiometrię DMOF, co silnie zwiększa wymiary DMOF w kierunku prostopadłym do NLC kryształu, podczas ściskania w niepenetrującym PTM (oba te analogiczne związki gospodarza i związki inkluzyjne są opisane w tych samych referencyjnych osiach kryształu). Dzięki silnym i odwrotnym odpowiedziom elastycznym, DMOF można uznać za czujnik molekularny zdolny do wykrywania cząsteczek o różnych rozmiarach w jego środowisku.

Zsyntetyzowaliśmy również i zbadaliśmy porowaty MOF, zdolny do samonaprawy swojego monokryształu po uszkodzeniu wywołanym wysokim ciśnieniem. Ściskanie jest kompensowane przez przechylenia i zmiany konformacyjne ligandów, co prowadzi do ferroelastycznego przejścia do wysokociśnieniowej fazy β. Dalsza kompresja prowadzi do wyraźnie widocznych rys i pęknięć wzdłuż granic domen. Po odpuszczeniu ciśnienia ślady uszkodzeń znikają, po każdym z powtarzających się cykli zwiększania i zmniejszania ciśnienia. Oprócz właściwości samoregeneracji, materiał wykazał wysoką wrażliwość na warunki kompresji. Obserwowane efekty zależą zarówno od cząsteczek gości wypełniających puste

przestrzenie, jak i od zastosowanej cieczy hydrostatycznej. Ta wrażliwość na rodzaj cząsteczek gościa i środowisko kryształu może być zastosowana w czujnikach.

Wywołane ciśnieniem zmiany w strukturze związków i związane z nimi reakcje chemiczne w polimerach koordynacyjnych można przewidzieć za pomocą trzech reguł. Pierwsza z nich związana jest ze zmianą stosunku promieni kationów metali i ligandów wraz ze wzrostem ciśnienia, co prowadzi do zwiększenia liczby koordynacyjnej. Ligandy wokół atomu centralnego powinny być elastyczne, aby modyfikować lub zmieniać swoją konformację. Niezbędna do zajścia takich transformacji jest również bliskość potencjalnego nowego liganda do centrum koordynacyjnego.

Podsumowując, istnieje wiele czynników, takich jak schemat koordynacji, topologia połączeń, rozmiar i kształt luk, charakter chemiczny ligandów, ich zdolność do tworzenia oddziaływań międzycząsteczkowych, rodzaj medium przenoszącego ciśnienie (PTM) lub szybkość kompresji, które mają wpływ na indukowane ciśnieniem transformacje kryształów. Kompresja takiego związku krystalicznego może przebiegać jako układ jedno- lub wieloskładnikowy, w zakresach zmian monotonicznych i poprzez przejścia fazowe. W strukturze jednoskładnikowej wysokie ciśnienie zmniejsza puste przestrzenie i odległości między cząsteczkami. Poprzez zmniejszoną objętość zwiększa się energia oddziaływań i zderzeń termicznych, co w przypadku określonych warunków może wywołać reakcję chemiczną. Z drugiej strony, ściskanie porowatych kryształów w cieczach o małych cząsteczkach może powodować znacznie inny efekt w porównaniu do ściskania w olejach i PTM o dużych cząsteczkach. Oprócz wielkości cząsteczek, również inne właściwości PTM, takie jak ich gęstość, lepkość i ciśnienie zamarzania, mogą promować lub uniemożliwiać tworzenie nowych interakcji polimer-PTM. Różnorodność możliwych reakcji materiałów strukturalnych na bodźce zewnętrzne często prowadzi do silnie anizotropowych i anomalnych efektów, takich jak ujemna ściśliwość liniowa i powierzchniowa, przejścia fazowe, amorfizacja, inkluzje gości, a nawet reakcje topochemiczne.

Appendices

A1

Dynamic Resolution of Piezosensitivity in Single Crystals of π-Conjugated Molecules

S. Bhattacharyya*, S. Sobczak*, **A. Półrolniczak***, S. Roy, D. Samanta, A. Katrusiak, T. K.Maji.

Chemistry–A European Journal 25 (24), 6092-6097, **2019.**

ChemPubSoc Europe

DOI: 10.1002/chem.201900054

CHEMISTRY A European Journal Communication

High-Pressure Chemistry

Dynamic Resolution of Piezosensitivity in Single Crystals of π-Conjugated Molecules

Sohini Bhattacharyya[+],[a] Szymon Sobczak[+],[b] Aleksandra Półrolniczak[+],[b] Syamantak Roy,[a] Debabrata Samanta,[a] Andrzej Katrusiak,*[b] and Tapas Kumar Maji*[a]

Abstract: Targeted synthesis of piezoresponsive small molecules and in-depth understanding of their mechanism is of utmost importance for the development of smart devices. This work reports the synthesis, structure and piezosensitivity of a bola-amphiphile 1,4-bis(pentyloxy)-2,5-bis(2-pyridineethynyl)-benzene (**C5-PPB**). Depending on the rate of compression, two different phases in **C5-PPB** can be generated. The ambient-pressure α-phase is stable up to 0.8 GPa, beyond which it undergoes an isostructural transformation to β-phase, accompanied by a clearly visible elongation of the crystal. This α-to-β phase transition requires the sample to be compressed slowly. When quickly compressed, phase α persists to about 1.5 GPa, beyond which its amorphization starts, accompanied by the appearance of irregular grooves on the largest faces. Mechanical pressure also affects the optical property of **C5-PPB**, which shows reversible mechanochromism with a green to cyan transformation in the emission, associated with a 15 nm shift in the maxima. The conductivity of **C5-PPB** as a direct outcome of its crystal packing has also been studied.

Development of purely organic π-conjugated oligomers that are light, flexible and external-stimuli responsive is highly desirable for multifarious applications in smart devices.[1] Molecules that are capable of responding to external mechanical forces[2] are sought after for human–machine or robotic interfaces, sensors, security inks, memory storage, and healthcare devices.[3] In condensed forms like crystals, liquid crystals, or micelles, the piezosensitivity of a particular material depends extensively on its intermolecular interactions and packing, governed by H-bonding, π–π, C–H···π, or dipole–dipole interactions.[4] When these interactions undergo alterations under mechanical perturbation, the emission spectrum or intensity may vary, which is regarded as mechanochromism or piezochromism and finds numerous practical applications.[5] However, the innate complexities of intermolecular forces and structure factors render piezosensitivity of such systems unpredictable and their rational design and synthesis still remains a major challenge.[3,6] In many cases, piezochromic molecules have appeared as isolated serendipitous occurrences where the change in luminescence is irreversible and achieving reversibility requires a subtle balance between different supramolecular interactions.[7] The in-depth understanding of the mechanism of piezosensitivity requires its correlation with the structural changes occurring under pressure,[8] which can be characterized by studying the single-crystal structure under hydrostatic compression. In this context, π-conjugated polymeric systems, such as *oligo*-(p-phenylenevinylene) (OPV) and *oligo*-(p-phenyleneethynylene) (OPE) derivatives[9] are ideal candidates. Such molecules, comprising a rigid conjugated backbone along with tunable side chains and functionalizable end terminals, offer the perfect combination of weak and strong forces to create a stimuli-responsive supramolecular architecture.[10] The rigid π-conjugated backbone gives rise to charge migration,[11] intense luminescence,[12] and may also lead to the formation of conformational polymorphs through rotational freedom around the single bonds connecting the conjugated units.[13] The interference with the crystal packing caused by such molecular movement forms the basis of stimuli-responsive luminescent materials.[14] Similar systems synthesized by us previously have shown a host of exciting stimuli-responsive properties like liquid crystallinity, mechanochromism, and photoconductivity as a direct outcome of their structures.[13] We predicted that a π-conjugated system without any strong directional H-bonding may manifest interesting piezosensitivity owing to a synergistic effect between the various weak van der Waals forces. In this work, we report the synthesis, structure and characterization of such a bola-amphiphile 1,4-bis(pentyloxy)-2,5-bis(2-pyridineethynyl)benzene (**C5-PPB**), which has been designed with polar pyridine terminals and non-polar alkyl chains, thus creating an interplay of weak interactions in the supramolecular assembly (Scheme 1). We have performed in-depth analysis of the compression rate-dependent polymorphism under hydrostatic pressure and reversible mechanochromism upon grinding in **C5-PPB.**

[a] *S. Bhattacharyya,[+] Dr. S. Roy, Dr. D. Samanta, Prof. Dr. T. K. Maji*
Chemistry and Physics of Materials Unit
School of Advanced Materials (SAMat)
Jawaharlal Nehru Centre for Advanced Scientific Research
Bangalore 560064 (India)
E-mail: tmaji@jncasr.ac.in
Homepage: www.jncasr.ac.in/tmaji/

[b] *S. Sobczak,[+] A. Półrolniczak,[+] Prof. A. Katrusiak*
Faculty of Chemistry, Adam Mickiewicz University
Umultowska 89b, 61-614 Poznań (Poland)
E-mail: katran@amu.edu.pl
Homepage: hpc.amu.edu.pl

[+] *These authors contributed equally to this work.*

Supporting information and the ORCID identification number(s) for the author(s) of this article can be found under: https://doi.org/10.1002/chem.201900054.

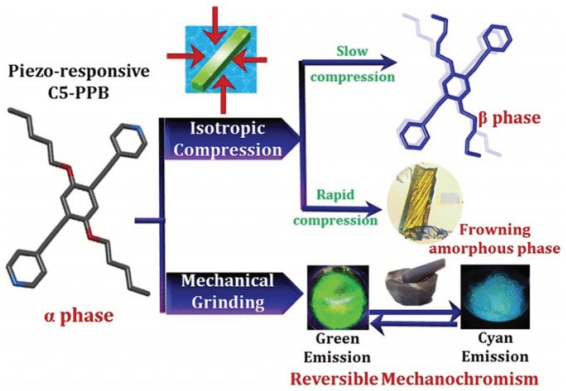

Scheme 1. Schematic representation of the piezo-response in **C5-PPB**.

C5-PPB has been synthesized by a multistep synthesis involving Sonogashira–Hagihara C–C coupling reaction from 1,4-diethynyl-2,5-bis(pentyloxy)benzene.[24] The pure bulk of **C5-PPB**, obtained after meticulous purification, was crystallized by slow evaporation of ethanol from its concentrated solution. Single-crystal X-ray diffraction (SCXRD) of the needle-like **C5-PPB** crystal (Figure 1 a) revealed that it crystallizes in triclinic

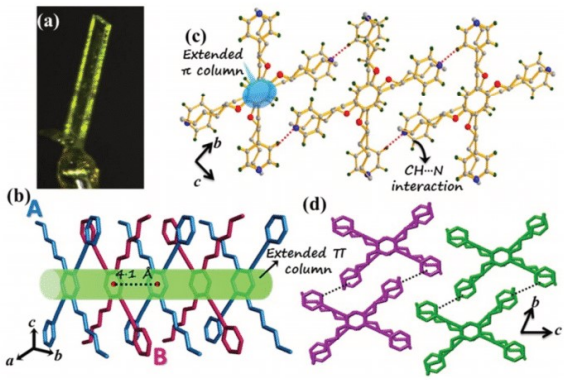

Figure 1. (a) Photograph of a single crystal of **C5-PPB**. (b) Consecutive molecules of **C5-PPB** arranged in ABA fashion in the *a* direction forming extended π-column. (c) 2D sheets formed by C–H···N bonding between two adjacent π-columns of **C5-PPB**. (d) Two different 2D sheets demarcated by purple and green colors interact through weak van der Waals forces.

$P\bar{1}$ space group, with two independent molecules located on inversion centers (hence Z = 2, and two halves of symmetry-independent molecules are present) arranged in a staggered fashion. The terminal pyridines are twisted at a dihedral angle of 12° with respect to the central phenyl ring. This ambient phase is regarded as the α-phase. In the crystal structure of phase α, the OPE back bone of one molecule overlaps with the alkyl chain of another along the crystallographic *a* direction. Further, in the *a* direction, the central phenyl rings of adjacent molecules interact via a weak parallel offset π–π stacking interaction with a distance of 4.1 Å.[4d,e] Thus, the molecules arranged in an ABA fashion form 1D chain with an extended π-column (Figure 1 b).[24] Along the crystallographic *b* direction, two such 1D chains communicate via C–H···N (C···N distance is 3.545 Å; ∠C–H···N angle is 156.5°) interaction between the N-atom of one molecule and the pyridinic β-H of its adjacent one to form a 2D network along the *ab* plane (Figure 1 c). These 2D arrays interact with each other by weak van der Waals forces along the crystallographic *a* direction (Figure 1 d). In addition, multiple C–H···π interactions also exist between the terminal phenyl rings and the alkyl C–H bonds of two adjacent molecules (C–H···π distances are between 2.861–2.967 Å; ∠C–H···π angles are in the range of 148.08–159.7°).[4f,24]

We envisaged such a system to be piezosensitive owing to the absence of any rigid directional interactions between the individual molecules and investigated the crystals under a high hydrostatic pressure in a diamond anvil cell (DAC).[14] A single crystal of **C5-PPB** was compressed both rapidly and slowly in the DAC and was observed to undergo drastic visible changes, which were also monitored by SCXRD. During compression, the following two different sets of effects were visually observed: (i) strong monotonic compression followed by the appearance of irregular "wrinkles" on the crystal face; (ii) a transition front traveling along the crystal plane, followed by an abrupt shape change. These observations initially seemed to be inconsistent, but were detected for the same crystal sample even on subsequent experiments. The compression of phase α is monotonic up to 0.9 GPa (Figure 2 b). When the crystal is compressed rapidly from 0.8 to about 1.2 GPa, phase α is retained, and a visible monotonic compression of the crystal is observed. When such a crystal is further compressed slowly, it still resides in phase α. However, when compressed to about 1.5 GPa, irregular "wrinkles" appear on the faces of the crystal, marking its amorphization (Figure 2). If phase α is compressed beyond 0.8 GPa very slowly, a drastic discontinuous phase transition occurs at 0.9 GPa,[24] associated with a large negative-linear strain, visibly elongating the crystals in one direction and contracting them in another, forming phase β (Figure 2 and Movie S1 in the Supporting Information).[24] This α-to-β transition does not change the crystal symmetry nor Wyckoff sites, so this can be identified as an isostructural phase transition. The single crystal integrity is often another characteristic of isostructural transitions.[15a] In this case, the isostructural transition between ambient phase α and high-pressure phase β is accompanied by a volume drop of 7% and strong conformational changes of two independent molecules, while the crystal symmetry of triclinic space group $P\bar{1}$ ($Z=2$) is retained. At the transition, the unit-cell parameter *a* abruptly expands by 20%, *b* shrinks by ~20%, and *c* by ~10%.[24] Characteristically, isostructural phase transitions are discontinuous (of the 1st order according to Ehrenfest's classification) and are associated with a volume drop in compressed crystals along with a hysteresis.[15] These general features are consistent with our observations of the sharp transition between phases α and β. The process of amorphization is generally diffused[16] and accordingly, the amorphization of phase α proceeds over the range of pressure from about 1.35 to 1.95 GPa at room temperature (Fig-

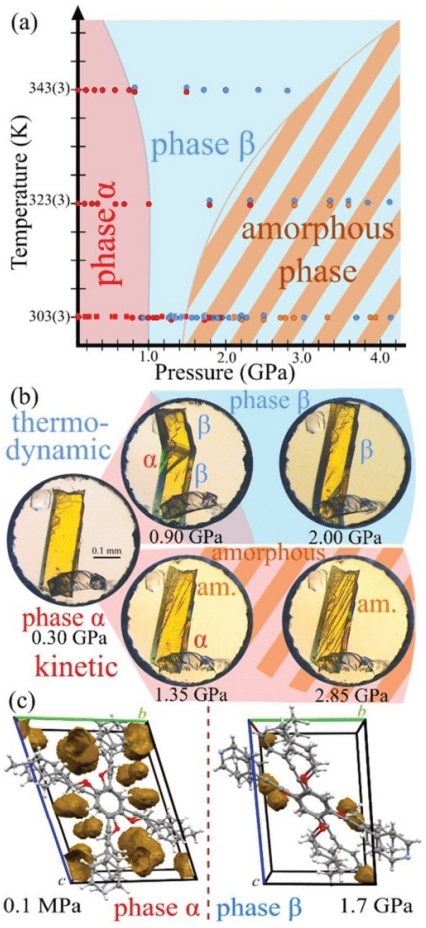

Figure 2. (a) Phase diagram of **C5-PPB**, based on the sample compressed in three different temperatures. Blue and pink colors mark phase stability regions and the orange stripes trace amorphous region for over-compressed phase α. Squares indicate points of the X-ray diffraction measurements and circles mark visual observations of the crystal shape. (b) The sample **C5-PPB** single crystal (left) first compressed rapidly (bottom) to 1.5 GPa, when the wrinkles mark the onset of amorphization, and then after releasing the pressure it was (top) compressed again slowly to 0.9 GPa, where the transition to phase β starts and transition fronts travel through the sample, transition fronts travel up and down through the sample, until it completes the transformation (top right). (c) Projections of **C5-PPB** molecules and voids (accommodating the probing sphere 0.8 Å in radius) in phases α and β along [100].

ure 2a). At higher temperature the amorphization range is shifted toward higher pressure, opposite to the boundary between phases α and β. The π–π interaction between the central phenyl rings in two adjacent molecules disappears as the distance between them increases from 4.1 Å in α-phase at ambient pressure to 4.9 Å at 1.7 GPa. Moreover, the molecular arrangements also vary drastically.[24] At 1.51 GPa, the distance between the central aromatic rings of neighboring molecules in phase α is reduced by 0.275 Å in phase β, along with the elongation of the two *n*-pentoxy chains, which explains the strong abrupt elongation of the crystal along direction *a* (Figure S7). In phase β the Wyckoff positions of molecules and their arrangement are retained; however, the conformation of independent molecules changes significantly (Figures 1 and Figure 2c). The torsion angles of pentyloxy chains change up to ≈160° (Figure S9), the terminal pyridines with respect to the central benzene rings rotate only slightly, but the rigid ethynyl bridge bends in the β phase and the curvature increases with the increasing pressure. Thus two different transformations of the **C5-PPB** crystal can be described as: (i) the kinetic compression leading to "frowning" amorphous phase; and (ii) the thermodynamic compression, leading to phase β, which is stable till at least 4.0 GPa. However, the β phase can be circumvented, by compressing the crystal starting from 0.8 GPa quickly, at an estimated rate higher than 0.1 GPa s^{-1}. The crystal rippling marks the start of gradual amorphization. At about 1.9 GPa the sample faces "frown" with approximately parallel "wrinkles", marking the collapsed regions in the sample (Figure 2b) and at this pressure no Bragg reflections can be detected, indicating the full amorphization.

We established that, at increased temperature, the critical pressure of the α-to-β transition is slightly decreased, but that of amorphization is somewhat increased, as mapped in the phase diagram with superimposed effects of both kinetic and thermodynamic compression (Figure 2a). At ambient conditions the crystal structure contains large voids (Figure 2c). They are too small to accommodate guest molecules, but are essential for inherent crystal properties, as evident from the β phase, where the molecules alter their conformation to fill up the void space (Figure 2c). It appears that such drastic conformational changes correlated between neighboring molecules require time, and upon fast compression, the conformers of phase α are "frozen" by rapidly increasing intermolecular interactions.

Hence, the quick compression of phase α eventually leads to random collapse of molecular stacks and subsequently to crystal amorphization. The macroscopic effect of the wrinkles on the crystal faces is a direct effect of the molecular stacks collapsing in groups in different directions, like bookshelves falling randomly in a library. In literature, there are numerous examples of the kinetic effects of the compression of liquids and crystals, as well as examples of so-called flash cooling.[17] However, **C5-PPB** is different because its kinetic path leads to crystal amorphization connected with a massive collapse of the voids in the crystal structure. Hence, it can amorphize when phase α is over-pressurized quickly, which is manifested by the "wrinkling" of the sample faces. These macroscopically visible distortions of the crystal shape distinguish **C5-PPB** from regular crystalline phase transitions that show parallel lines running exactly along the crystallographic planes on the faces of the sample.[18] The significantly irregular "wrinkling" is aligned along one direction on the sample, which resembles a corrugated foil. The direction of "wrinkles" is determined by initial structural collapse and the corrugation of the structure (Figure 2 and Movie S1 in the Supporting Information). However, the "wrinkles" are irregular in direction and depth and their direction changes occur monotonically without sharp turns (characteristic for crystals). It can be noted that in the crystal

undergoing the amorphization, a subtle pattern of lines appear in the largest crystal face (see the photograph at 1.35 GPa in Figure 2b). It is therefore plausible that a subtle isostructural phase transition precedes the amorphization.[19] The strong macroscopic effects in **C5-PPB** are spectacular for both the slow and fast modes of compression and additionally for the spectroscopic reasons. In these respects the strong transformations of **C5-PPB** can be listed among other macroscopic phenomena observed in crystals (although their structural background can be very different), like color changes,[5d–i] crystal jumping,[20] bending,[21] twisting,[22] etc.[23]

Upon observing the piezosensitivity of **C5-PPB** single crystals, we were interested in observing the optical response of the compound to small anisotropic pressures for practical application. OPE systems are well known for their luminescent behavior,[1a] and **C5-PPB** is no different. Molecularly dissolved methanolic solution of **C5-PPB** shows two peaks in the absorption spectrum with λ_{max} at 310 and 375 nm.[24] It shows a wide emission band, ranging from 400 to 550 nm, with a maximum at 442 nm (Figure S3b) However, in the solid state, **C5-PPB** molecules remain in the aggregated state, showing a redshifted wide absorption band with a typical vibronic feature from 350 nm (Figure S3c) and emission maximum at 507 nm (ex 350 nm). Mechanical grinding of the single crystals of **C5-PPB** with a mortar and pestle for ≈30 min changes the emission from fluorescent green to cyan (Figure 3a). This corresponds to a ≈15 nm blueshift in the emission maximum and λ_{max} shifts to 492 nm (Figure 3b). This blue-shifted emission can be attributed to the breaking of weak supramolecular forces in the dense crystal state of **C5-PPB**. As a rare instance of reversible mechanochromism, the grounded sample, on being left undisturbed for ≈8 h, reverts its emission to its original green spectrum, which is reflected by its emission spectrum overlapping with that of the single crystalline form. The weak supramolecular interactions reorient and re-establish themselves over time, thereby reverting to the original green emission. This is also reinforced by the distinctly different powder X-ray diffraction (PXRD) patterns of **C5-PPB** before and after grinding, implying structural reorganization (Figure 3c). Indexing the peaks reveal that the first peak at $2\theta = 6^\circ$ corresponding to (001) plane, shifts to $2\theta = 5.7^\circ$ after grinding. The (001) plane is the molecular *ab* plane that lies in between the 2D networks formed by CH···N interaction between the π-columns. The appearance of this peak at a lower angle implies an increase in the distance between the 2D networks in the *c* direction. The peak at $2\theta = 9^\circ$ corresponding to (011) plane is significantly diminished after grinding. The (011) plane contains the extended π-column of the structure and significant decrease in the intensity of its corresponding peaks indicates an increase in the distance between the π-stacked molecules.[24] The PXRD collected after 24 h of grinding is almost the same as the pristine compound.

To get a deeper insight into the structural changes associated with the mechanochromic behavior, time-dependent density functional theory (TD-DFT) computations were performed at CAM-B3LYP/6–31+G* level, on three different model systems (models 1–3, Figure S6), which account for the weak π–π and CH···N interactions. Model 1 illustrates a single molecule, model 2 shows a π-stacked dimer, and model 3 considers CH···N interactions. Notably, model 1 showed absorption maximum at 342 nm ($f = 1.2$, HOMO→LUMO), which shows an 8 nm blueshift from the absorption maximum of model 2 ($\lambda_{max} = 350$ nm, $f = 0.69$, HOMO→LUMO+1) (Figures S5 and S6). In contrast, model 1 shows a 4 nm redshift in the absorption maximum from model 3 ($\lambda_{max} = 338$ nm, $f = 1.2$, HOMO→LUMO). Experimentally, we observed a slight blueshift in excitation spectra post grinding, which is a clear indication of the breaking of π–π stacking. Utilizing the above transitions, emission wavelengths were calculated to be 389 nm and 397 nm, for model 1 and 2, respectively, implying an 8 nm blueshift

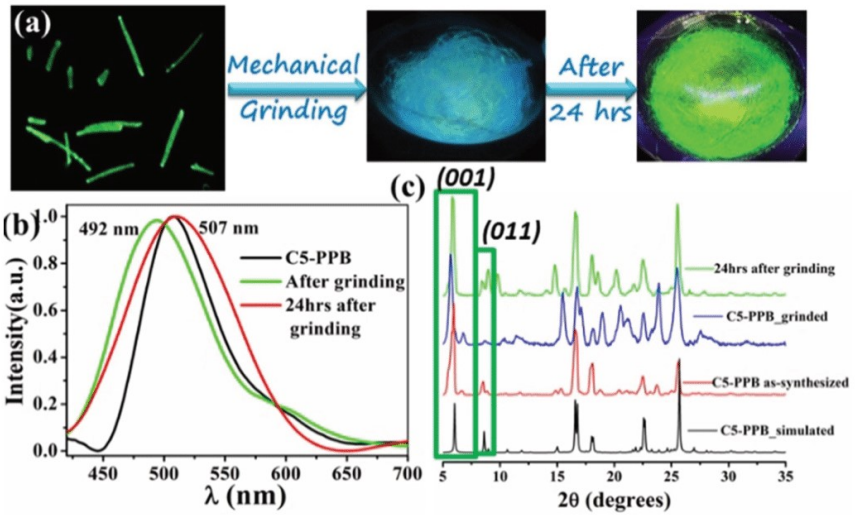

Figure 3. (a) Photographs of the **C5-PPB** sample under a UV lamp before and after grinding. (b) Emission spectra of **C5-PPB** before and after grinding. (c) PXRD patterns of **C5-PPB** before and after grinding.

upon complete removal of π–π stacking, which is in agreement with experimental findings. We have also observed in the SCXRD structure obtained at 1.7 GPa that the distance between the central phenyl rings of two adjacent molecules increases to almost ≈4.9 Å, thereby diminishing the π–π interaction. Thus, in the case of both mechanical anisotropic and high isotropic pressure, the π–π interaction is disrupted.

For use in practical applications, apart from piezosensitivity, inherent conductivity is also an important property. The conductivity of **C5-PPB** was measured across the needle-shaped single crystal both in the longitudinal as well as the lateral directions. The measured conductivity in the longitudinal direction is 1.75×10^{-7} S cm^{-1}, whereas that in the lateral direction is 3.31×10^{-9} S cm^{-1} (Figure S10ab). This stark difference can be explained simply by looking into the structure, where the (100) and (−100) faces confine the crystal at the ends along its long direction, whereas faces (001) and (011) are parallel to this longest crystal dimension along direction [100]. From the SCXRD analysis, along the (100) plane, the parallel displaced π–π stacking is present and hence along the longitudinal direction, facile through space charge transfer yields a high value of conductivity. However, along the width or thickness either the weak CH···N interaction or weak van der Waals interaction is present, (Figure S10cd), which is ineffective for conductivity.

In conclusion, **C5-PPB** is an intriguing molecular system with an interesting supramolecular architecture, which shows unusual compression-rate-dependent piezosensitive behavior. The two different phenomena upon compressing the crystal are, first, the kinetic transformation of the crystal into the amorphous phase upon rapid compression and, second, the thermodynamic transformation of the crystal into an isostructural phase upon slow compression. Such in-depth study on the structural changes occurring in a piezoresponsive organic molecule is rare. Reversible mechanochromism coupled with conductivity in this piezosensitive molecule makes it a potential candidate for applications in smart devices. Proper integration of this molecule in devices could offer a range of possibilities, which we are currently investigating in our lab.

CCDC 1871836, 1869429, 1869438, and 1894690 contain the supplementary crystallographic data for this paper. These data are provided free of charge by The Cambridge Crystallographic Data Centre.

Acknowledgements

The authors are grateful to Mr. Saurav Islam for help with conductivity studies. S.B. acknowledges INSPIRE fellowship, DST, Govt. of India for Fellowship. T.K.M. is grateful to the Department of Science and Technology (DST, Project No. MR-2015/001019 and Project No.TRC-DST/C.14.10/16-2724, JNCASR), Govt. of India and JNCASR for financial support. S.B. and T.K.M. are grateful to Sheikh Saqr Laboratory, JNCASR for SCXRD facility. S.S., A.P., and A.K. are grateful to the Polish National Science Centre (grant OPUS 10 No. UMO-2015/19/B/ST5/00262), S.S. to grant POWR.03.02.00-00-I023/17 and A.P. to grant POWR.03.02.00-00-I026/16 co-financed by the EU European Social Fund under the Operational Program Knowledge Education Development.

Conflict of interest

The authors declare no conflict of interest.

Keywords: bola-amphiphile · chromophores · high-pressure chemistry · piezosensitive · reversible mechanochromism

[1] a) R. Thomas, S. Varghese, G. U. Kulkarni, *J. Mater. Chem.* **2009**, *19*, 4401 – 4406; b) A. R. Ramesh, K. G. Thomas, *Chem. Commun.* **2010**, *46*, 3457 – 3459; c) H.-Y. He, Y.-L. Zhou, Y. Hong, L.-G. Zhu, *J. Mol. Struct.* **2005**, *737*, 97 – 101.

[2] a) X. Yan, F. Wang, B. Zheng, F. Huang, *Chem. Soc. Rev.* **2012**, *41*, 6042 – 6065; b) V. S. Minkov, S. V. Goryainov, E. V. Boldyreva, C. H. Görbitz, *J. Raman Spectrosc.* **2010**, *41*, 1748 – 1758; c) S. A. Moggach, C. H. Görbitz, J. E. Warren, *CrystEngComm* **2010**, *12*, 2322; d) M. Pravica, B. Yulga, S. Tkachev, Z. Liu, *J. Phys. Chem. A* **2009**, *113*, 9133 – 9137; e) Y. Wang, Z. Zhou, T. Wen, Y. Zhou, N. Li, F. Han, Y. Xiao, P. Chow, J. Sun, M. Pravica, A. L. Cornelius, W. Yang, Y. Zhao, *J. Am. Chem. Soc.* **2016**, *138*, 15751 – 15757.

[3] V. Lebedev, E. Laukhina, E. Moreno-Calvo, C. Rovira, V. Laukhin, I. Ivanov, S. M. Dolotov, V. F. Traven, V. V. Chernyshev, J. Veciana, *J. Mater. Chem. C* **2014**, *2*, 139 – 146.

[4] a) C. Gu, N. Huang, Y. Chen, L. Qin, H. Xu, S. Zhang, F. Li, Y. Ma, D. Jiang, *Angew. Chem. Int. Ed.* **2015**, *54*, 13594 – 13598; *Angew. Chem.* **2015**, *127*, 13798 – 13802; b) J. Wu, Y. Cheng, J. Lan, D. Wu, S. Qian, L. Yan, Z. He, X. Li, K. Wang, B. Zou, J. You, *J. Am. Chem. Soc.* **2016**, *138*, 12803 – 12812; c) Y. Guan, M. L. Jones, A. E. Miller, S. E. Wheeler, *Phys. Chem. Chem. Phys.* **2017**, *19*, 18186 – 18193; d) C. R. Martinez, B. L. Iverson, *Chem. Sci.* **2012**, *3*, 2191 – 2201; e) M. Nishio, Y. Umezawa, J. Fantini, M. S. Weissd, P. Chakrabarti, *Phys. Chem. Chem. Phys.* **2014**, *16*, 12648 – 12683; f) M. Nishio, *CrystEngComm* **2004**, *6*, 130 – 158.

[5] a) S. Yagai, T. Seki, H. Aonuma, K. Kawaguchi, T. Karatsu, T. Okura, A. Sakon, H. Uekusa, H. Ito, *Chem. Mater.* **2016**, *28*, 234 – 241; b) P. Xue, J. Ding, P. Wang, R. Lu, *J. Mater. Chem. C* **2016**, *4*, 6688 – 6706; c) C. Feng, K. Wang, Y. Xu, L. Liu, B. Zou, P. Lu, *Chem. Commun.* **2016**, *52*, 3836 – 3839; d) A. Jaffe, Y. Lin, W. L. Mao, H. I. Karunadasa, *J. Am. Chem. Soc.* **2015**, *137*, 1673 – 1678; e) L. Wang, K. Wang, B. Zou, *J. Phys. Chem. Lett.* **2016**, *7*, 2556 – 2562; f) S. Gupta, T. Pandey, A. K. Singh, *Inorg. Chem.* **2016**, *55*, 6817 – 6824; g) M. Andrzejewski, A. Katrusiak, *J. Phys. Chem. Lett.* **2017**, *8*, 929 – 935; h) M. Andrzejewski, A. Katrusiak, *J. Phys. Chem. Lett.* **2017**, *8*, 279 – 284; i) M. Andrzejewski, N. Casati, A. Katrusiak, *Dalton Trans.* **2017**, *46*, 14795 – 14803.

[6] Y. Jiang, *Mater. Sci. Eng. C* **2014**, *45*, 682 – 689.

[7] a) R. Misra, T. Jadhav, B. Dhokale, S. M. Mobin, *Chem. Commun.* **2014**, *50*, 9076 – 9078; b) Y. Dong, J. Zhang, X. Tan, L. Wang, J. Chen, B. Li, L. Ye, B. Xu, B. Zou, W. Tian, *J. Mater. Chem. C* **2013**, *1*, 7554 – 7559; c) P. S. Hariharan, N. S. Venkataramanan, D. Moon, S. P. Anthony, *J. Phys. Chem. C* **2015**, *119*, 9460 – 9469.

[8] S. Ghosh, M. K. Mishra, S. Ganguly, G. R. Desiraju, *J. Am. Chem. Soc.* **2015**, *137*, 9912 – 9921.

[9] U. H. F. Bunz, *Chem. Rev.* **2000**, *100*, 1605 – 1644.

[10] a) S. Roy, V. M. Suresh, T. K. Maji, *Chem. Sci.* **2016**, *7*, 2251 – 2256; b) H. Li, D. R. Powell, R. K. Hayashi, R. West, *Macromolecules* **1998**, *31*, 52 – 58.

[11] V. K. Praveen, C. Ranjith, E. Bandini, A. Ajayaghosh, N. Armaroli, *Chem. Soc. Rev.* **2014**, *43*, 4222 – 4242.

[12] T. M. Fasina, J. C. Collings, J. M. Burke, A. S. Batsanov, R. M. Ward, D. Albesa-Jove, L. Porres, A. Beeby, J. A. K. Howard, A. J. Scott, W. Clegg, S. W. Watt, C. Viney, T. B. Marder, *J. Mater. Chem.* **2005**, *15*, 690 – 697.

[13] a) S. Roy, A. Hazra, A. Bandyopadhyay, D. Raut, P. L. Madhuri, D. S. S. Rao, U. Ramamurty, S. K. Pati, S. Krishna Prasad, T. K. J. Maji, *J. Phys. Chem. Lett.* **2016**, *7*, 4086 – 4092; b) S. Roy, M. Das, A. Bandyopadhyay, S. K. Pati, P. P. Ray, T. K. Maji, *J. Phys. Chem. C* **2017**, *121*, 23803 – 23810; c) S. Roy, D. Samanta, S. Bhattacharyya, P. Kumar, A. Hazra, T. K. Maji, *J. Phys. Chem. C* **2018**, *122*, 21598 – 21606.

[14] L. Merrill, W. A. Bassett, *Rev. Sci. Instrum.* **1974**, *45*, 290 – 294.
[15] a) V. E. Schneider, E. E. Tornau, *Phys. Status Solidi* **1982**, *111*, 565 – 574; b) G. Jaeger, *Arch. Hist. Exact Sci.* **1998**, *53*, 51 – 81; c) P. Borrmann, O. Mülken, J. Harting, *Phys. Rev. Lett.* **2000**, *84*, 3511 – 3514.
[16] a) J. Koike, *Phys. Rev. B* **1993**, *47*, 7700 – 7704; b) O. Mishima, *Nature* **1996**, *384*, 546 – 549; c) R. J. Hemley, A. P. Jephcoat, H. K. Mao, L. C. Ming, M. H. Manghnani, *Nature* **1988**, *334*, 52 – 54; d) E. Ma, *Scr. Mater.* **2003**, *49*, 941 – 946.
[17] a) E. Boldyreva, *Cryst. Growth Des.* **2007**, *7*, 1662 – 1668; b) N. A. Tumanov, E. V. Boldyreva, B. A. Kolesov, A. V. Kurnosov, R. Quesada Cabrera, *Acta Crystallogr. Sect. B* **2010**, *66*, 458 – 471; c) K. Adrjanowicz, A. Grzybowski, K. Grzybowska, J. Pionteck, M. Paluch, *Cryst. Growth Des.* **2013**, *13*, 4648 – 4654; d) M. Fisch, A. Lanza, E. Boldyreva, P. Macchi, N. Casati, *J. Phys. Chem. C* **2015**, *119*, 18611 – 18617; e) B. A. Zakharov, N. A. Tumanov, E. V. Boldyreva, *CrystEngComm* **2015**, *17*, 2074 – 2079; f) A. Y. Fedorov, D. A. Rychkov, E. A. Losev, B. A. Zakharov, J. Stare, E. V. Boldyreva, *CrystEngComm* **2017**, *19*, 2243 – 2252; g) G. Resnati, E. Boldyreva, P. Bombicz, M. Kawano, *IUCrJ* **2015**, *2*, 675 – 690; h) S. Sobczak, A. Katrusiak, *J. Phys. Chem. C* **2017**, *121*, 2539 – 2545; i) B. A. Zakharov, E. V. Boldyreva, *CrystEngComm* **2019**, *21*, 10 – 22.
[18] a) A. Katrusiak, *Acta Crystallogr. Sect. B* **1990**, *46*, 246 – 256; b) S. V. Goryainov, E. N. Kolesnik, E. V. Boldyreva, *Phys. B* **2005**, *357*, 340 – 347; c) W. Cai, A. Katrusiak, *CrystEngComm* **2012**, *14*, 4420 – 4424; d) E. Patyk, J. Skumiel, M. Podsiadło, A. Katrusiak, *Angew. Chem. Int. Ed.* **2012**, *51*, 2146 – 2150; *Angew. Chem.* **2012**, *124*, 2188 – 2192; e) E. A. Kapustin, V. S. Minkov, E. V. Boldyreva, *Acta Crystallogr. Sect. B* **2014**, *70*, 517 – 532; f) B. A. Zakharov, E. V. Boldyreva, *J. Mol. Struct.* **2014**, *1078*, 151 – 157; g) S. Ghosh, M. K. Mishra, S. B. Kadambi, U. Ramamurty, G. R. Desiraju, *Angew. Chem.* **2015**, *127*, 2712 – 2716; h) A. A. Matvienko, D. V. Maslennikov, B. A. Zakharov, A. A. Sidelnikov, S. A. Chizhik, E. V. Boldyreva, *IUCrJ* **2017**, *4*, 588 – 597.
[19] a) M. Szafrański, A. Katrusiak, *J. Phys. Chem. Lett.* **2017**, *8*, 2496 – 2506; b) M. Szafrański, A. Katrusiak, *J. Phys. Chem. Lett.* **2016**, *7*, 3458 – 3466.
[20] a) J. Ridout, L. S. Price, J. A. K. Howard, M. R. Probert, *Cryst. Growth Des.* **2014**, *14*, 3384 – 3391; b) J. Bernstein, *Polymorphism in Molecular Crystals*, Oxford University Press, U.K., **2002**; c) T. Steiner, W. Hinrichs, W. Saenger, R. Gigg, *Acta Crystallogr. Sect. B* **1993**, *49*, 708 – 718; d) O. Crottaz, F. Kubel, H. Schmid, *J. Mater. Chem.* **1997**, *7*, 143 – 146; e) M. C. Etter, A. R. Siedle, *J. Am. Chem. Soc.* **1983**, *105*, 641 – 643; f) J. Ding, R. Herbst, K. Praefcke, B. Kohne, W. A. Saenger, *Acta Crystallogr. Sect. B* **1991**, *47*, 739 – 742; g) S. Zamir, J. Bernshtein, D. Greenwood, *J. Mol. Cryst. Liq. Cryst.* **1994**, *242*, 193 – 200; h) M. A. Fernandes, D. C. Levendis, F. R. L. Schoening, *Acta Crystallogr. Sect. B* **2004**, *60*, 300 – 314; i) H. F. Lieberman, R. J. Davey, D. M. T. Newsham, *Chem. Mater.* **2000**, *12*, 490 – 494; j) Z. Skoko, S. Zamir, P. Naumov, J. Bernshtein, *J. Am. Chem. Soc.* **2010**, *132*, 14191 – 14202; k) M. Kaftory, M. Botoshansky, M. Kapon, V. Shteiman, *Acta Crystallogr. Sect. B* **2001**, *57*, 791 – 799; l) J. Gigg, R. Gigg, S. Payne, R. Conant, *J. Chem. Soc. Perkin Trans. 1* **1987**, 2411 – 2414.
[21] a) C. M. Reddy, R. C. Gundakaram, S. Basavoju, M. T. Kirchner, K. A. Padmanabhan, G. R. Desiraju, *Chem. Commun.* **2005**, 3945; b) P. Naumov, S. C. Sahoo, B. A. Zakharov, E. V. Boldyreva, *Angew. Chem. Int. Ed.* **2013**, *52*, 9990 – 9995; *Angew. Chem.* **2013**, *125*, 10174 – 10179; c) M. Lusi, J. Bernstein, *Chem. Commun.* **2013**, *49*, 9293 – 9295; d) O. S. Bushuyev, T. C. Corkery, C. J. Barrett, T. Friščić, *Chem. Sci.* **2014**, *5*, 3158; e) O. S. Bushuyev, A. Tomberg, T. Friščić, C. J. Barrett, *J. Am. Chem. Soc.* **2013**, *135*, 12556; f) S. Ghosh, M. K. Mishra, S. B. Kadambi, U. Ramamurty, G. R. Desiraju, *Angew. Chem. Int. Ed.* **2015**, *54*, 2674; *Angew. Chem.* **2015**, *127*, 2712; g) M. K. Panda, S. Ghosh, N. Yasuda, T. Moriwaki, G. D. Mukherjee, C. M. Reddi, P. Naumov, *Nat. Chem.* **2015**, *7*, 65; h) O. S. Bushuyev, A. Tomberg, J. R. Vinden, N. Moitessier, C. J. Barrett, T. Friščić, *Chem. Commun.* **2016**, *52*, 2103 – 2106.
[22] a) S. Kobatake, S. Takami, H. Muto, T. Ishikawa, M. Irie, *Nature* **2007**, *446*, 778 – 781; b) K. Uchida, S. Sukata, Y. Matsuzawa, M. Akazawa, J. J. D. de Jong, N. Katsonis, Y. Kojima, S. Nakamura, J. Areephong, A. Meetsma, B. L. Feringa, *Chem. Commun.* **2008**, 326 – 328; c) M. Morimoto, M. Irie, *J. Am. Chem. Soc.* **2010**, *132*, 14172 – 14178; d) F. Terao, M. Morimoto, M. Irie, *Angew. Chem. Int. Ed.* **2012**, *51*, 901 – 904; *Angew. Chem.* **2012**, *124*, 925 – 928; e) S. Kobatake, H. Hasegawa, K. Miyamura, *Cryst. Growth Des.* **2011**, *11*, 1223 – 1229; f) A. K. Saini, K. Natarajan, S. M. Mobin, *Chem. Commun.* **2017**, *53*, 9870 – 9873; g) S. Hayashi, A. Asano, N. Kamiya, Y. Yokomori, T. Maeda, T. Koizumi, *Sci. Rep.* **2017**, *7*, 9453; h) S. Hayashi, T. Koizumi, N. Kamiya, *Cryst. Growth Des.* **2017**, *17*, 6158 – 6162.
[23] a) X. Cui, A. L. Rohl, A. Shtukenberg, B. Kahr, *J. Am. Chem. Soc.* **2013**, *135*, 3395 – 3398; b) D. Kitagawa, H. Tsujioka, F. Tong, X. Dong, C. J. Bardeen, S. Kobatake, *J. Am. Chem. Soc.* **2018**, *140*, 4208 – 4212; c) P. Naumov, S. Chizhik, M. K. Panda, N. K. Nath, E. Boldyreva, *Chem. Rev.* **2015**, *115*, 12440 – 12490; d) H. Wang, P. Chen, Z. Wu, J. Zhao, J. Sun, R. Lu, *Angew. Chem. Int. Ed.* **2017**, *56*, 9463 – 9467; *Angew. Chem.* **2017**, *129*, 9591 – 9595.
[24] See the Supporting Information.

Manuscript received: January 4, 2019
Revised manuscript received: February 27, 2019
Accepted manuscript online: March 12, 2019
Version of record online: April 10, 2019

A2

Large negative linear compressibility of a porous molecular co-crystal

S. Sobczak, **A. Półrolniczak**, P. Ratajczyk, W. Cai, A. Gładysiak, V. I Nikolayenko, D. C Castell, L. J Barbour, A. Katrusiak.

Chemical Communications 56 (31), 4324-4327, **2020.**

ChemComm

ROYAL SOCIETY OF CHEMISTRY

COMMUNICATION

View Article Online
View Journal | View Issue

Cite this: *Chem. Commun.*, 2020, **56**, 4324

Received 17th January 2020,
Accepted 9th March 2020

DOI: 10.1039/d0cc00461h

rsc.li/chemcomm

Large negative linear compressibility of a porous molecular co-crystal†

Szymon Sobczak, [a] Aleksandra Półrolniczak, [a] Paulina Ratajczyk, [a] Weizhao Cai, [a] Andrzej Gładysiak, [a] Varvara I. Nikolayenko, [b] Dominic C. Castell, [b] Leonard J. Barbour *[b] and Andrzej Katrusiak *[a]

Flexible and transformable molecules, particularly those responding to external stimuli, are needed for designing sensors and porous compounds capable of storing or separating gases and liquids. Under normal conditions the photochromic compound, 1,2-bis[2-methyl-5-(pyridyl)-3thienyl]cyclopentene (BTCP) forms a porous co-crystal with 1,4-diiodotetrafluorobenzene (dItFB). It traps acetone (Ac) molecules in the pores. Owing to a unique system of pores in the polar framework, the crystal is sensitive to the humidity in the air and to the chosen liquid environment. When compressed in non-penetrating media, the crystal displays a strong negative linear compressibility (NLC) along [100].

The search for environmentally-friendly methods for storing fuels[1–6] and for removing pollution and waste[7–9] drives the current interest in various kinds of porous materials. Crystalline compounds with well-defined pores and cages are especially promising for these purposes. Although the field of porous materials is dominated by microporous zeolites and metal–organic frameworks (MOFs), molecular systems can be attractive for several reasons.[10,11] Owing to the structural and chemical variability generated by modular assembly, it is possible to change the pore sizes and to fine-tune the shape and functionality of the pores in materials free of metal ions. The inclusion of stimulus-responsive molecules can result in unprecedented properties of such porous molecular systems.

Interesting phenomena related to stimulus-responsive compounds include interconversions between isomeric forms and topochemical reactions triggered by light. The molecules of such compounds are conformationally flexible and capable of undergoing low-energy reactions, involving breaking and forming covalent bonds.

To investigate the high-pressure behaviour of this class of materials we have chosen a bis-3-thienylcyclopentene derivative of 1,2-bis[2′-methyl-5′-(pyrid-4″-yl)-thien-3′-yl]perfluoro-cyclopentene (BTCP).[12–18] When irradiated with ultraviolet light, this group of compounds undergoes solid-state photocyclization, yielding a stable isomeric form with a closed ring. Exposure to visible light results in the ring-open form.[16,18] The reactivity of BTCP, as shown in Fig. 1 derivatives can be triggered in relatively large aggregates. Even single crystals can undergo bulk conversions, involving reversible structural changes, such as pore opening.[16] It is well-known that high pressure often induces prominent changes in crystal structure,[19,20] phase transitions,[21–28] sorption of solvent molecules[29–34] and chemical reactions.[35–41] Moreover, it was found that flexible molecules assembled into aggregates or polymeric frameworks under hydrostatic pressure can exhibit counterintuitive elastic properties, including negative linear and area compression.[36,42–45]

Here we report the isothermal compression of a porous molecular co-crystal solvate, hereafter abbreviated as BTCPs·dItFB·Ac, of 1,2-bis[2′-methyl-5′-(pyrid-4″-yl)-thien-3′-yl]perfluoro-cyclopentene with 1,4-diiodotetrafluorobenzene (dItFB) and acetone (Ac).[46] We have established that in the range of

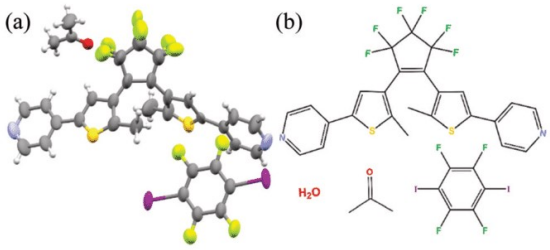

Fig. 1 (a) The asymmetric unit of co-crystal BTCPs·dItFB·Ac and (b) the structural formula of BTCP, dItFB as well as the guests described in our work. In (a), the anisotropic thermal parameters are shown at the 50% probability level and the disordered Ac molecule is shown in one of its half-occupied sites only.

[a] *Department of Chemistry, Adam Mickiewicz University, Poznań, Poland. E-mail: katran@amu.edu.pl*
[b] *Department of Chemistry and Polymer Science, University of Stellenbosch, Matieland 7600, South Africa. E-mail: ljb@sun.ac.za*

† Electronic supplementary information (ESI) available: Experimental details, literature survey concerning NLC coefficients, detailed conformational analisis and tabularized detailed crystallographic data. CCDC 1886608–1886615. For ESI and crystallographic data in CIF or other electronic format see DOI: 10.1039/d0cc00461h

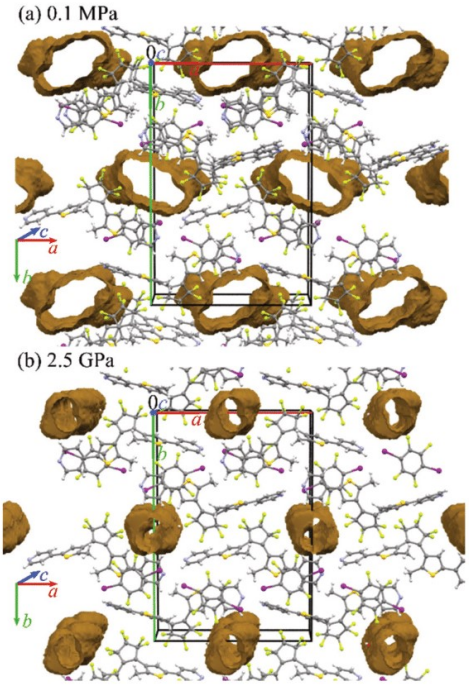

Fig. 2 The size and arrangement of voids (a) at ambient pressure and (b) at 2.5 GPa. The voids are shown for a 1.2 Å probe radius and grid spacing 0.2 Å using the program Mercury.

0–2.5 GPa at room temperature this crystal exhibits pronounced negative linear compressibility (NLC).

BTCP and dltFB co-crystallize from acetone under ambient conditions, with acetone molecules trapped in guest-accessible pockets (Fig. 2). We have established that the crystals lose part of their solvent content when exposed to air, and that the quality of such dried crystals can be recovered with a few drops of water. This results in subsequent improvement of the X-ray diffraction data, yielding higher resolution and a lower R_{int} parameter. The water molecules penetrate the pores of the BTCPs·dItFB·Ac crystal, causing some elongation along [001] (Table 1). The unit cell volume of the partially hydrated co-crystals increases by 10.8(7) Å^3, *i.e.*, 2.7 Å^3 per asymmetric unit. This H_2O adsorption is associated with anisotropic strain of the crystal: parameters *b* and *c* elongate by about 0.07 Å and 0.015 Å, respectively, while parameter *a* shortens by −0.02 Å (Table 1). However, no water molecules could be located in the crystal structure of the crystals exposed to moisture, which suggests non-stoichiometric sorption of H_2O into disordered positions in the pores. Although the uptake of water in molecular crystals and MOFs usually increases the volume, it has been shown that adsorption of water can also result in a significant reduction of volume.[47–49]

A single crystal of BTCPs·dItFB·Ac, which had been stored in a dry environment, was compressed in glycerol. Although disordered H_2O molecules could not be located up to 1.95 GPa, it was possible to model one water molecule per asymmetric unit at 2.5 GPa. This suggests that their ordering takes place at higher pressure. Karl Fischer titration of the glycerol confirmed the presence of somewhat less that 2% (wt) of water, which could be the origin of the water molecules located in the pores of the compressed sample. Single-crystal X-ray diffraction data were recorded at pressures of 0.4, 0.7, 1.09, 1.59, 1.95 and 2.5 GPa. High-pressure experiments were carried out in a Merrill-Bassett diamond-anvil cell (DAC), modified by mounting the diamond anvils directly on steel supports with conical windows.[50] The DAC was centred using the gasket shadowing method.[51] Starting from the ambient-pressure model, the high-pressure crystal structures were refined using the least-squares method of SHELXL.[52] The pressure in the DAC was calibrated by the ruby fluorescence method, using a Photon Control spectrometer with enhanced resolution, affording an accuracy of 0.02 GPa.[53,54] X-Ray data were measured on a four-circle Oxford-Diffraction Xcalibur diffractometer equipped with an EOS-CCD detector. Due to the strongly disordered acetone molecule in all high-pressure measurements, the SQUEEZE algorithm of PLATON was applied.[55] The crystallographic data and experimental details are summarized in Table 1 and Table S4 (ESI†) and have been deposited in CIF format at the Cambridge Structural Database with numbers CCDC 1886608–1886615.†

Isothermal compression of a single crystal of BTCPs·dItFB·Ac immersed in glycerol induces negative linear compressibility (NLC) along [100], *i.e.*, perpendicular to the pore channels. The NLC of the co-crystal along this direction is unprecedented in magnitude for an organic molecular crystal, reaching −30 TPa^{-1} between 0.1 MPa and 0.4 GPa (*cf.* Table S1 in the ESI†).[56] The crystal compressibility is clearly nonlinear (Fig. 3) and the NLC magnitude gradually reduces to −15.54 TPa^{-1}

Table 1 Selected crystallographic data of co-crystal BTCP·dItFB·Ac (*cf.* Table S4 in ESI for details)

Pressure [GPa]	0.0001	0.0001	0.40	0.70	1.09	1.59	1.95	2.50
Environment	Air	Water	Glycerol	Glycerol	Glycerol	Glycerol	Glycerol	Glycerol
Space group	$Pna2_1$	$Pna2_1$	$Pna2_1$	$Pna2_1$	$Pna2_1$	$Pna2_1$	$Pna2_1$	$Pna2_1$
a (Å)	17.2716(8)	17.2451(6)	17.475(9)	17.449(4)	17.559(5)	17.604(14)	17.564(10)	17.606(4)
b (Å)	27.171(3)	27.2415(16)	26.52(5)	26.511(15)	26.315(16)	25.83(6)	25.64(5)	25.580(17)
c (Å)	7.9406(7)	7.9554(3)	7.662(7)	7.536(11)	7.259(8)	7.13(4)	7.07(3)	6.944(9)
V (Å^3)	3726.5(6)	3737.3(3)	3551(8)	3486(5)	3354(4)	3240(20)	3185(15)	3127(5)
Z/*Z*′	4/1	4/1	4/1	4/1	4/1	4/1	4/1	4/1
D_x (g cm^{-3})*	1.803*	1.808*	1.903*	1.938*	2.014*	2.085*	2.121*	2.161*

*D_x – the initial stoichiometry BTCP·dItFB·Ac without water content was assumed for the density calculations.

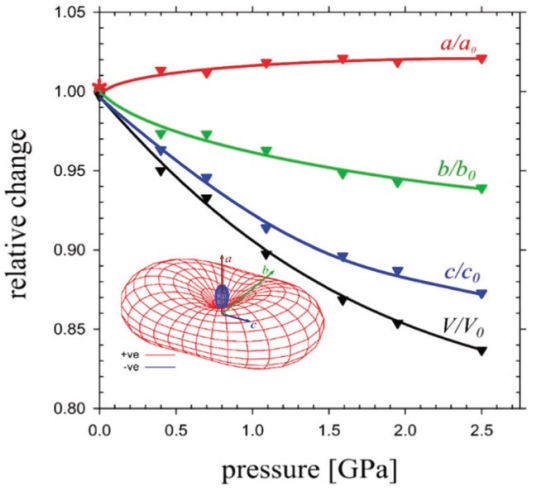

Fig. 3 Compression of co-crystal BTCP·dItFB·Ac in glycerol plotted relative to the 0.1 MPa dimensions. The error bars are smaller than the plotted symbols. The inset shows a graphical representation of the compressibility tensor calculated between the 0.1 MPa and 0.7 GPa (*cf.* Fig. S3 and Table S3 in ESI†).[56]

between 0.1 MPa and 0.7 GPa, Table S1 (ESI†). The NLC in molecular crystals originates from anisotropic structural features. For the BTCP cocrystal the NLC can be rationalized using the wine-rack mechanism, as the NLC effect occurs along the elongation direction of the cross-section of the pores (compare Fig. 2 and 3). The compression also involves changes in the conformation of molecules, and in their arrangement.

The initial compression up to 0.4 GPa affects the BTCP conformation. The perfluorocyclopentene and heterocyclic aromatic rings of BTCP approximate the shape of an isosceles triangle. The rings are flat and of well-known regular geometry. However, owing to the single bonds that join them, the molecule is flexible. As the pressure increases, the molecule becomes elongated. We have established that the molecular shape of BTCP is most affected by pressure up to 0.4 GPa, when the distance between terminal pyridine rings elongates by 1.7%

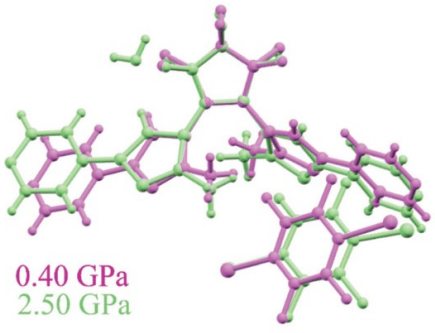

Fig. 4 The two molecules of BTCP from 0.40 GPa and 2.5 GPa superimposed on the perfluorocyclopentene ring.

(compared to 2.4% at 2.50 GPa). This elongation coincides with the NLC effect along [100]. The pressure effect on the intramolecular distance between two reactive carbon atoms in the thienyl groups is unfavourable for closing the ring.[57] Only in the initial pressure range does this distance decrease insignificantly, but at 2.5 GPa it elongates considerably (Fig. 4).

In summary, we have investigated a porous and polar co-crystal solvate BTCP·dItFB·Ac. At ambient conditions, it absorbs or releases water depending on the surrounding moisture. Under pressure, the crystal displays strongly anisotropic compression coupled to the conformation of BTCP molecules. To our knowledge,[43] the negative linear compressibility of over -30 TPa^{-1} is the strongest ever reported for an organic molecular crystal; similarly, we have observed that BTCP·dItFB·Ac displays an impressive positive linear compression of about 90 TPa^{-1}, corresponding to the reduction by 12% at 2.5 GPa of the *c* unit cell parameter.

SS, AP and AK are grateful to the grant OPUS 10 No. UMO-2015/19/B/ST5/00262. SS also thanks grant POWR.03.02.00-00-I023/17 and AP grant POWR.03.02.00-00-I026/16 co-financed by the European Union through the European Social Fund under the Operational Program Knowledge Education Development for the finical support. LJB, VIN and DCC acknowledge the National Research Foundation of South Africa for support of this work.

Conflicts of interest

There are no conflicts of interest to declare.

Notes and references

1 L. J. Murray, M. Dincă and J. R. Long, *Chem. Soc. Rev.*, 2009, **38**, 1294.
2 J. A. Mason, J. Oktawiec, M. K. Taylor, M. R. Hudson, J. Rodriguez, J. E. Bachman, M. I. Gonzalez, A. Cervellino, A. Guagliardi, C. M. Brown, P. L. Llewellyn, N. Masciocchi and J. R. Long, *Nature*, 2015, **527**, 357–361.
3 W. R. Browne and B. L. Feringa, *Nat. Nanotechnol.*, 2006, **1**, 25–35.
4 A. Dhakshinamoorthy, A. M. Asiri and H. García, *Angew. Chem., Int. Ed.*, 2016, **55**, 5414–5445.
5 M. Gallo and D. Glossman-Mitnik, *J. Phys. Chem. C*, 2009, **113**, 6634–6642.
6 S. Noro, *Metal-Organic Frameworks*, Wiley-VCH Verlag GmbH & Co. KGaA, Weinheim, Germany, 2013, vol. 5.
7 J. Liu, P. K. Thallapally and D. Strachan, *Langmuir*, 2012, **28**, 11584–11589.
8 B. Aguila, D. Banerjee, Z. Nie, Y. Shin, S. Ma and P. K. Thallapally, *Chem. Commun.*, 2016, **52**, 5940–5942.
9 S. Jakobsen, D. Gianolio, D. S. Wragg, M. H. Nilsen, H. Emerich, S. Bordiga, C. Lamberti, U. Olsbye, M. Tilset and K. P. Lillerud, *Phys. Rev. B: Condens. Matter Mater. Phys.*, 2012, **86**, 125429.
10 T. Hasell and A. Cooper, *Nat. Rev. Mater.*, 2016, **1**, 16053.
11 J. R. Holst, A. Trewin and A. I. Cooper, *Nat. Chem.*, 2010, **2**, 915–920.
12 K. Matsuda, Y. Shinkai and M. Irie, *Inorg. Chem.*, 2004, **43**, 3774–3776.
13 F. Luo, C. Bin Fan, M. B. Luo, X. L. Wu, Y. Zhu, S. Z. Pu, W. Y. Xu and G. C. Guo, *Angew. Chem., Int. Ed.*, 2014, **53**, 9298–9301.
14 X. F. Feng, F. Luo, L. Zhang, A. M. Zheng, C. S. Yan, L. Le Gong, C. Bin Fan, H. Q. Wu and Z. Q. Liu, *Chem. Commun.*, 2016, **53**, 763–766.
15 K. Matsuda, K. Takayama and M. Irie, *Chem. Commun.*, 2001, 363–364.

16 H. Sato, R. Matsuda, S. Kitagawa, Y. Zheng, H. J. Jeon and P. Wu, *Nat. Commun.*, 2017, **8**, 100.
17 V. I. Nikolayenko, S. A. Herbert and L. J. Barbour, *Chem. Commun.*, 2017, **53**, 11142–11145.
18 K. Nomiyama, M. Irie, K. Matsuda, M. Isayama, Y. Shinkai and T. Yamaguchi, *Chem. Lett.*, 2003, **32**, 1178–1179.
19 C. Sanloup, *The deep earth*, Springer, Netherlands, Dordrecht, 2012, vol. 140.
20 Elena Boldyreva and P. Dera, *High-Pressure Crystallography*, Springer Science & Business Media, 2010.
21 S. Sobczak and A. Katrusiak, *J. Phys. Chem. C*, 2017, **121**, 2539–2545.
22 E. Patyk, J. Skumiel, M. Podsiadło and A. Katrusiak, *Angew. Chem., Int. Ed.*, 2012, **51**, 2146–2150.
23 M. Fisch, A. Lanza, E. Boldyreva, P. Macchi and N. Casati, *J. Phys. Chem. C*, 2015, **119**, 18611–18617.
24 E. V. Boldyreva, S. N. Ivashevskaya, H. Sowa, H. Ahsbahs and H.-P. Weber, *Dokl. Phys. Chem.*, 2004, **396**, 111–114.
25 Y. Wang, K. Li, A. Sano-Furukawa, F. Hong, H. Zheng, A. Katrusiak, F. Liao, M. Andrzejewski, T. Hattori, L. Wang, H. Mao and Y. Meng, *J. Phys. Chem. C*, 2016, **120**, 29510–29519.
26 F. P. A. Fabbiani, D. R. Allan, A. Dawson, W. I. F. David, P. A. McGregor, I. D. H. Oswald, S. Parsons and C. R. Pulham, *Chem. Commun.*, 2003, 3004–3005.
27 F. P. A. Fabbiani, D. R. Allan, W. I. F. David, A. J. Davidson, A. R. Lennie, S. Parsons, C. R. Pulham and J. E. Warren, *Cryst. Growth Des.*, 2007, **7**, 1115–1124.
28 F. P. A. Fabbiani and C. R. Pulham, *Chem. Soc. Rev.*, 2006, **35**, 932–942.
29 F. X. Coudert, *Chem. Mater.*, 2015, **27**, 1905–1916.
30 S. Sobczak and A. Katrusiak, *Cryst. Growth Des.*, 2018, **18**, 1082–1089.
31 S. C. McKellar and S. A. Moggach, *Acta Crystallogr., Sect. B: Struct. Sci., Cryst. Eng. Mater.*, 2015, **71**, 587–607.
32 S. A. Moggach, T. D. Bennett and A. K. Cheetham, *Angew. Chem., Int. Ed.*, 2009, **48**, 7087–7089.
33 S. A. Moggach, P. A. Wright, S. C. McKellar, A.-M. Banu, A. Greenaway, K. Ward, A. J. Graham, T. Düren and J. P. S. Mowat, *J. Am. Chem. Soc.*, 2014, **136**, 8606–8613.
34 J. Liu, S. Li, K. Yang, B. Zou, G. Zou, K. Wang, B. Liu and Q. Li, *J. Phys. Chem. C*, 2014, **118**, 5848–5853.
35 M. Andrzejewski and A. Katrusiak, *J. Phys. Chem. Lett.*, 2017, **8**, 929–935.
36 W. Cai, A. Gładysiak, M. Anioła, V. J. Smith, L. J. Barbour and A. Katrusiak, *J. Am. Chem. Soc.*, 2015, **137**, 9296–9301.
37 J. P. Tidey, H. L. S. Wong, J. McMaster, M. Schröder and A. J. Blake, *Acta Crystallogr., Sect. B: Struct. Sci., Cryst. Eng. Mater.*, 2016, **72**, 357–371.
38 J. E. Warren, M. Murrie, S. A. Moggach, P. Parois, A. R. Lennie, N. Rowantree, S. Parsons, E. K. Brechin and K. W. Galloway, *CrystEngComm*, 2009, **11**, 2601.
39 R. J. Angel, N. L. Ross, E. C. Spencer, J. A. K. Howard and B. E. Hanson, *J. Am. Chem. Soc.*, 2009, **131**, 4022–4026.
40 J. K. Clegg, A. J. Brock, K. A. Jolliffe, L. F. Lindoy, S. Parsons, P. A. Tasker and F. J. White, *Chem. – Eur. J.*, 2017, **23**, 12480–12483.
41 A. Półrolniczak, S. Sobczak and A. Katrusiak, *Inorg. Chem.*, 2018, **57**, 8942–8950.
42 W. Li, M. R. Probert, M. Kosa, T. D. Bennett, A. Thirumurugan, R. P. Burwood, M. Parinello, J. A. K. Howard and A. K. Cheetham, *J. Am. Chem. Soc.*, 2012, **134**, 11940–11943.
43 A. B. Cairns and A. L. Goodwin, *Phys. Chem. Chem. Phys.*, 2015, **17**, 20449–20465.
44 R. H. Baughman, S. Stafström, C. Cui and S. O. Dantas, *Science*, 1998, **279**, 1522–1524.
45 W. Zieliński and A. Katrusiak, *Cryst. Growth Des.*, 2014, **14**, 4247–4253.
46 V. I. Nikolayenko, D. C. Castell, D. P. van Heerden and L. J. Barbour, *Angew. Chem., Int. Ed.*, 2018, **57**, 12086–12091.
47 W. Zieliński and A. Katrusiak, *CrystEngComm*, 2015, **17**, 5468–5473.
48 M. Andrzejewski, N. Casati and A. Katrusiak, *Dalton Trans.*, 2017, **46**, 14795–14803.
49 V. I. Nikolayenko, A. Heyns and L. J. Barbour, *Chem. Commun.*, 2017, **53**, 11306–11309.
50 L. Merrill and W. A. Bassett, *Rev. Sci. Instrum.*, 1974, **45**, 290–294.
51 A. Budzianowski and A. Katrusiak, High-pressure crystallographic experiments with a CCD detector, in *High-Pressure Crystallography*, ed. A. Katrusiak and P. F. McMillan, Kluwer Academic Publisher, Dordrecht.
52 G. M. Sheldrick, *Acta Crystallogr., Sect. C: Struct, Chem.*, 2015, **71**, 3–8.
53 G. J. Piermarini, S. Block, J. D. Barnett and R. A. Forman, *J. Appl. Phys.*, 1975, **46**, 2774–2780.
54 H. K. Mao, J. Xu and P. M. Bell, *J. Geophys. Res.*, 1986, **91**, 4673–4676.
55 A. L. Spek, *Acta Crystallogr., Sect. C: Struct, Chem.*, 2015, **71**, 9–18.
56 M. J. Cliffe and A. L. Goodwin, *J. Appl. Crystallogr.*, 2012, **45**, 1321–1329.
57 X. Lin, J. Jia, P. Hubberstey, M. Schröder and N. R. Champness, *CrystEngComm*, 2007, **9**, 438–448.

A3

Solvent-controlled elongation and mechanochemical strain in a metal-organic framework

A. Półrolniczak, S. Sobczak, V. Nikolayenko, L. Barbour, A. Katrusiak.

Dalton Transactions 50 (47), 17478-17481, **2021.**

Dalton Transactions

ROYAL SOCIETY OF CHEMISTRY

COMMUNICATION

View Article Online
View Journal | View Issue

Cite this: *Dalton Trans.*, 2021, **50**, 17478

Received 13th June 2021,
Accepted 4th November 2021

DOI: 10.1039/d1dt01937f

rsc.li/dalton

Solvent-controlled elongation and mechanochemical strain in a metal–organic framework†

Aleksandra Półtrolniczak, ‡[a] Szymon Sobczak, ‡[a] Varvara I. Nikolayenko,[b] Leonard J. Barbour *[b] and Andrzej Katrusiak *[a]

Under high pressure, crystals of $[Zn(m\text{-}btcp)_2(bpdc)_2]\cdot 2DMF\cdot H_2O$, referred to as DMOF are particularly sensitive to the type of pressure-transmitting media (PTM) employed: large PTM molecules seal the pores and DMOF is compressed as a closed system, whereas small PTM molecules are pushed into the pores, thereby altering the stoichiometry of DMOF. Compression in glycerol and Daphne 7474 leads to negative linear compressibility (NLC), while a mixture of methanol : ethanol : water 'hyperfills' the pores of the chiral framework, adjusting its 3-dimensional strain and resulting in pressure-induced amorphization around 1.2 GPa. The uptake of the small-molecule PTM strongly increases the dimensions of DMOF in the direction perpendicular to that of the NLC of the crystal.

Properties of porous metal–organic frameworks (MOFs) can be tailored specifically for applications such as gas storage and separation,[1] nanosensing,[2] catalysis of chemical reactions,[3] medical drug delivery[4] and others.[5] By combining flexible organic ligands with rigid inorganic nodes, we can construct structurally flexible MOFs with high thermal stability. However, under external stimuli, MOFs can undergo strong conformational changes resulting in phase transitions or even chemical reactions.[6–14] A thorough understanding of the mechanisms behind these structural rearrangements is essential for the rational design of new materials.

In response to various kinds of stimuli (*e.g.* light, heat, pressure and magnetic field), optoelectrical, optomechanical and optochemical effects are coveted for practical applications. Upon irradiation with light of a particular wavelength, the crystals of certain photochromic molecules change colour,[15,16] which is often accompanied by structural, electronic and even chemical rearrangements.[2,16] One of the most thoroughly investigated classes of compound comprises derivatives of bis-3-thienylcyclopentenes (*btcps*) capable of topochemical photocyclisation to form stable closed-ring isomers.[17,18] *Btcp* compounds were first employed for the construction of MOFs by Luo *et al.*[19] and later also by other groups.[20–24]

We previously reported a series of four MOFs prepared from $Zn(NO_3)_2$ and 1,2-bis[2-methyl-5-(4-pyridyl)-3-thienyl]-perfluorocyclopentene (*m-btcp*) or 1,2-bis[2-ethyl-5-(4-pyridyl)-3-thienyl]-perfluorocyclopentene (*e-btcp*), combined with either the rigid 4,4′-biphenyldicarboxylic acid (H_2bpdc) or the flexible 4,4′-oxybisbenzoic acid (H_2oba). Owing to ligand flexibility[25] and the degree of interpenetration, solid-state photocyclization only occurred in $[Zn(e\text{-}btcp)_2(oba)_2]$ (DMOF3) upon irradiation with 365 nm UV light.[23]

Extreme hydrostatic pressure is also a strong and efficient stimulus capable of inducing phase transitions,[26–28] enforcing the transport of molecules in porous materials[29–31] and even triggering chemical reactions.[26,32,33] Owing to their framework structures, MOFs can exhibit unique mechanochemical properties under such conditions (*e.g.*, negative linear expansion and negative area compressibility).[7,11,12,34] The applications that arise from this effects are of growing interest due to the development of pressure sensors and actuators for high-pressure underwater and geological installations, hydrothermal chambers, autoclaves and pressure reactors.[12,34] The generation of anisotropic compression in a material under hydrostatic stress is often related to the flexibility of linkers, which dominates the strain of the MOF's framework.[12] It should be stressed that the physical definition of compressibility is reserved for 'closed systems' of fixed stoichiometry and in one phase of the compound (compressibility should not be calculated across phase transitions). These conditions are fulfilled for the compression in large-molecule PTMs. However,

[a]*Department of Materials Chemistry, Faculty of Chemistry, Adam Mickiewicz University, Umultowska 89b, 61-614 Poznań, Poland. E-mail: katran@amu.edu.pl*

[b]*Department of Chemistry and Polymer Science, University of Stellenbosch, 7602, Matieland, South Africa. E-mail: ljb@sun.ac.za*

†Electronic supplementary information (ESI) available: Details regarding loading of the diamond anvil cell. CCDC 1956801–1956804, 1956866–1956870 for DMOF compressed in glycerol, 1956872–1956875 Daphne 7474 and 1956823–1956826, 1956193 for MEW. For ESI and crystallographic data in CIF or other electronic format see DOI: 10.1039/d1dt01937f

‡These authors contributed equally.

small-molecule PTMs can trigger the transport of guests to and from the pores and the stoichiometry of the sample crystal changes as a function of pressure. Such a sample, when exposed to high pressure, can even increase in volume due to the uptake of new guests.

In this context we now present structural data relating to the effects of hydrostatic pressure, involving different hydrostatic media, on single crystals of the 3D host framework $[Zn(m\text{-}btcp)_2(bpdc)_2]\cdot 2DMF\cdot H_2O$ (denoted as DMOF). DMOF crystallises in the orthorhombic space group $P2_12_12_1$. The central zinc ion is tetrahedrally coordinated to two *bpdc* dianions and two *m-btcp* molecules (Scheme 1). These units are interconnected to form a honeycomb-like topology composed of chiral four-connected nets with fivefold interpenetration.[23] The structure contains large guest-accessible channels extending along *a* (Fig. 1), with elliptical cross-sections that are elongated along *b*. The pores are easily accessible by small-solvent molecules, with the as-synthesised structure containing DMF and water guest molecules.

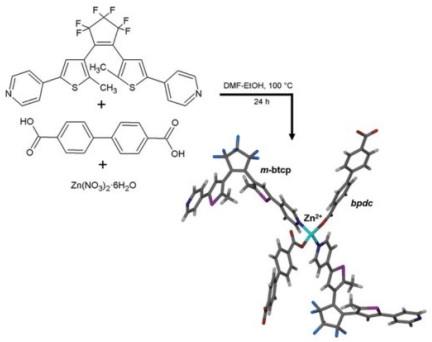

Scheme 1 Solvothermal preparation of DMOF from $Zn(NO_3)_2$, *m-btcp* and H_2*bpdc*.

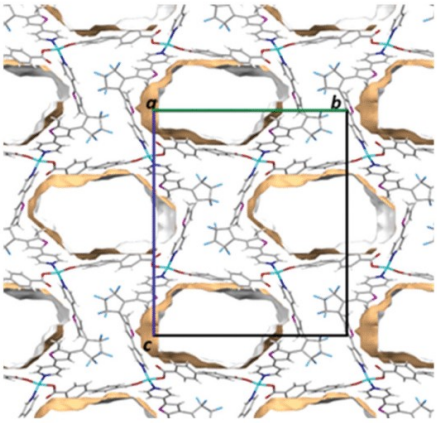

Fig. 1 Guest-accessible space (*ca.* 33% of the total volume) in the structure of DMOF as viewed along *a*; calculated using the program mercury[35] (probe radius 1.5 Å).

Since we had been unable to cyclise the *m-btcp* component of DMOF by means of photoirradiation, we elected to also investigate the effects of extreme compression for this purpose (see ESI† for details). Crystals of as-synthesised DMOF were loaded into a Merrill–Bassett diamond-anvil cell (DAC) and, owing to the presence of large channels, separate diffraction experiments were carried out using the non-penetrating hydrostatic fluids glycerol and Daphne 7474, or a penetrating mixture of methanol : ethanol : water (MEW). As a result, a straightforward mechanism linking the crystal structure and its compression (in the non-penetration PTMs) and mechanochemical strain (in penetrating PTM) can be elucidated. Relevant crystallographic parameters are summarised in Table 1. A common feature of hydrostatic compression of porous crystals is that the magnitude along the pores (here along *a*) is the least compressed/strained.[36]

In non-penetrating media DMOF is most compressed along *c* with $\beta_c = -1/c\cdot\partial c/\partial p = 24(5)$ TPa^{-1}, while negative linear compression (NLC) occurs along *b* (Fig. 2, 3 and Table S1†). The compressibility of −16(3) TPa^{-1} along *b*, calculated between 0.1 MPa and 1.7 GPa, corresponds to the elongation of this unit-cell dimension by 0.75 Å. The strong changes in *b* and *c* originate from the elliptical cross-section of the pores (the unit-cell parameters *b* and *c* are correlated to the semi-major and semi-minor axes of the pores, respectively). Although increasing pressure causes narrowing of the pore along its short cross-sectional dimension (*i.e.*, along *c*), the pores do not collapse. It is also important to note that the compressibilities along both *b* and *c* are linked owing to framework deformation (*i.e.*, the wine-rack mechanism hinged on the cations, and conformational changes in the ligands rather than on the metal cations only, which is typical of MOFs with rigid linkers[37,38]). In principle, the effect of the elliptical pores should be similar to that for discrete molecules (such as ROY, methanol monohydrate, POM, and others) and metal-hinged MOFs.

In the penetrating medium MEW, the mechanochemical strains along *b* and *c* are reversed compared to the compressibilities along these directions in non-penetrating PTMs (Fig. 2). The mechanochemical strain along *b* becomes positive ($\beta_b = 27(6)$ TPa^{-1}), while that along *c* is negative ($\beta_c = -44(3)$ TPa^{-1}), as calculated between structures at 0.1 MPa and 1.18 GPa (Fig. 2, 3 and Table S2†). This change is ascribed to the intake of new guest molecules, which 'inflate' the channels, thus causing elongation of *c* (*i.e.* along the semi-minor axis of the elliptical channel). Owing to wine-rack coupling through the framework, this shortens the semi-major axis of the channel along *b*.

The process of superfilling (or hyperfilling)[33] increases the initial unit-cell volume by about 100 Å^3 at 0.25 GPa (Fig. 2 and Table 1). This implies an intake (in volume) of approximately 5 non-hydrogen atoms per unit cell into the crystal structure, which corresponds to the *ca.* 74 additional electrons located within the pores, as estimated by the SQUEEZE subroutine of Platon. Further compression in MEW magnifies the adsorption

Table 1 Selected crystallographic data for DMOF and its clathrate with methanol : ethanol : water (M : E : W)

Pressure [GPa]	0.0001	0.19	0.8	1.5	0.25	0.56	0.85	1.18
Environment	Atmospheric	Daphne 7474	Glycerol	Glycerol	M : E : W	M : E : W	Me : E : W	M : E : W
Space group	$P2_12_12_1$	$P2_12_12_1$	$P2_12_12_1$	$P2_12_12_1$	$P2_12_12_1$	$P2_12_12_1$	$P2_12_12_1$	$P2_12_12_1$
a (Å)	7.11393(12)	7.011(17)	6.730(2)	6.513(9)	7.1001(8)	7.1015(18)	7.072(4)	7.029(3)
b (Å)	24.9253(4)	25.05(2)	25.256(15)	25.67(3)	24.68(2)	24.22(3)	24.225(15)	24.125(10)
c (Å)	29.0241(8)	28.81(5)	28.79(4)	27.96(7)	29.899(7)	30.248(17)	30.38(5)	30.55(4)
V (Å^3)	5146.45(19)	5059(16)	4893(7)	4675(14)	5240(5)	5202(8)	5205(10)	5181(8)
D_x [a] (g cm^{-3})	1.162	1.182	1.222	1.279	1.141	1.149	1.149	1.154
Z/Z'	4/1	4/1	4/1	4/1	4/1	4/1	4/1	4/1

[a] D_x – the initial stoichiometry $C_{39}H_{24}F_6N_2O_4S_2Zn{\cdot}C_3H_6NO$ was assumed and no water content was considered for the density calculations.

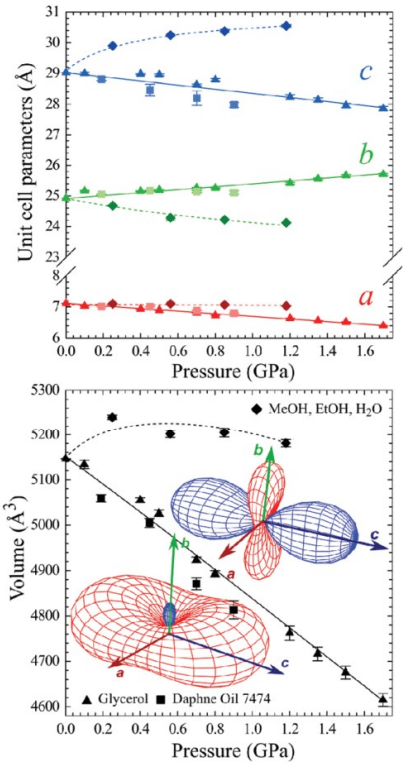

Fig. 2 Pressure dependence of the unit-cell parameters (top) and volume (bottom) for isothermal compression of DMOF in the non-penetrating oils Daphne 7474 (squares) and glycerol (triangles), and the penetrating MEW mixture (diamonds). The lines are for guiding the eye.

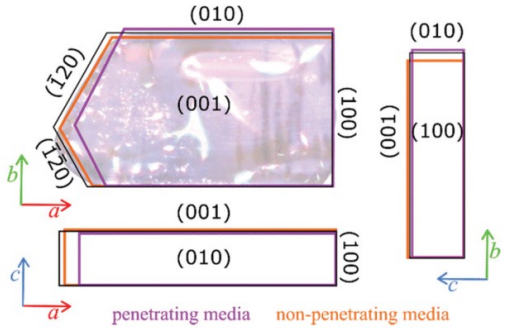

Fig. 3 Crystal contours (black) overlayed with a photo of a DMOF crystal (at 0.1 MPa), and the contours of this sample compressed in non-penetrating (orange, 1.20 GPa) and penetrating (purple, 1.18 GPa) media. The crystal contours are shown in three projections, to better represent the effect of negative linear compression (NLC) along the [*y*] direction (in non-penetrating media) and the activated expansion along the [*z*] direction (in penetrating media), respectively.

phenomenon, thus allowing additional molecules to penetrate the structure. This intake proceeds continuously until a pressure of 1.2 GPa is reached, after which the DMOF framework likely collapses; no diffraction pattern was observed above 1.2 GPa, suggesting that the crystal becomes amorphous. Analogous mechanochemical behaviour was also observed in other MOFs.[33] It is characteristic that the compression of DMOF crystals in non-penetrating PTM does not result in the amorphization or deterioration of the crystal quality, whereas the penetrating PTM leads to the crystal amorphization. This behaviour is different than that in most porous crystals, where the internal pressure of the PTM compressed inside the pores supports their walls, which precludes their collapse. It appears that the uptake of the PTM continues with pressure and at some point destabilize the framework, or that pressure higher than 1.2 GPa triggers shifts of the guests and collapses of portions of the pores.

Although we did not observe the hoped-for cyclisation of *m-btcp*, we have established that DMOF exhibits interesting mechanochemical behaviour when compressed in non-penetrating and penetrating media. Owing to the strong and inverse elastic responses between negative and positive deformation in two orthogonal directions, DMOF can be considered as a molecular sensor capable of detecting molecules of different sizes in its compressed environment. The most interesting property of DMOF is that its NLC in the non-penetrating media contrasts with the elongation along another direction in a penetrating PTM. This unique feature could be applied as a switch of sensors of fluids (operating under pressure, like in oil pipes) or micro mechanisms controlled by hydraulic systems. Certainly, a library of materials with such exceptional mechanical and mechanochemical properties is needed.

Conflicts of interest

There are no conflicts to declare.

Acknowledgements

AP, SS and AK are grateful to the Polish National Science Centre (grant OPUS 10 No. UMO-2015/19/B/ST5/00262). SS also thanks grant POWR.03.02.00-00-I023/17 and AP grant POWR.03.02.00-00-I026/16 co-financed by the European Union through the European Social Fund under the Operational Program Knowledge Education Development for the finical support. VIN and LJB thank the National Research Foundation (NRF) of South Africa for financial support.

Notes and references

1 H. Li, K. Wang, Y. Sun, C. T. Lollar, J. Li and H. C. Zhou, *Mater. Today*, 2018, **21**, 108–121.
2 E. A. Dolgopolova, A. M. Rice, C. R. Martin and N. B. Shustova, *Chem. Soc. Rev.*, 2018, **47**, 4710–4728.
3 J. Lee, O. K. Farha, J. Roberts, K. A. Scheidt, S. T. Nguyen and J. T. Hupp, *Chem. Soc. Rev.*, 2009, **38**, 1450–1459.
4 G. Férey, C. Serre, C. Kreuz, L. Cynober, Y. K. Hwang, T. Baati, P. Horcajada, T. Chalati, B. Gillet, S. Gil, P. Clayette, J.-S. Chang, D. Heurtaux, J. F. Eubank, P. Couvreur, C. Sebrie, R. Gref, P.-N. Bories and V. Marsaud, *Nat. Mater.*, 2009, **9**, 172–178.
5 H. C. J. Zhou and S. Kitagawa, *Chem. Soc. Rev.*, 2014, **43**, 5415–5418.
6 A. J. Graham, J. C. Tan, D. R. Allan and S. A. Moggach, *Chem. Commun.*, 2012, **48**, 1535–1537.
7 F. X. Coudert, *Chem. Mater.*, 2015, **27**, 1905–1916.
8 Z. Su, Y. R. Miao, G. Zhang, J. T. Miller and K. S. Suslick, *Chem. Sci.*, 2017, **8**, 8004–8011.
9 W. Cai and A. Katrusiak, *Nat. Commun.*, 2014, **5**, 4337.
10 A. Półrolniczak, S. Sobczak and A. Katrusiak, *Inorg. Chem.*, 2018, **57**, 8942–8950.
11 G. Tabacchi, *ChemPhysChem*, 2018, **19**, 1249–1297.
12 I. E. Collings and A. L. Goodwin, *J. Appl. Phys.*, 2019, **126**, 181101.
13 A. Lanza, L. S. Germann, M. Fisch, N. Casati and P. Macchi, *J. Am. Chem. Soc.*, 2015, **137**, 13072–13078.
14 P. Vervoorts, J. Keupp, A. Schneemann, C. L. Hobday, D. Daisenberger, R. A. Fischer, R. Schmid and G. Kieslich, *Angew. Chem.*, 2021, **133**, 800–806.
15 N. K. Kulachenkov, D. Sun, Y. A. Mezenov, A. N. Yankin, S. Rzhevskiy, V. Dyachuk, A. Nominé, G. Medjahdi, E. A. Pidko and V. A. Milichko, *Angew. Chem., Int. Ed.*, 2020, **59**, 15522–15526.
16 R. Pardo, M. Zayat and D. Levy, *Chem. Soc. Rev.*, 2011, **40**, 672–687.
17 S. Kobatake, K. Uchida, E. Tsuchida and M. Irie, *Chem. Commun.*, 2002, **2**, 2804–2805.
18 D. Kitagawa, H. Nishi and S. Kobatake, *Angew. Chem., Int. Ed.*, 2013, **52**, 9320–9322.
19 F. Luo, C. B. Fan, M. B. Luo, X. L. Wu, Y. Zhu, S. Z. Pu and W. Xu, *Angew. Chem., Int. Ed.*, 2014, **53**, 9298–9301.
20 D. E. Williams, J. A. Rietman, J. M. Maier, R. Tan, A. B. Greytak, M. D. Smith, J. A. Krause and N. B. Shustova, *J. Am. Chem. Soc.*, 2014, **136**, 11886–11889.
21 H. Sato, R. Matsuda, S. Kitagawa, Y. Zheng, H. J. Jeon and P. Wu, *Nat. Commun.*, 2017, **8**, 100.
22 K. Matsuda, K. Takayama and M. Irie, *Inorg. Chem.*, 2004, **43**, 482–489.
23 V. I. Nikolayenko, S. A. Herbert and L. J. Barbour, *Chem. Commun.*, 2017, **53**, 11142–11145.
24 Y. Zheng, H. Sato, P. Wu, H. J. Jeon, R. Matsuda and S. Kitagawa, *Nat. Commun.*, 2017, **8**, 100.
25 S. Sobczak, A. Półrolniczak, P. Ratajczyk, W. Cai, A. Gładysiak, V. I. Nikolayenko, D. C. Castell, L. J. Barbour and A. Katrusiak, *Chem. Commun.*, 2020, **56**, 4324–4327.
26 A. Katrusiak, *Acta Crystallogr., Sect. B: Struct. Sci., Cryst. Eng. Mater.*, 2019, **75**, 918–926.
27 P. G. Yot, Q. Ma, J. Haines, Q. Yang, A. Ghoufi, T. Devic, C. Serre, V. Dmitriev, G. Férey, C. Zhong and G. Maurin, *Chem. Sci.*, 2012, **3**, 1100–1104.
28 C. L. Hobday, C. H. Woodall, M. J. Lennox, M. Frost, K. Kamenev, T. Düren, C. A. Morrison and S. A. Moggach, *Nat. Commun.*, 2018, **9**, 1–9.
29 A. J. Graham, D. R. Allan, A. Muszkiewicz, C. A. Morrison and S. A. Moggach, *Angew. Chem., Int. Ed.*, 2011, **50**, 11138–11141.
30 S. A. Moggach, T. D. Bennett and A. K. Cheetham, *Angew. Chem.*, 2009, **121**, 7221–7223.
31 K. W. Chapman, G. J. Halder and P. J. Chupas, *J. Am. Chem. Soc.*, 2009, **131**, 17546–17547.
32 S. Sobczak and A. Katrusiak, *Inorg. Chem.*, 2019, **58**, 11773–11781.
33 S. C. McKellar and S. A. Moggach, *Acta Crystallogr., Sect. B: Struct. Sci., Cryst. Eng. Mater.*, 2015, **71**, 587–607.
34 A. B. Cairns and A. L. Goodwin, *Phys. Chem. Chem. Phys.*, 2015, **17**, 20449–20465.
35 C. F. Macrae, I. J. Bruno, J. A. Chisholm, P. R. Edgington, P. Mccabe, E. Pidcock, L. Rodriguez-monge, R. Taylor, J. Van De Streek and P. A. Wood, *J. Appl. Crystallogr.*, 2008, **41**, 466–470.
36 J. C. Tan, T. D. Bennett and A. K. Cheetham, *Proc. Natl. Acad. Sci. U. S. A.*, 2010, **107**, 9938–9943.
37 A. U. Ortiz, A. Boutin, A. H. Fuchs and F.-X. Coudert, *J. Chem. Phys.*, 2013, **138**, 174703.
38 S. M. J. Rogge, M. Waroquier and V. Van Speybroeck, *Acc. Chem. Res.*, 2018, **51**, 138–148.

A4

Self-healing ferroelastic metal-organic framework sensing guests, pressure and chemical environment

A. Półrolniczak, A. Katrusiak.

Materials Advances 2 (14), 4677-4684, 2021.

Materials Advances

ROYAL SOCIETY OF CHEMISTRY

PAPER

View Article Online
View Journal | View Issue

Check for updates

Cite this: *Mater. Adv.*, 2021, 2, 4677

Self-healing ferroelastic metal–organic framework sensing guests, pressure and chemical environment†

Aleksandra Półtrolniczak and Andrzej Katrusiak *

Received 5th February 2021,
Accepted 21st May 2021

DOI: 10.1039/d1ma00111f

rsc.li/materials-advances

Strong strain shuttering ferroelastic crystals that self-heal after releasing the strain have been revealed for a new metal–organic framework $[Cd(BDC)(AZPY)]_n$ (BDC = terephthalic acid; AZPY = 4,4′-azobispyridine), with the Cd(II) cation hepta-coordinated. It has been obtained in the form of single crystals without and with guests, acetonitrile or DMF (dimethylformamide). This pleochroic porous complex, hereafter referred to as AMU3, is built of two interwoven frameworks with the planar AZPY linkers (C_{2h} symmetric) orientationally disordered on the D_{2h} sites. The disorder of AZPY linkers persists down to 100 K at least, but it is eliminated by high pressure. The onset of AZPY ordering in the 0.2–0.9 GPa range depends both on the guest and on the hydrostatic fluid. The mechanism of AMU3 ferroelasticity involves the AZPY disordering in prototypic orthorhombic phase α of space-group *Cmce*. The AZPY ordering reduces the symmetry of phase β to monoclinic subgroup $P2_1/n$. The shear strain in the bulk of ferroelastic orientational-state domains is accommodated by the tilts and conformational changes of the ordered AZPY linkers, while along the boundaries between domains the Cd–N bonds break. On releasing the pressure the Cd–N bonds are restored and the signs of the cracks disappear.

Introduction

Rational design and synthesis of functional metal–organic frameworks (MOFs) requires a palette of accessories in the form of chemical components of predictable features and transitions in various thermodynamic conditions. The key factors are the topological architectures of MOFs and a selection of appropriate building blocks.[1–3] Usually, frameworks of desired topologies can be obtained by selecting the size and valence of cations, as well as geometrically defined building blocks of organic linkers.[4] Such materials are often thermally and mechanically stable even after removing the guest molecules.[5–9] These features are found in ligands commonly used as organic building blocks, for example rigid benzene di-, tri-, and tetra-carboxylates, and azolate-based ligands, as well as their derivatives. Also flexible molecules, such as 4,4′-azo(bis)pyridine (AZPY, Fig. 1), are known for effective bridging coordination capabilities.[10–12] The AZPY linkers often exhibit disorder, most often in two positions due to the strong conjunction of the alternative π-electron bonds across the molecule and the flat pyridyl moieties.[13,14] In azopyridine there are two types of coordination sites involving the nitrogen atoms: those in pyridyl moieties and those in the azo bridge. The pyridyl ring has been employed in a variety of coordination geometries. Depending on the metal center, it is possible to construct a wide range of compounds, such as multinuclear complexes (in the forms of dimers, squares, and rectangles), molecular frameworks (for instance brick-wall, herringbone, or wave-like motifs), and coordination polymers. The coordination mode involving the azo bridge is less common. A variety of MOFs containing AZPY have been prepared and characterized.[15–18] In such sorbent materials, the primary sites of gas adsorption in the pores are very important. As a result of free basic centers ('azo' nitrogens) in the AZPY molecule, these nitrogen atoms can serve as the primary adsorbers. Moreover, the AZPY linkers can undergo conformational changes, activated by light.[19–23]

Owing to their internal structure, MOFs are highly elastic and pressure-sensitive.[24–29] These features can be further increased by flexible linkers and large voids. Pressure is a thermodynamic variable that affects the volume of crystals more efficiently than it is done by temperature.[30–32] Under

Department of Materials Chemistry, Faculty of Chemistry, Adam Mickiewicz University, Uniwersytetu Poznańskiego 8, 61-614, Poznan, Poland. E-mail: katran@amu.edu.pl

† Electronic supplementary information (ESI) available: Experimental details, Raman spectra, results of quantum-mechanical calculations, compressibility and thermal expansion analysis, framework topology scheme, survey on the CCDC database concerning the AZPY linker, void volume changes, pleochroic effect, compressibility calculations, and detailed crystallographic data; supplementary movie: self-healing of AMU3 (mp4); CCDC 2046185–2046192, 2046198–2046205, 2046207–2046212, 2046216–2046220 and 2046409. For ESI and crystallographic data in CIF or other electronic format see DOI: 10.1039/d1ma00111f

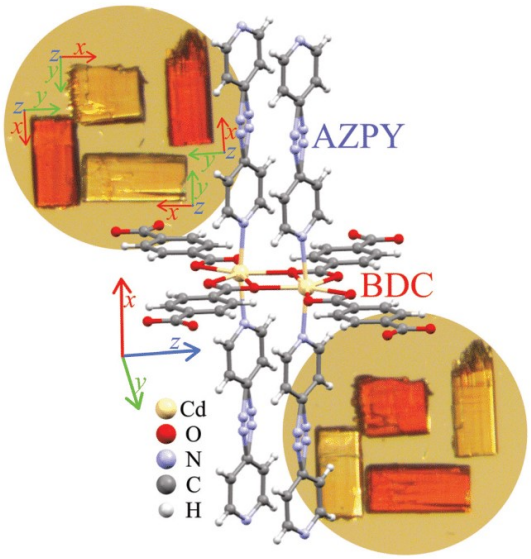

Fig. 1 The double Cd(II) centre coordinated by AZPY and BDC linkers in AMU3 under normal conditions, including both sites of disordered AZPY linkers. In the first inset, several single-crystal AMU3 samples are aligned parallel and perpendicular to the polarized light, then rotated by 90° for the second inset.

high pressure all (one-phase) materials contract in volume.[33,34] This compression can be isotropic or anisotropic. The compression of most materials is positive in all directions; however occasionally the negative linear compression[35–39] and negative area[40–43] compression are observed. Anomalous compression can be caused by an uptake of guest[29,44–48] or its release,[49–51] as well as solid-state phase transitions[52,53] and chemical reactions.[54–61] The most typical pressure-induced changes affect the voids, which are most relevant to sorption and elastic properties of MOFs. Many crystals undergoing phase transitions induced by hydrostatic pressure, or when subjected to none uniform stress, fracture and even break into pieces, which disqualifies their application or significantly limits the scope and time of their performance. There are also materials capable of self-healing their fractures,[62,63] which is particularly needed in the active sensor parts.[64–66]

Here we report a new MOF, Cd(BDC)(AZPY), abbreviated as AMU3, synthesized of 4,4′-azopyridine and terephthalic acid (1,4-benzenedicarboxylic acid = BDC) with $Cd(NO_3)_2{\cdot}4H_2O$, and solvent guest molecules. We have performed the pore activation process of AMU3·DMF (DMF = dimethylformamide) leading to guest-free AMU3 that when soaked with acetonitrile (MeCN) yielded AMU3·MeCN. We found that all these compounds are ferroelastic, and that their critical pressure and orientation-states strongly depend on the exchangeable guests. The exchange of guests provides a convenient method for tuning the ferroelastic properties, required for the materials used in chemo-mechanic transducers and various sensor applications. Under pressure the AMU3 crystals become fractured, but they exhibit a self-healing property in the prototypic phase.

Experimental

We have synthesized single-crystals of AMU3 by a slow-diffusion technique. In this method the substrates are dissolved in low- and high-density solvents and then placed one above another in a test tube. The speed of diffusion can be controlled by introducing an intermediate layer, usually of a mixture of pure solvents (1 : 1 vol.). Then the test tube is tightly closed. In this way, within 8 days orange elongated block AMU3 crystals are formed. After removing from the solvent, they are stable in air. Detailed information about the synthesis is presented in the ESI.†

Pore activation

The applications for gas storage or gas-phase catalysis are scalable with large internal surface areas. In some MOFs the pores are blocked by molecules of solvents or other substances used for synthesis. Some of the frameworks collapse during the pore activation process, *i.e.* the removal of guest molecules. The most effective and general strategies for removing guest molecules are (i) conventional heating and exposure to vacuum; (ii) solvent exchange; (iii) supercritical CO_2 ($scCO_2$) processing; (iv) freeze-drying; and (v) chemical treatment.[67]

For activating the pores in AMU3 we chose the methods of (ii) solvent exchange and (iv) $scCO_2$ processing. The Cd(BDC)(AZPY)·DMF crystals have been immersed in chloroform and left for 3 days. The subsequent single-crystal diffraction measurements detected no guest molecules in the pores. During the pore activation, the quality of single-crystals decreased, which was manifested by a lower resolution of the diffraction data and broader reflections. After immersing the activated crystals in acetonitrile, its molecules penetrated into the pores and the quality of single-crystals improved. In the case of $scCO_2$ processing, we have also obtained the guest-free structure, but mainly in the form of fine powder, naturally appearing green in the scattered light, which is the complement of deep orange colour of the light transmitted through the crystals. A similar change between the complementing deep-orange and green shades occurs between high-quality single crystals and the damaged samples (Fig. 2).

Non-ambient X-ray diffraction

We performed three series of high-pressure studies, each for the AMU3 crystal with different guest molecules in the pores and for different pressure-transmitting media (PTM). AMU3·DMF was compressed in a 16 : 3 : 1 (vol.) mixture of methanol : ethanol : water (MEW) and in glycerin, assuring the hydrostatic conditions up to 10.5 GPa and ~3.5 GPa, respectively.[68] We observed a monotonic compression of AMU3·DMF up to 0.4 GPa, when a phase transition changed the crystal symmetry from orthorhombic space group *Cmce* to monoclinic space group $P2_1/n$.

High-pressure experiments on AMU3 were performed in a Merrill–Bassett diamond anvil cell (DAC),[69] modified by mounting the diamond anvils directly onto the steel supports with conical windows. The pressure in the DAC was calibrated by the ruby-fluorescence method with a photon control spectrometer,

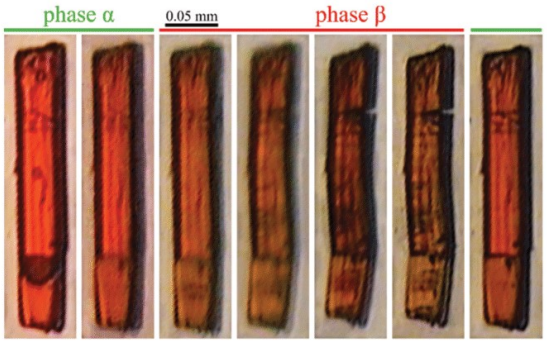

Fig. 2 AMU3·DMF crystal compressed and decompressed in methanol : ethanol : water mixture used as the hydrostatic medium. The green shade of the sample in phase β is the light scattered on microfractures. The crystal axes in phase α are [z] along the viewing direction; [y] horizontal and [x] vertical.

affording the accuracy of 0.03 GPa.[70,71] The gaskets were made of a 0.3 mm thick tungsten foil with spark-eroded holes of 0.5 mm in diameter. The X-ray diffraction data were measured on an Xcalibur EOS-CCD diffractometer with Mo Kα radiation (λ = 0.71073 Å). The DAC was centered by the gasket-shadow method.[72] The collected data were preliminarily reduced with the *CrysAlisPro* suite, version 171.38.46.[73] *OLEX2* was used.[74] The structure was solved by direct methods with *SHELXS* and least-squares refined with *SHELXL*.[75,76]

The ambient-pressure structure was the starting model for the refinements of low-temperature and high-pressure structures. In high-pressure experiments the DAC absorption corrections and gasket shadowing were calculated by the program *REDSHABS*.[77,78] The low-temperature data were measured for the single-crystal mounted on a microloop on an Xcalibur EOS-CCD diffractometer equipped with a gas-flow Oxford Cryostream attachment between 100 and 297 K in 40 K steps. All non-H atoms were refined with anisotropic thermal parameters. H atoms were located in the difference Fourier map and from the molecular geometry. The final crystal data are summarized in Table 1 (*cf.* Tables S7–S10, ESI†).

Results and discussion

The AMU3 crystal is built of two interwoven frameworks Cd(BDC)(AZPY), as illustrated in Fig. 3. In phase α the CdBDC

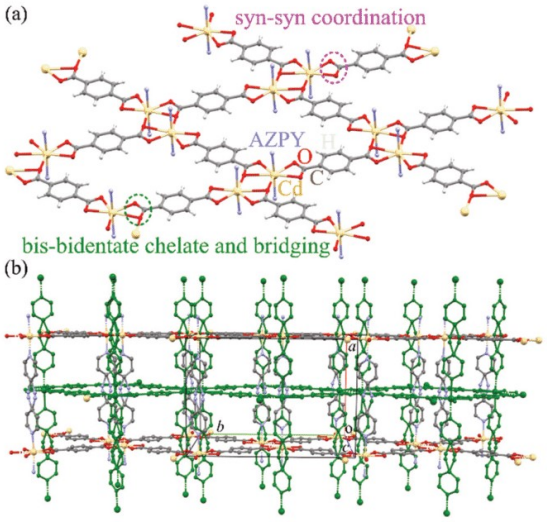

Fig. 3 (a) One CdBDC sheet, with added N-atoms of AZPY linkers, extending along crystal plane (100); and (b) autostereogram of two interwoven frameworks, one coloured green, with AZPY linkers penetrating through the holes of two CdBDC sheets of another framework shown in yellow (Cd), grey (C), red (O) and blue (N). The DMF molecules and H atoms are skipped for clarity.

sheets are perfectly planar, as they are located on mirror planes perpendicular to the crystal [100] direction. In these sheets there are large holes inside the rings of four BDC anions coordinating Cd cations. The Cd cations are present in double-core tandem arrangement coordinated by four BDC anions, all within the planar sheet. On both sides of the CdBDC sheets, each Cd cation forms two other coordination bonds to AZPY molecules aligned parallel to direction [100]. Each CdBDC sheet is connected with next CdBDC sheets by the AZPY linkers, which on both sides penetrate through the rings of the closest CdBDC sheets belonging to the other framework.

Lattice strain

At ambient pressure the lattice of interwoven Cd(BDC)(AZPY) frameworks is orthorhombic, because the disordered AZPY molecules in the planar conformation are perpendicular to the CdBDC sheets (Fig. 3 and Fig. S5, ESI†). The disordered AZPY molecules acquire the average D_{2h} symmetry, which is higher compared to the C_{2h} symmetry of the ordered molecule

Table 1 Selected crystallographic data of AMU3 phases α and β compressed in methanol : ethanol : water (MEW, 16 : 3 : 1 vol.) mixture and glycerin (Gly)

Phase		α	α	α	β	β	β	α	β	α	β
PTM:		None	None	MEW	MEW	MEW	MEW	Gly	Gly	MEW	MEW
Guest:		DMF	MeCN	DMF	DMF	DMF	DMF	DMF	DMF	MeCN	MeCN
Pressure (GPa)		0.0001	0.0001	0.3	0.8	1.27	3.66	0.4	1.12	0.6	0.8
Space group		*Cmce*	*Cmce*	*Cmce*	$P2_1/n$	$P2_1/n$	$P2_1/n$	*Cmce*	$P2_1/n$	*Cmce*	$P2_1/n$
Unit-cell:	*a* (Å)	13.7238(4)	13.6976(4)	13.643(3)	12.162(3)	11.996(4)	11.362(6)	13.729(2)	12.241(12)	13.6195(11)	12.372(3)
	b (Å)	20.7039(6)	20.7250(7)	20.739(3)	13.928(18)	13.77(3)	13.31(3)	20.856(4)	13.970(11)	20.7923(17)	14.15(3)
	c (Å)	14.7091(4)	14.6495(5)	14.20(2)	12.574(3)	12.629(4)	13.269(8)	14.403(2)	12.627(11)	14.241(15)	12.433(4)
	β (°)	90	90	90	113.67(3)	113.84(4)	115.07(7)	90	113.67(9)	90	113.58(3)
V (Å^3)		4179.4(2)	4158.7(2)	4019(6)	1951(3)	1908(5)	1818(5)	4124.0(12)	1978(3)	4033(4)	1995(4)
Z/Z'		8/0.5	8/0.5	8/0.5	4/1	4/1	4/1	8/0.5	4/1	8/0.5	4/1

in the planar conformation. The ordered AZPY molecules in their energetically optimized conformation are skew, as the diazo-bridge shifts the axes of the pyridyls aside by 2.8 Å, which would induce a shear displacement of the sheets along the crystal axis y_o (index 'o' indicates the orthorhombic phase α). No such ferroelastic strain and no ordering of the AZPY linkers was observed on cooling the crystals down to 100 K. At such low temperatures the dynamic disorder of either the diazo-bridge or all of the AZPY molecule is highly unlikely. The dynamic disorder of the azo-bridge would imply either quick rotations of all AZPY molecules (their conformation fixed planar) along their longest axis or a pedal-like movement of the pyridyls, which would require overcoming the potential-energy barrier between favoured planar conformations. Thus it is plausible that in the AMU3 phase α the static disorder of the AZPY linkers is present not only at low temperatures but also above room temperature. Therefore we have studied the AMU3 crystals under high hydrostatic pressure, which eliminates the disorder primarily through the volume reduction, and not through the temperature-controlled energy of vibrations. Indeed, at high pressure an onset of ordering of AZPY molecules induces the phase transition to monoclinic phase β. The phase transition occurs at the critical pressure (p_c), which depends on the guest molecules and hydrostatic medium (Fig. 4).

Our X-ray diffraction structural determinations show that at p_c the AZPY linkers become ordered and their conformation changes from planar to twisted – the inclination of the pyridine rings increases with pressure: at 1 GPa they are inclined by 2.02° (between the average planes of pyridine rings C2′ C3′ C4′ C5′ C6′ N1′ N2′ and C2″ C3″ C4″ C5″ C6″ N1″ N2″, as indicated in Fig. 5) and at 3.66 GPa this inclination increases to 30.76° (Fig. 5). Thus the flexibility of the AZPY linkers is connected with the ferroelastic properties of the AMU3 crystal. Its prototypic phase α is associated with the AZPY linkers disordered,

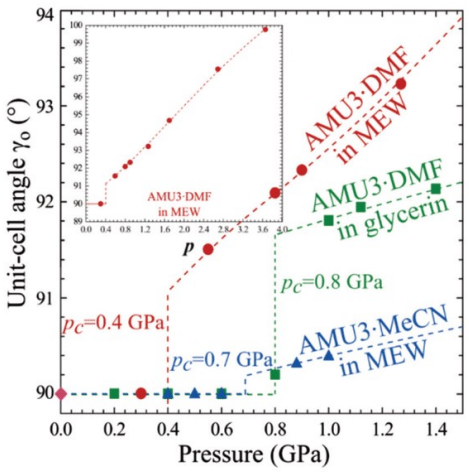

Fig. 4 Monoclinic strain in AMU3·DMF and AMU3·MeCN as a function of pressure. The inset extends the pressure range for AMU3·DMF compressed in methanol : ethanol : water (MEW, 16 : 3 : 1 vol.) mixture.

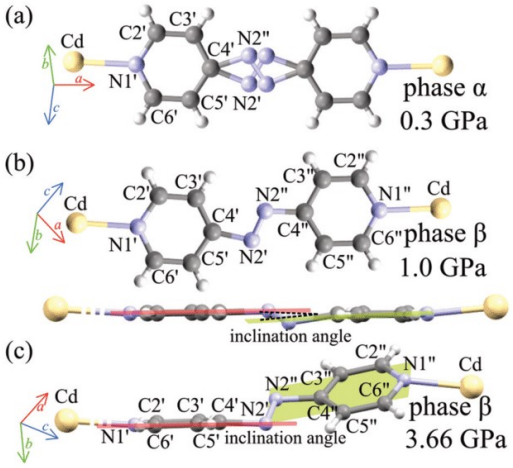

Fig. 5 The AZPY linker in Cd(BDC)(AZPY): (a) disordered in phase α; (b) ordered and somewhat distorted from coplanarity in phase β (viewed perpendicular and parallel to the pyridyl rings); and (c) ordered-twisted at 3.66 GPa.

while the shear strain of orientational states in phase β is regulated by the tilts of ordered AZPY linkers and their conformation.

The transition between phases α and β can be described by the order parameter η connected with the ordering of the AZPY molecules:

$$\eta = \left|\mathrm{SOF}(\mathrm{N}_2') - \mathrm{SOF}(\mathrm{N}_2'')\right|,$$

where N_2' denotes azo group N2′ = $\mathrm{N2}''_{\mathrm{A}}$, and N_2'' is N2″ = $\mathrm{N2}'_{\mathrm{A}}$ (subscript 'A' indicates the symmetry operation through the mirror plane perpendicular to crystal direction [100]), $\mathrm{SOF}(\mathrm{N}_2')$ and $\mathrm{SOF}(\mathrm{N}_2'')$ are the site occupation factors of the disordered azo groups (*cf.* Fig. 5 for atomic labels N2′, N2″ and their disordered sites). In phase α the SOF values are equal to 0.5, so the order parameter η = 0, and for phase β the ordered azo groups give η = 1.

The Bravais lattice *C* of phase α is orthorhombic, but in phase β it becomes monoclinic *P*, as illustrated in Fig. 6. For describing the shear strain of the lattice we have chosen the γ_o angle of the unit cell in phase α (subscript 'o' refers to orthorhombic phase α, 'm' to monoclinic phase β). The unit-cell vectors between phases α (a_o, b_o, c_o) and β (a_m, b_m, c_m) are transformed through matrices:

$$\begin{pmatrix} a_m \\ b_m \\ c_m \end{pmatrix} = \begin{pmatrix} 0.5 & -0.5 & 0 \\ 0 & 0 & -1 \\ 0.5 & 0.5 & 0 \end{pmatrix} \begin{pmatrix} a_o \\ b_o \\ c_o \end{pmatrix}$$

and

$$\begin{pmatrix} a_o \\ b_o \\ c_o \end{pmatrix} = \begin{pmatrix} 1 & 0 & 1 \\ -1 & 0 & 1 \\ 0 & -1 & 0 \end{pmatrix} \begin{pmatrix} a_m \\ b_m \\ c_m \end{pmatrix}$$

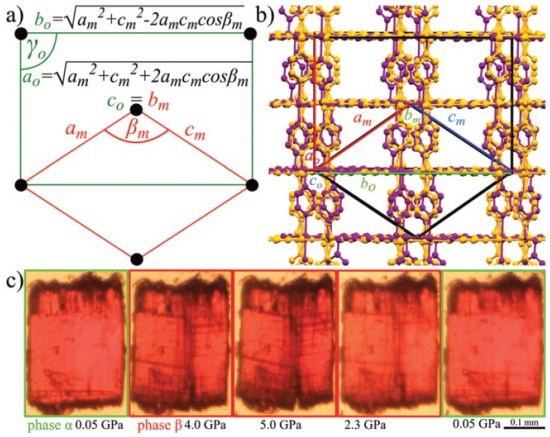

Fig. 6 (a) Lattice relations between the prototypic orthorhombic phase α (green) and monoclinic orientational state (red) in ferroelastic crystal AMU3. (b) Orthorhombic (yellow) and monoclinic (purple) AMU3 structures (measured at 0.1 MPa and 1.27 GPa, respectively), compared by overlaying their ball-and-stick drawings. Indexes 'o' and 'm' refer to phases α and β, respectively. (c) Photographs of a sample crystal with defects appearing in the compressed β phase along planes $(100)_o$ and $(010)_o$, and the cleavage of the crystal along $(010)_o$ (*cf.* Movie S1, ESI†).

Thus the monoclinic strain η' of phase β can be measured as the distortion of angle γ_o from 90°

$$\eta' = \pm(\gamma_o - 90^\circ),$$

where signs plus and minus correspond to two possible ferroelastic orientational states, $\gamma_o = \cos^{-1}\{(a_m^2 - c_m^2)/(a_o \cdot b_o)\}$, $a_o = (a_m^2 + c_m^2 + 2a_m c_m \cos\beta_m)^{1/2}$ and $b_o = (a_m^2 + c_m^2 - 2a_m c_m \cos\beta_m)^{1/2}$. It is also possible to choose the order parameter η'' of this ferroelastic as a difference between the primitive cell parameters: $\eta'' = \pm(a_m - c_m)$, or the relevant diagonals of the *C*-lattice cell.

Crystal damage and self-healing

The lattice strain described above results in the cleavage of the crystal samples. The cleavage occurs at about 3 GPa, *i.e.* well above the phase transition when the shear strain η' increases to about 5° (the inset in Fig. 4), and so the angle between the cleaved planes becomes *circa* 10° (Fig. 2). It appears that between 0.4 and 2.0 GPa (for the AMU3·DMF sample compressed in methanol:ethanol:water) the shear strain is partly accommodated by the elasticity of the crystal, and also by micro fractures, which produces a greenish tint of the scattered light (Fig. 2), or as plane defects clearly visible as thin lines in Movie S1 (see the ESI†). It is apparent from the pleochroic colours that the domain walls are formed along crystal planes $(010)_o$ and/or $(100)_o$. The directions of defects can be easily identified according to the pleochroic colours (*cf.* Movie S1, ESI†). These domain walls along $(010)_o$ and $(100)_o$ are present in the sample shown in Fig. 6c. The orientation of the domain walls illustrate the monoclinic strain building up in the sample crystal and that it breaks just along one of the planes, which is sufficient for releasing the strain. Movie S1 (ESI†) shows that the large fractures formed above 3.0 GPa almost completely disappear for reiterated cycles of increased and decreased pressure. Such a self-healing property is sought for its practical applications.[62,79–81] The structural mechanism revealed for the AMU3 crystals, and in particular the rotations and tilts of the linkers as well as their conformational distortions, can be used for designing new self-healing materials.

Strain-structure coupling

As described above, the η' strain originates from the AZPY linkers and their N–Cd coordination bonds. The tilts of the AZPY molecules are consistent in shifting the CdBDC sheets along axis b_o. The order and disorder of the AZPY linkers in phases α and β have some effects on their sorption properties. The shear strain folds the framework and in this way the voids are reduced in volume (Fig. 7). The disordered AZPY linkers occupy more space, so the disorder elimination in phase β increases the space available for guests, but at still higher pressure the shear strain is to some extent limited by the framework stiffness. After the disorder elimination a further volume reduction of the voids is achieved through the conformational twisting of the AZPY molecules. We have found that these transformations depend on the guest and are sensitive to the crystal environment. The guests clearly affect the unit-cell dimensions and their compression, as shown in Fig. S3 in the ESI.† The disorder persists even at the liquid-nitrogen temperature, whereas it is efficiently eliminated at a fraction of one GPa. Thus the AZPY linkers can be used for designing the elastic properties of MOF crystals, and making

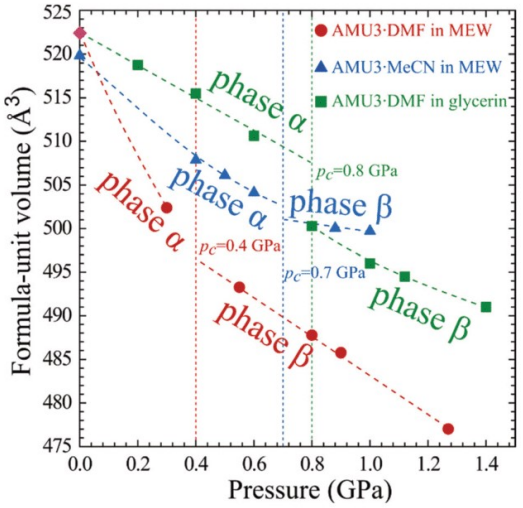

Fig. 7 Formula-unit volume for AMU3·DMF compressed in methanol : ethanol : water 16 : 3 : 1 mixture (MEW, red circles), AMU3·MeCN (acetonitrile) in MEW (blue triangles), and with DMF as a guest molecule compressed in glycerin (green squares). The ESDs are smaller than the plotted symbols.

them sensitive to chemical and mechanical stimuli, which can change their sorption and breathing properties. Fig. S6 (ESI†) shows that a considerable number of crystals containing AZPY molecules is disordered. It indicates that the pressure-induced transformations analogous to those in AMU3 may concern also other compounds.

It should be noted that the AMU3 crystals strongly change their volume under pressure and that this effect depends both on the guest molecules and on the PTM (Fig. 7 and Tables S1–S6, ESI†). The compression of phase α-AMU3·DMF compressed in MEW is over three times stronger compared to that of α-AMU3·DMF compressed in glycerin. Surprisingly, the largest volume change is observed for AMU3·DMF compressed in MEW, which in principle should allow the water and methanol molecules to penetrate easily into the pores, while the compression of AMU3·DMF in glycerin is least responsive to pressure. We have connected the observed compressibility differences with large voids in the AMU3 structure, and with the ability of the crystals to extrude the DMF molecules. This extrusion requires the presence of the MEW mixture, possibly because of the substitution of the DMF guests with much smaller water and methanol molecules from the crystal environment. Such an exchange is not possible for significantly more viscous glycerin liquid and with molecules much larger than the MEW components. The strong compression of α-AMU3·DMF is most likely caused by the altered contents of the voids. This reasoning is consistent with the transition pressure of α-AMU3·DMF compressed in MEW being lower than that of α-AMU3·DMF compressed in glycerin. The crystal with smaller guests or with partly filled voids can be expected to transform to the β phase at a lower pressure than that with the filled voids, and hence are better supported from inside and less prone to collapse.[82] The volume reduction of α-AMU3·MeCN compressed in MEW is intermediate between those of α-AMU3·DMF compressed in glycerin and in MEW, which strongly suggests that the contents of voids in α-AMU3·DMF compressed in MEW is reduced. All these observations indicate that the large volume reduction of α-AMU3·DMF compressed in MEW cannot be regarded as compressibility in the physical sense, but that it is connected to the reduced composition of the crystal.

Pleochroism of AMU3

Phase α-AMU3 has the structural property that all AZPY linkers are aligned parallel in the crystal structure, and all BDC linkers are perpendicular to this direction. Consequently, the optical properties of AMU3 crystals are strongly anisotropic, which leads to their strong pleochroism. The crystals are either transparent or red, as shown in Fig. 1 and Fig. S8 (ESI†). In phase β their perpendicular positions are off-set by a few degrees only, and the strong pleochroism remains.

Conclusions

Pleochroic crystals of AMU3 display several features attractive for sensor applications, as they are prone to the guest exchange, but are hardly affected by temperature and only the pressure leads to the ferroelastic strain. The crystals exhibit self-healing properties, which repair the damage induced by the phase transition to the ferroelastic orientational states. This type of damage disqualifies many ferroelastic materials from practical applications. We have shown that the interplay of the framework topology with the flexibility of linkers can lead to specific types of structural transformations of MOFs. In AMU3 the rigid sheets of Cd(II)-BDC contrast with the AZPY linkers disordered in two orientations. The disorder is coupled to the lattice strain and is sensitive to the guest types and to the crystal environment, which can be applied in chemo-mechanical transducers in sensors. The survey of MOFs involving AZPY linkers reveals a considerable number of similarly disordered structures (76 out of 173), which can display analogous properties. Furthermore, the number of disordered azopyridine linkers in any kind of compound is similarly high: there are 466 structures with the 'disorder' descriptor in the CCDC version 2020.0, and some properties of AMU3 can be applicable to those structures, too. These numbers show that the possible disorder and conformational properties of AZPY molecules can be considered when designing the structures of MOFs aimed at specific properties and applications.

Conflicts of interest

There are no conflicts to declare.

Acknowledgements

Authors are grateful to Dr Szymon Sobczak for his advice and helpful comments. This research was supported by funding from the Polish National Science Centre: OPUS 10 No. UMO-2015/19/B/ST5/00262; PRELUDIUM 18 No. UMO-2019/35/N/ST5/01838 and grant POWR.03.02.00-00-I026/16 co-financed by the EU European Social Fund under the Operational Program Knowledge Education Development.

Notes and references

1 H. C. Zhou, J. R. Long and O. M. Yaghi, *Chem. Rev.*, 2012, **112**, 673–674.
2 J. Liu, D. Zhu, C. Guo, A. Vasileff and S. Qiao, *Adv. Energy Mater.*, 2017, **1700518**, 1–26.
3 D. Zhao, D. J. Timmons, D. Yuan and H.-C. Zhou, *Acc. Chem. Res.*, 2011, **44**, 123–133.
4 N. Novendra, J. M. Marrett, A. D. Katsenis, H. M. Titi, M. Arhangelskis, T. Friščić and A. Navrotsky, *J. Am. Chem. Soc.*, 2020, **142**, 21720–21729.
5 J. E. Mondloch, O. Karagiaridi, O. K. Farha and J. T. Hupp, *CrystEngComm*, 2013, **15**, 9258–9264.
6 K. A. Zenere, S. G. Duyker, E. Trzop, E. Collet, B. Chan, P. W. Doheny, C. J. Kepert and S. M. Neville, *Chem. Sci.*, 2018, **9**, 5623–5629.
7 H. Li, M. Eddaoudi, M. O'Keeffe and O. M. Yaghi, *Nature*, 1999, **402**, 276–279.

8 H. J. Park, D. Lim, W. S. Yang, T. Oh and M. P. Suh, *Chem. – Eur. J.*, 2011, **17**, 7251–7260.
9 J. Sotelo, C. H. Woodall, D. R. Allan, E. Gregoryanz, R. T. Howie, K. V. Kamenev, M. R. Probert, P. A. Wright and S. A. Moggach, *Angew. Chem.*, 2015, **127**, 13530–13534.
10 G. Sezer, M. Arici, İ. Erucar, O. Z. Yeşilel, H. U. Özel, B. T. Gemici and H. Erer, *J. Solid State Chem.*, 2017, **255**, 89–96.
11 A. M. Ako, C. S. Hawes, B. Twamley and W. Schmitt, *CrystEngComm*, 2017, **19**, 994–1000.
12 R. Haldar, S. Bonakala, P. Kanoo, S. Balasubramanian and T. K. Maji, *CrystEngComm*, 2014, **16**, 4877–4885.
13 S. Noro, M. Kondo, T. Ishii, S. Kitagawa and H. Matsuzaka, *J. Chem. Soc., Dalton Trans.*, 1999, 1569–1574.
14 G. J. Halder and C. J. Kepert, *Aust. J. Chem.*, 2005, **58**, 311–314.
15 S. Sanram, J. Boonmak and S. Youngme, *Inorg. Chim. Acta*, 2018, **469**, 11–19.
16 A. Vlad, M. Cazacu, M. Zaltariov, A. Bargan, S. Shova and C. Turta, *J. Mol. Struct.*, 2014, **1060**, 94–101.
17 R. Kumar, K. Jayaramulu, T. K. Maji and C. N. R. Rao, *Dalton Trans.*, 2014, **43**, 7383–7386.
18 G. Günay, O. Z. Yesilel, H. Erer, S. Keskin and A. Tabak, *Polyhedron*, 2015, **100**, 108–113.
19 Y. Chen, H. Yu, M. Quan, L. Zhang, H. Yang and Y. Lu, *RSC Adv.*, 2015, **5**, 4675–4680.
20 K. Aoki, M. Nakagawa and K. Ichimura, *J. Am. Chem. Soc.*, 2000, **122**, 10997–11004.
21 C. Bin Fan, Z. Q. Liu, L. Le Gong, A. M. Zheng, L. Zhang, C. S. Yan, H. Q. Wu, X. F. Feng and F. Luo, *Chem. Commun.*, 2017, **53**, 763–766.
22 Z.-J. Lin, T.-F. Liu, B. Xu, L.-W. Han, Y.-B. Huang and R. Cao, *CrystEngComm*, 2011, **13**, 3321–3324.
23 P. Kanoo, A. C. Ghosh, S. T. Cyriac and T. Kumar, *Chem. – Eur. J.*, 2012, **18**, 237–244.
24 I. E. Collings and A. L. Goodwin, *J. Appl. Phys.*, 2019, **126**, 1–13.
25 A. J. Graham, D. R. Allan, A. Muszkiewicz, C. A. Morrison and S. A. Moggach, *Angew. Chem., Int. Ed.*, 2011, **50**, 11138–11141.
26 S. A. Moggach, T. D. Bennett and A. K. Cheetham, *Angew. Chem., Int. Ed.*, 2009, **48**, 7087–7089.
27 S. C. Mckellar and S. A. Moggach, *Acta Crystallogr.*, 2015, **B71**, 587–607.
28 J. Navarro-Sánchez, I. Mullor-Ruíz, C. Popescu, D. Santamaría-Pérez, A. Segura, D. Errandonea, J. González-Platas and C. Martí-Gastaldo, *Dalton Trans.*, 2018, **47**, 10654–10659.
29 A. Celeste, A. Paolone, J. Itie, F. Borondics, B. Joseph, O. Grad, G. Blanita, C. Zlotea and F. Capitani, *J. Am. Chem. Soc.*, 2020, **140**, 15012–15019.
30 E. V. Boldyreva, *J. Mol. Struct.*, 2003, **647**, 159–179.
31 V. S. Minkov, N. A. Tumanov, R. Q. Cabrera and E. V. Boldyreva, *CrystEngComm*, 2010, **12**, 2551–2560.
32 R. Lee, J. A. K. Howard, M. R. Probert and J. W. Steed, *Chem. Soc. Rev.*, 2014, **43**, 4300–4311.
33 R. H. Baughman, R. H. Baughman and S. Stafstro, *Science*, 1998, **279**, 1522.
34 I. D. H. Oswald and C. M. Beavers, *CrystEngComm*, 2019, **21**, 4420–4421.
35 A. B. Cairns and A. L. Goodwin, *Phys. Chem. Chem. Phys.*, 2015, **17**, 20449–20465.
36 W. Cai and A. Katrusiak, *Nat. Commun.*, 2014, **5**, 1–8.
37 Z. Chen, B. Xu, Q. Li, Y. Meng, Z. Quan and B. Zou, *Inorg. Chem.*, 2020, **59**, 1715–1722.
38 J. Binns, K. V. Kamenev, K. E. R. Marriott, G. J. McIntyre, S. A. Moggach, M. Murrie and S. Parsons, *Chem. Commun.*, 2016, **52**, 7486–7489.
39 W. Li, M. R. Probert, M. Kosa, T. D. Bennett, A. Thirumurugan, R. P. Burwood, M. Parinello, J. A. K. Howard and A. K. Cheetham, *J. Am. Chem. Soc.*, 2012, **134**, 11940–11943.
40 W. Cai, A. Gładysiak, M. Anioła, V. J. Smith, L. J. Barbour and A. Katrusiak, *J. Am. Chem. Soc.*, 2015, **137**, 9296–9301.
41 S. A. Hodgson, J. Adamson, S. J. Hunt, M. J. Cliffe, A. B. Cairns, A. L. Thompson, M. G. Tucker, N. P. Funnell and A. L. Goodwin, *Chem. Commun.*, 2014, **50**, 5264–5266.
42 T. Lim, *Phys. Status Solidi B*, 2017, **1600682**, 1–11.
43 G. Feng, W. X. Zhang, L. Dong, W. Li, W. Cai, W. Wei, L. Ji, Z. Lin and P. Lu, *Chem. Sci.*, 2019, **10**, 1309–1315.
44 S. Sobczak, A. Półrolniczak, P. Ratajczyk, W. Cai, A. Gładysiak, V. I. Nikolayenko, D. C. Castell, L. J. Barbour and A. Katrusiak, *Chem. Commun.*, 2020, **56**, 4324–4327.
45 D. Fairen-Jimenez, S. A. Moggach, M. T. Wharmby, P. A. Wright, S. Parsons and T. Düren, *J. Am. Chem. Soc.*, 2011, **133**, 8900–8902.
46 S. C. McKellar, J. Sotelo, A. Greenaway, J. P. S. Mowat, O. Kvam, C. A. Morrison, P. A. Wright and S. A. Moggach, *Chem. Mater.*, 2016, **28**, 466–473.
47 N. Nijem, P. Canepa, U. Kaipa, K. Tan, K. Roodenko, S. Tekarli, J. Halbert, I. W. H. Oswald, R. K. Arvapally, C. Yang, T. Thonhauser, M. A. Omary and Y. J. Chabal, *J. Am. Chem. Soc.*, 2013, **135**, 12615–12626.
48 P. Z. Moghadam, J. F. Ivy, R. K. Arvapally, A. M. Dos Santos, J. C. Pearson, L. Zhang, E. Tylianakis, P. Ghosh, I. W. H. Oswald, U. Kaipa, X. Wang, A. K. Wilson, R. Q. Snurr and M. A. Omary, *Chem. Sci.*, 2017, **8**, 3989–4000.
49 S. Sobczak and A. Katrusiak, *Cryst. Growth Des.*, 2018, **18**, 1082–1089.
50 G. J. Halder, C. J. Kepert, B. Moubaraki, K. S. Murray and J. D. Cashion, *Science*, 2002, **298**, 1762–1765.
51 P. D. Southon, L. Liu, E. A. Fellows, D. J. Price, G. J. Halder, K. W. Chapman, B. Moubaraki, K. S. Murray, J. F. Létard and C. J. Kepert, *J. Am. Chem. Soc.*, 2009, **131**, 10998–11009.
52 M. Fisch, A. Lanza, E. Boldyreva, P. Macchi and N. Casati, *J. Phys. Chem. C*, 2015, **119**, 18611–18617.
53 B. A. Zakharov and E. V. Boldyreva, *CrystEngComm*, 2019, **21**, 10–22.
54 A. Półrolniczak, S. Sobczak and A. Katrusiak, *Inorg. Chem.*, 2018, **57**, 8942–8950.
55 S. Sobczak and A. Katrusiak, *Inorg. Chem.*, 2019, **58**, 11773–11781.
56 S. Sobczak, W. Drożdż, G. Lampronti, A. Belenguer, A. Katrusiak and A. R. Stefankiewicz, *Chem. – Eur. J.*, 2018, **24**, 8769–8773.

57 A. Lanza, L. S. Germann, M. Fisch, N. Casati and P. Macchi, *J. Am. Chem. Soc.*, 2015, **137**, 13072–13078.
58 E. C. Spencer, M. S. R. N. Kiran, W. Li, U. Ramamurty, N. L. Ross and A. K. Cheetham, *Angew. Chem., Int. Ed.*, 2014, **53**, 5583–5586.
59 M. Andrzejewski and A. Katrusiak, *J. Phys. Chem. Lett.*, 2017, **8**, 279–284.
60 D. R. Allan, A. J. Blake, D. Huang, T. J. Prior and M. Schröder, *Chem. Commun.*, 2006, 4081–4083.
61 J. A. Gould, M. J. Rosseinsky and S. A. Moggach, *Dalton Trans.*, 2012, **41**, 5464–5467.
62 R. P. Wool, *Soft Matter*, 2008, **4**, 400–418.
63 P. Naumov, S. Chizhik, P. Commins and E. Boldyreva, in *Mechanically Responsive Materials for Soft Robotics*, ed. H. Koshima, Wiley-VCH Verlag GmbH& Co. KGaA, 1st edn, 2020, pp. 105–137.
64 D. Kim, D. R. Whang and S. Y. Park, *J. Am. Chem. Soc.*, 2016, **138**, 8698–8701.
65 L. Feng, J. L. Li, G. S. Day, X. L. Lv and H. C. Zhou, *Chem*, 2019, **5**, 1265–1274.
66 Y. Yang, X. Ding and M. W. Urban, *Prog. Polym. Sci.*, 2015, **49–50**, 34–59.
67 P. Kumar, B. Anand, Y. F. Tsang, K. H. Kim, S. Khullar and B. Wang, *Environ. Res.*, 2019, **176**, 108488.
68 A. Katrusiak, *International Tables for Crystallography*, vol. H, ch. 2.7, 2019, pp. 156–173.
69 L. Merrill and W. A. Bassett, *Rev. Sci. Instrum.*, 1974, **45**, 290–294.
70 H. K. Mao, J. Xu and P. M. Bell, *J. Geophys. Res.*, 1986, **91**, 4673.
71 G. J. Piermarini, S. Block, J. D. Barnett and R. A. Forman, *J. Appl. Phys.*, 1975, **46**, 2774–2780.
72 A. Budzianowski and A. Katrusiak, *High-Pressure Crystallography*, Kluwer Acad. Publ. Dordrecht, Netherlands, 2004, pp. 101–112.
73 Agilent, Technol. UK Ltd, Yarnton, Oxford, UK.
74 O. V. Dolomanov, L. J. Bourhis, R. J. Gildea, J. A. K. Howard and H. Puschmann, *J. Appl. Crystallogr.*, 2009, **42**, 339–341.
75 G. M. Sheldrick, *Acta Crystallogr., Sect. A: Found. Crystallogr.*, 2008, **64**, 112–122.
76 G. M. Sheldrick, *Acta Crystallogr., Sect. C: Cryst. Struct. Commun.*, 2015, **71**, 3–8.
77 A. Katrusiak, REDSHABS – Program for correcting reflections intensities for DAC absorption, gasket shadowing and sample-crystal absorption, Adam Mickiewicz University, Poznan, Poland, 2003.
78 A. Katrusiak, *Zeitschrift fur Krist.*, 2004, **219**, 461–467.
79 G. Wypych, *Self-Healing materials: Principles and technology*, ChemTec Publishing, 1st edn, 2017.
80 M. D. Hager, S. van der Zwaag and U. S. Schubert, *Self-healing Materials*, Springer International Publishing, 1st edn, 2016.
81 S. K. Ghosh, *Self-healing Materials: Fundamentals, Design Strategies, and Applications*, Wiley-VCH, 2008.
82 F.-X. Coudert, *Chem. Mater.*, 2015, **27**, 1905–1916.

A5

Solid-state associative reactions and the coordination compression mechanism

A. Półrolniczak*, S. Sobczak*, A. Katrusiak.

Inorganic Chemistry 57 (15), 8942-8950, 2018.

Inorganic Chemistry
Cite This: Inorg. Chem. 2018, 57, 8942−8950
Article
pubs.acs.org/IC

Solid-State Associative Reactions and the Coordination Compression Mechanism

Aleksandra Półrolniczak,[†] Szymon Sobczak,[†] and Andrzej Katrusiak*

Department of Materials Chemistry, Faculty of Chemistry, Adam Mickiewicz University, Umultowska 89b, 61-614 Poznan, Poland

Supporting Information

ABSTRACT: Coordination polymers and metal−organic frameworks can be modified by high pressure, according to its effects on the radii of central and ligand atoms. The pressure reduces the ligands' radii, and the coordination number is usually increased. Such transformations of the coordination quite generally conform to the inverse rule of pressure and temperature effects, although the temperature-induced transformations are much less frequently observed. The two-dimensional coordination polymer $Cd(APP)_2NO_3{\cdot}NO_3$ [APP = 1,4-bis(3-aminopropyl)-piperazine] undergoes a pressure-induced isostructural phase transition triggered by a topochemical reaction, yielding $Cd(APP)_2(NO_3)_2$. The transition retains the symmetry of both phases, and their structures have been determined by X-ray diffraction for the single crystals compressed in a diamond-anvil cell. The reaction increases the Cd coordination, from 6-fold in phase I to 7-fold in phase II, where the new Cd−O bond involves an additional nitrate anion in the Cd coordination sphere.

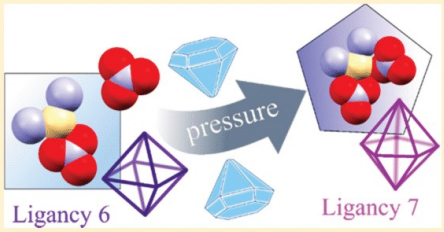

INTRODUCTION

High pressure has become an established highly efficient tool for inducing strong structural transformations in various types of chemical compounds.[1−3] In their structures, the parameters most susceptible to pressure are intermolecular contacts and soft conformational rotations. Unsaturated compounds exposed to the pressure exceeding 10 GPa often polymerize randomly and yield amorphous phases, difficult for structural characterization.[4−13] Therefore, invaluable are pressure-induced reactions retaining the crystalline products,[14−24] suitable for determining the atomic positions by X-ray diffraction at subsequent stages of the reaction. Such transformations of a coordination polymer (CP)[25−27] can also fine-tune its properties and induce new functionalities, leading to their practical applications.

It was shown recently that the postsynthetic modification (PSM) of porous coordination polymers (PCPs)[28] is an efficient way for obtaining new modified materials. To date, the PSM was performed in several ways, but the categories of pressure-enforced and mechanochemical modifications belong to the most efficient methods. Two types of pressure-induced PSMs can be distinguished: ligand-exchange and bond-rearrangement reactions. This transformation often involves the breaking[29−32] and formation[19,20,22−24,29,33,34] of new bonds with metallic centers. Such nonoxidative and oxidative reactions usually change the coordination number, and in some cases, coordination complexes polymerize into CPs.[14,15,17] However, no systematic analysis generalizing these pressure effects has been performed.

Presently, we report a pressure-controlled reaction of a CP, where NO_3 anions "detached" in the voids at 0.1 MPa, above 0.4 GPa forms a coordination bond to the Cd cation. As a result, the coordination number of this CP is increased. To our knowledge, this is the first pressure-induced topochemical reaction of a CP, where the metal cation becomes coordinated by an NO_3^- anion unbonded in nearby voids at ambient conditions. This unprecedented pressure-catalyzed associative reaction has been rationalized by the compression of ionic radii of ligands coordinating Cd^{2+} and those in its vicinity.

RESULTS AND DISCUSSION

At 0.4 GPa, complex $Cd(APP)_2NO_3{\cdot}NO_3$ [APP = 1,4-bis(3-aminopropyl)piperazine] undergoes an associative reaction, leading to the product $Cd(APP)_2(NO_3)_2$, as shown in Scheme 1. In this reaction, a new coordination bond is formed and the coordination number increases from 6 to 7. This reaction proceeds around the central cation, while the strain in its more distant crystalline environment is absorbed by flexible APP linkers and their displacements. Therefore, this reaction can be classified as a solid-state phase transition, as described below.

Crystal Strain. At ambient conditions, the crystal of hydrated $Cd(APP)_2NO_3{\cdot}NO_3$ is built of polymeric sheets extending along the crystal plane $(10\bar{2})$, separated by water molecules (Figures 1 and S1). In this two-dimensional polymer, cation Cd^{2+} is 6-fold-coordinated by four amine N atoms of four APP molecules and two O atoms of one nitrate group. The voids between the APP struts accommodate another NO_3^- anion and two water molecules per formula unit. The structure and properties of the $Cd(APP)_2NO_3{\cdot}NO_3$

Received: April 4, 2018
Published: July 6, 2018

DOI: 10.1021/acs.inorgchem.8b00913
Inorg. Chem. 2018, 57, 8942−8950

Scheme 1. Solid–Solid Reaction of $Cd(APP)_2NO_3{\cdot}NO_3$ at 0.4 GPa, Leading to 7-Fold-Coordinated Cd^{2+} in $Cd(APP)_2(NO_3)_2$

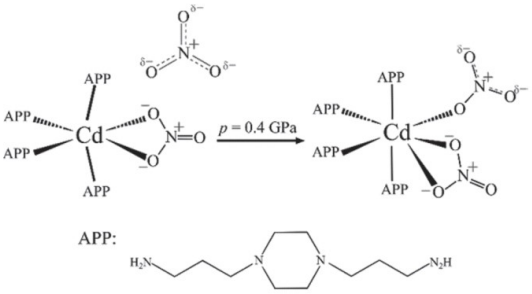

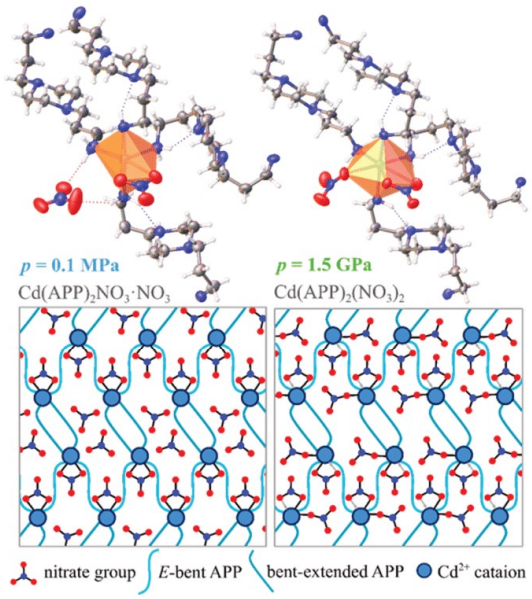

Figure 1. (Left) Cation Cd^{2+} 6-fold-coordinated by four APP molecules and one bidentate nitrate anion in $Cd(APP)_2NO_3{\cdot}NO_3$. (Right) 7-Fold coordination in $Cd(APP)_2(NO_3)_2$ after the reaction. Schemes of the corresponding polymeric layers are shown in the bottom; note two APP conformers. *E*-bent and bent-extended, discriminated in the legend (cf. Figure S3).

crystal strongly depend on the conformation of amine APP struts. The shapes of two independent APP linkers are very similar in their central parts. This central part consists of a piperazine ring, which is relatively rigid in the chair conformation. However, the flexible N-substituted equatorial 3-aminopropyl chains can be considerably bent or extended.

The typical structural effects of compression, i.e., shortened intermolecular contacts, reduced voids, and distorted soft conformational parameters, proceed monotonically in $Cd(APP)_2NO_3{\cdot}NO_3{\cdot}2H_2O$ at 0.2 GPa. At 0.4 GPa, a strong discontinuous anomaly in the crystal compression (Figure 2) marks a first-order transition from the low-pressure phase I to the high-pressure phase II.

At this transition, the unit-cell parameter *a* lengthens by ca. 4%, the parameter *b* shrinks by ca. 6%, and the crystal volume is reduced by 4%, while the space-group symmetry $P2_1/c$ remains preserved, consistent with the isostructural type of phase transition. The strong strain caused by the transition in the crystal sample resulted in its fragmentation into the coexisting portions of the $Cd(APP)_2NO_3{\cdot}NO_3$ and $Cd(APP)_2(NO_3)_2$ phases. Their superimposed diffraction patterns in the recorded images were manifested as split reflections (see the insets in Figure 2). The split reflections occurred because of the strong strain between phases I and II, although their space-group symmetry remained unchanged. Because of the hysteresis of the transformation, both phases I and II (Table 1) coexisted at 0.4 GPa, and the unit-cell dimensions and structural model obtained at this pressure point are the averages of both contributing compounds $Cd(APP)_2NO_3{\cdot}NO_3$ and $Cd(APP)_2(NO_3)_2$, but not an intermediate stage of the reaction. In some of our experiments, particularly on small crystals, they became fully monocrystalline again after the phase transition above 0.5 GPa. Similar single-crystal-to-single-crystal isostructural transitions were previously observed also for other compounds.[35,36] However, some larger samples of $Cd(APP)_2NO_3{\cdot}NO_3$ above the transition broke into several smaller pieces of phase II, albeit with a very strong preferential orientation maintained during the compression, which allowed structural studies using the single-crystal diffraction technique. We have also observed visually that new elongated very thin crystals grew on the surface of the sample in phase II (cf. the Experimental Section); however, their diffraction could not be detected in the recorded images.

High-Pressure Association. At ambient pressure, the Cd-coordinated octahedron is distorted, mainly because of one bidentate nitrate ligand $N1O_3$ (Figure 1). Consequently, the corresponding edge O1–O2 of the octahedron is significantly shorter, of 2.159 Å, than others, between 3.238 Å (O3–N8) and 4.103 Å (N1–O1). The nitrate ligand can be either symmetrically bidentate, asymmetrically bidentate, or unidentate.[37,38] Cd cations display a strong preference for the symmetric bidentate coordination by the nitrate ligands, which is manifested in the exceptionally high stability of such complexes.[39]

In this context, the associative reaction induced by pressure in $Cd(APP)_2NO_3{\cdot}NO_3$ is quite surprising (Figures 3 and S3). When hydrostatic pressure reaches 0.4 GPa, the structure collapses because the associative reaction increases the 6-fold Cd^{2+} coordination in phase I to the 7-fold coordination in phase II (Scheme 1). The new Cd–O4 bond is formed when nitrate $N2O_3^-$ is pushed closer to Cd^{2+}. Thus, at the transition point, the compressibility increases,[40] and the crystal abruptly transforms into the more dense phase II.

The activation process of this association reaction requires that the associating group ($N2O_3^-$) be located near the metallic center. At ambient pressure, the anion $N2O_3^-$ lies in the vicinity of the octahedrally coordinated Cd^+ cation. With increased pressure, the Cd···O4 distance reduces from 3.884 Å at 0.1 MPa to 3.849 Å at 0.25 GPa (Figure 3a). At 0.4 GPa, this distance abruptly shortens to about 2.70 Å in phase II, which clearly marks the formation of the new coordination bond, Cd–O4. This associative reaction is accompanied by a lengthening of the bond Cd–O2, from 2.639 to 2.855 Å, and a somewhat smaller lengthening of Cd–O1, from 2.504 to 2.612 Å. Of all four Cd–N coordination bonds, only one, Cd–N1,

DOI: 10.1021/acs.inorgchem.8b00913
Inorg. Chem. 2018, 57, 8942–8950

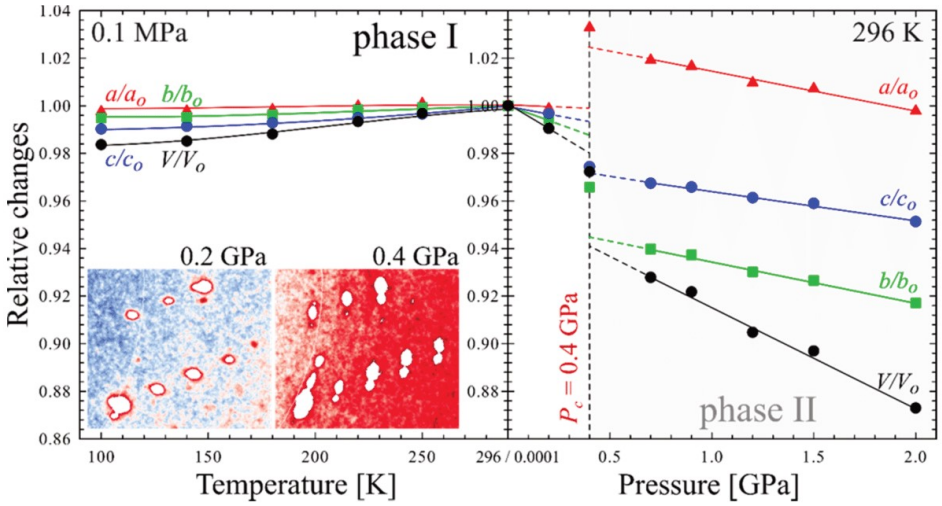

Figure 2. Relative changes of the unit-cell dimensions of crystal $Cd(APP)_2NO_3{\cdot}NO_3$: (left) cooled at 0.1 MPa; (right) compressed in isopropyl alcohol at 296 K. The vertical dashed line marks the reaction pressure. The insets illustrate the splitting of reflections in X-ray diffraction images due to the coexistence of phases I and II at 0.4 GPa (cf. Figure S2). The expansion and compression strains are graphically represented in Figures S9–S11.

Table 1. Selected Crystallographic Data of Dihydrates $Cd(APP)_2NO_3{\cdot}NO_3$ and $Cd(APP)_2(NO_3)_2$[a]

	phase I			phase I/II	phase II				
	0.0001 GPa	0.0001 GPa	0.20(3) GPa	0.40(3) GPa	0.70(3) GPa	0.90(3) GPa	1.20(3) GPa	1.50(3) GPa	2.00(3) GPa
temperature (K)	100	298	298	298	298	298	298	298	298
space group	$P2_1/c$	$P2_1/c$	$P2_1/c$	$P2_1/c$	$P2_1/c$	$P2_1/c$	$P2_1/c$	$P2_1/c$	$P2_1/c$
unit-cell parameters									
a (Å)	18.4776(15)	18.5224(1)	18.500(9)	19.130(2)	18.8771(14)	18.8295(6)	18.7012(11)	18.6563(9)	18.4820(11)
b (Å)	12.3500(10)	12.4128(9)	12.3460(9)	11.987(4)	11.6650(17)	11.6345(9)	11.5450(15)	11.5005(12)	11.3833(12)
c (Å)	13.3403(11)	13.4718(8)	13.4265(2)	13.126(6)	13.032(3)	13.0109(15)	12.951(3)	12.919(2)	12.815(3)
β (deg)	95.072(9)	95.580(6)	95.356(11)	95.263(19)	94.664(11)	94.543(5)	94.148(10)	94.078(7)	93.572(10)
volume (Å^3)	3032.3(4)	3082.7(4)	3053.3(16)	2997.1(17)	2860.2(9)	2841.4(4)	2788.8(7)	2764.8(6)	2690.8(7)
Z/Z'	4/1	4/1	4/1	4/1	4/1	4/1	4/1	4/1	4/1
D_x (g cm^{-3})	1.474	1.450	1.464	1.492	1.563	1.574	1.603	1.617	1.662

[a] D_x is calculated for the empirical formula $C_{20}H_{52}CdN_{10}O_8$ (M_r = 673.11), excluding the guest molecules (cf. Tables S4 and S5).

lengthens by ca. 0.1 Å. All coordination bonds hardly change in length at 0.20 GPa in phase I.

Our survey in the Cambridge Structural Database (Nov 2017 release)[41] shows that the distributions of the Cd–O/N distances in 6- and 7-fold-coordinated complexes with N and O donors are similar. In these complexes, the average Cd–N/O bond length is 2.4 Å and the longest bonds are 2.8–2.9 Å (Figure S8). According to these data, the associative reaction at 0.4 GPa increases the coordination number from 6 to 7. The changes of the APP conformations from 0.1 MPa to 2 GPa and of the lengths of the Cd–N and Cd–O bonds within phases I and II are very small (Figure S2 in SI), which testifies that the associative reaction is the main driving force of the transformation at 0.4 GPa.

The work contribution of the crystal compression $\int p\,dV$ to 0.4 GPa, when the reaction is triggered, is 1.9 kJ mol^{-1} (Figure 2), and the work performed at 0.4 GPa $p\Delta V$ is 7.4 kJ mol^{-1}. The summed energy of 9.3 kJ mol^{-1} is about 20 times smaller than the energy of Cd^{2+}–N/O bonds;[42] however, it does not include the entropy and chemical potential contributions or the significant energy changes of elongated Cd–N/O bonds.[43]

Compressed-Coordination Effects. The changes in coordination in compressed $Cd(APP)_2NO_3{\cdot}NO_3$ can be connected with a significant distortion of the CdN_4O_2 octahedron. Because of the bidentate bonds of nitrate $N1O_3$, the coordination octahedron O1···O2 edge is significantly shorter than the other edges N···N and N···O involving monodentate APP ligands (Figure 3). This significantly distorts the Cd-coordination sphere and opens a gap between O1 and N1: angle O1–Cd–N1 is close to 120° at ambient conditions, compared to O1–Cd–O2 of less than 50°(cf. Figure S5). At 0.4 GPa, atom O4 of nitrate $N2O_3$ is pushed into the gap between O1 and N1. This pressure-induced reaction can be rationalized in terms of the reduced radii of ligand atoms. Goldschmidt and Pauling's radius–ratio rule connects the coordination number with the radii of the ligands tightly arranged around the cation. It can be expected than the anionic and atomic radii are more affected by the pressure than the small cation at the center. In principle, the valence electrons in anions interact weaker with the nucleus, and they easier adjust to their environment than the outer electrons in the cations. This reasoning is consistent with our present result

DOI: 10.1021/acs.inorgchem.8b00913
Inorg. Chem. 2018, 57, 8942–8950

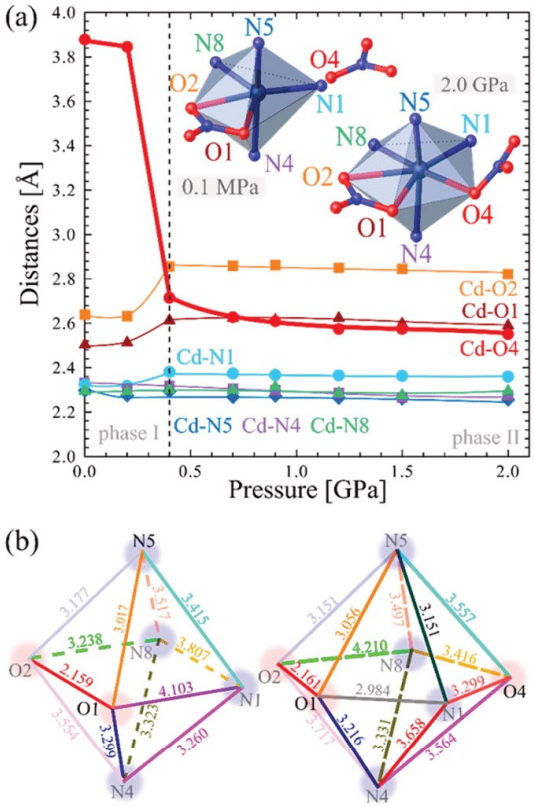

Figure 3. (a) Distances Cd–ligand. The insets show the coordination polyhedra in phases I (0.2 GPa) and II (2.0 GPa). The lines are for guiding the eye only. (b) Idealized coordination polyhedra and lengths of their edges in phases I (0.2 GPa) and II (0.75 GPa) (cf. their pressure dependences plotted in Figures S4–S7).

that high pressure increases the coordination number in $Cd(APP)_2NO_3{\cdot}NO_3$. The compressed anionic radii result in increased R_{Ligand}/R_{Cation} ratios, consistent with the radius–ratio rule, and the number of ligands increases. Also, this reaction affects the electronic configuration of the cation, which is the response for its decreasing repulsion with ligands (Figure 3).[12,44–46]

In the literature, there is a number of structural reports on the pressure-induced changes of the coordination of metal cations. We have established that for most of these transformations the increasing pressure either increases the number of ligands or causes their exchange. The transformation of $Cd(APP)_2NO_3{\cdot}NO_3$ conforms to this rule that high pressure increases the coordination number. The literature and our results have been compiled and are illustrated in Figure 4.

For example, Cai et al.[33] showed that in $[Zn(L)_2(OH)_2]_n{\cdot}$ Guest [where L is 4-(1*H*-naphtho[2,3-*d*]imidazol-1-yl)-benzoate and Guest is water or methanol (MeOH)] in pressure-induced phase II the tetrahedral coordination ZnO_3N changes to the 5-fold-coordinated ZnO_4N; Andrzejewski and Katrusiak[19] observed, along with the piezochromic phase transition in $CoCl_2bpp$, that the tetrahedral coordination

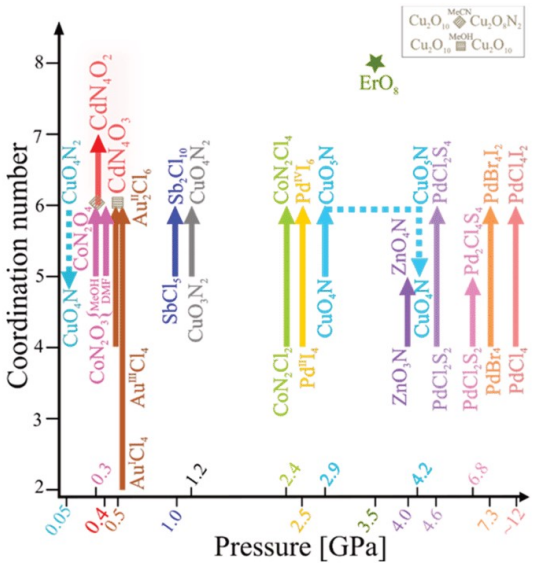

Figure 4. Coordination-number changes in CPs, MOFs, and complexes from the low-to-high-pressure structures indicated by arrows (see the text). The asterisk marks a rearrangement without the coordination-number change, and the dotted lines indicate that the coordination number decreases when the pressure increases.

$CoCl_2N_2$ increases to the octahedral coordination $CoCl_4N_2$; Lanza et al.[20] reported in $[Co_3(OH)_2btca_2]$ a transformation from 5-fold to octahedral coordination, involving a nucleophilic addition of MeOH/*N*,*N*-dimethylformamide (DMF) molecules to the Co^{2+} center; McKellar et al.[47] described a similar process that under hydrostatic pressure Cu-based metal–organic framework (MOF) STAM-1 (St. Andrews MOF-1) exchanges a water ligand at the axial metal site with MeOH and acetonitrile (MeCN); Spencer et al.[23] showed a rearrangement of bonds in the coordination sphere of $[tmenH_2][Er(HCOO)_4]_2$; Allan et al.[14] described a unique polymerization within $[PdCl_2([9]aneS_3)]$ ([9]aneS$_3$ = 1,4,7-trithiacyclononane), transforming a square-planar coordination to an octahedral coordination; Gould et al.[17] by compressing $[Cu(L\text{-}Asp)(H_2O)_2]$ (Asp = aspartate) increased the 5-fold coordination of Cu^{2+} to 6-fold coordination. Pressure-induced conversions of long contacts into primary bonds were observed also in the perovskite $CsHgCl_3$ (the octahedral coordination of Hg^+ becomes nearly ideal)[48] and in $CsGeBr_3$.[49] A pressure-induced solid-state reaction was observed in $Cs_2[PdX_4]{\cdot}I_2$ (X = Cl, Br, or I): the redox reaction converts $Cs_2[Pd^{2+}I_4]{\cdot}I_2$ to $Cs_2[Pd^{4+}I_6]$ at 2.5 GPa.[50] A closely related reaction $Au^I + Au^{III} = 2Au^{II}$ of 0.52 GPa in $CsAu^IAu^{III}Cl_6$, containing the chains of alternating square-planar $[AuCl_4]^-$ and linear $[AuCl_2]^-$ anions, transforms all of the 4-fold-coordinated Au^I to octahedrally coordinated Au^{II}.[51] Tidey et al.[52] reported for β-$[PdCl_2([9]aneS_2O)]$ the 4-to-5-fold coordination change, coupled with the dimeric complex formation. Bujak and Angel[53] postulated that above 1 GPa half of the Sb atoms in $[Me_2NHMe_2NH_3][SbCl_5]$ become 6-fold-coordinated and the other half retain their initial 5-fold coordination. Prescimone et al.[54] reported the pressure-induced elimination of one of the coordinating water molecules from half of the Cu^{2+} cations in

DOI: 10.1021/acs.inorgchem.8b00913
Inorg. Chem. 2018, 57, 8942–8950

$[Cu_2(OH)_2(H_2O)_2(tmen)_2](ClO_4)_2$ (tmen = tetramethylethylenediamine), leading to a change from 5-fold pyramidal coordination to a 6-fold distorted-octahedral coordination, where the sixth vertex is a perchlorate O atom. To our knowledge, the generally increased or rearranged coordination in compressed complexes has only two exceptions, which can be connected with competing compressed contacts, changing conformations, and other pressure-induced effects in the crystal structure (see the Supporting Information).[15,18]

It is noteworthy that MOFs and CPs are often classified as the intermediate compounds between the coordination and inorganic chemistry.[55] According to the IUPAC definition, MOFs constitute a subclass of CPs with organic ligands and voids accessible for guest molecules.[55] No such pores are present in CPs. The absence of pores in CPs is considered disadvantageous because they cannot be used as adsorbers of gases and other small-molecule compounds.[56] The associative reaction in $Cd(APP)_2NO_3{\cdot}NO_3$ at 0.4 GPa withdraws the NO_3^- anions from the voids, but they immediately collapse and no pores open up. However, it is possible that in other CPs high-pressure associative reaction can widen or open pores, which would allow the adsorption of some molecules from the environment, and then by the release of pressure, the pores would be closed and the guest molecules trapped inside. Such materials are sought for separating compounds, eliminating undesired components from air, and storing poisonous substances.[57−61]

Pressure-induced transformations are often compared to those induced by lowering of the temperature, and indeed the rule of inverse effects of temperature and pressure was formulated (abbreviated here as the "inverse p/T rule").[62] This relationship is associated with the reduction of thermal vibrations both at low temperature and under high pressure.[63] Compared to pressure-induced changes of the coordination number, there are relatively few reports on the coordination transformations resulting from temperature changes, particularly when one considers the much more frequent varied-temperature than varied-pressure studies.

All reports on temperature-induced associative reactions found by us in the literature have been scrutinized in the text below and are schematically illustrated in Figure 5. Zhang et al.[59] observed that in $[Ag_6Cl(atz)_4]OH{\cdot}6H_2O$ (atz = 3-amino-1,2,4-triazole anion) the coordination number of Ag cations is reduced from 4 to 2 above 293 K and it increases back to 4 below 103 K. Hu and Englert[64] showed that in $[ZnCl_2(bipy)]_n$ (bipy = 4,4′-bipyridine) the Zn ligancy decreases from 6 to 4 above 360 K and it increases back below 130 K. Xie et al.[65] reported that $UO_2(C_{18}H_{20}N_2O_4@CB6)_2Br_2$ [with a pseudorotaxane motif C6BPCA@CB6, where C6BPCA = 1,1′-(hexane-1,6-diyl)bis(4(carbonyl)pyridin-1-ium and CB6 = cucurbit[6]uril)] transforms between the 7-coordinated form in phase β-UP and the 6-coordinated one in phase α-UP respectively upon cooling and heating in the 170−320 K range. Zhu et al.[66] recorded a remarkable reversible association of free cations Eu^{3+} in $(H_3O^+)Eu_{0.5}[EuNa_{0.5}L(DMF)(H_2O)]{\cdot}(solvent)_x$ [L = 5,5′,5″-(1,3,5-triazine-2,4,6-triyltriimino)-triisophthalate hexaanion], below 193 K becoming $(H_3O^+)_2[Eu_3NaL_2(DMF)_5(H_2O)_2]{\cdot}(solvent)_y$ with 8-coordinated Eu^{3+}. Bernini et al.[67] changed the Yb^{3+} coordination in $[Yb(C_4H_4O_4)_{1.5}]$ between 8 and 7 by cooling it below 374 and heating it above 403 K, respectively (Figure 5).

All of the examples listed above agree with the inverse p/T rule. We have found only one exemption, the [(Cl)Hg(m-Cl)$_2$(hep-H)] [hep-H = 2-(2-hydroxyethyl)pyridine] structure reported by Mobin et al.,[68] where the coordination number increases from 4 to 5 and the framework dimensionality increases also when heated to 383 K. The reaction reverses when the high-temperature compound [(Cl)Hg(m-Cl)$_2$(hep-Cl)] is cooled and kept for 3 days at 298 K.

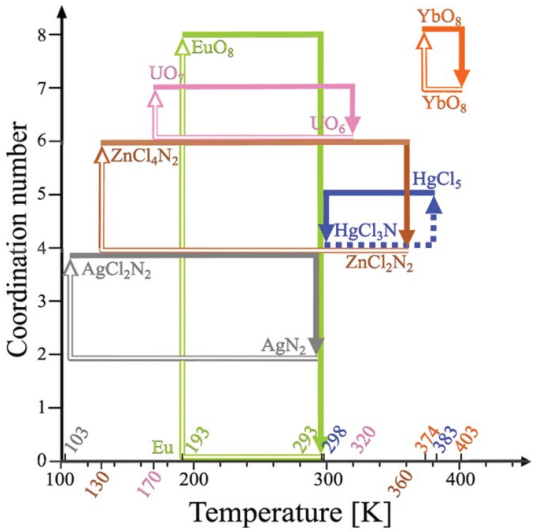

Figure 5. Coordination changes in CPs, MOFs, and complexes between the low- and high-temperature structures indicated by arrows (full and open lines refer to the heating and cooling runs; the dotted line marks the only exemption from the inverse p/T rule; cf. Figure 4).

It is apparent from Figure 5 that most of the structures (six compounds) comply with the inverse p/T rule, and at present, only one exemption supporting the direct p/T relationship is known. These systematic changes can be connected with the above-mentioned reduction of thermal vibrations. Indeed, it is known that the ionic radii are often established from the crystal structures determined at normal conditions.[69−73] Consequently, these experimentally determined radii incorporate the Debye−Waller factors,[74] which are both temperature- and pressure-dependent.

Fewer cases of temperature-induced changes in the coordination number compared to pressure-induced changes indicate that the effects of temperature are more subtle and susceptible to phase transformations, desorption, and other effects.[75,76] This conclusion is further supported by the considerable hysteresis of the transformations induced by temperature, of tens of Kelvin and even over 200 K. Therefore, the coordination changes at varied temperatures are less predictable compared to the systematic increase of the coordination number under high pressure, as described in this paper.

The changes in the magnitudes of atomic displacement parameters (ADPs) in $Cd(APP)_2NO_3{\cdot}NO_3$, plotted in Figure 6, show that, despite the stronger reduction in the ADP magnitudes at 100 K/0.1 MPa than those in phase II at 296 K/2.0 GPa, the temperature lowered at 0.1 MPa does not induce transformations of the crystal. However, the reaction is triggered by high pressure when the ADPs are hardly changed from their magnitudes at 296 K/0.1 MPa. It confirms that the

DOI: 10.1021/acs.inorgchem.8b00913
Inorg. Chem. 2018, 57, 8942−8950

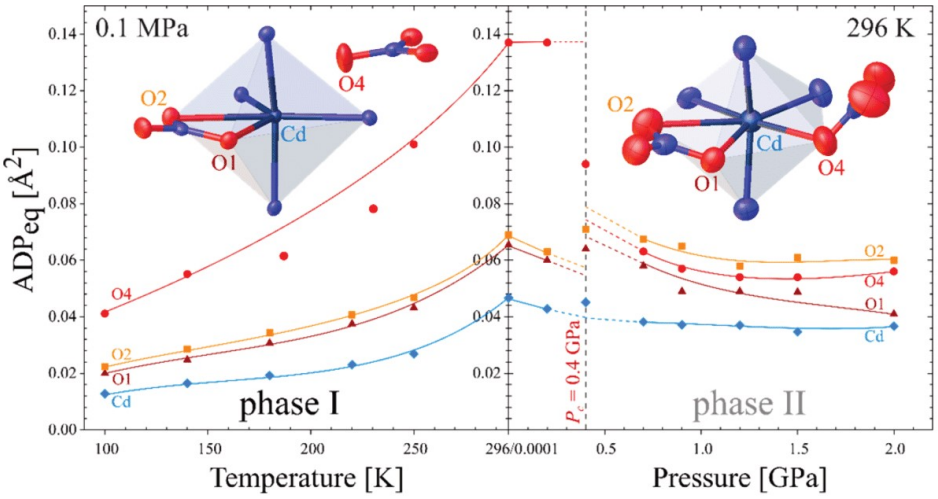

Figure 6. ADPs of atoms involved in the coordination sphere in $Cd(APP)_2NO_3{\cdot}NO_3$ plotted as a function of the temperature (left) and pressure (right). The insets show the relevant anisotropic thermal ellipsoids in the crystal, drawn at the 50% probability level.

high pressure is very efficient in inducing structural transformations and that the associated ADP changes play a minor role. It is characteristic that the considerable reduction of the ADP magnitude of the associatively bonded atom O4 is reduced after the reduction, and no pretransitional effect can be noted for this parameter.

■ CONCLUSIONS

Structural changes and chemical reactions induced by pressure in coordination complexes and polymers can be rationalized according to relatively simple rules describing (i) the effect of pressure on the radii of ligand atoms, (ii) the arrangement of ligands around the central cation, and (iii) the vicinity of other potential ligands. Rule i relies on the observation that the pressure reduces the radii of the ligand atoms and, hence, increases the R_{Cation}/R_{Ligand} ratio, which is favorable for the coordination number increase. The changes of the ligand-atom radii can originate from several effects, including the electronic structure and thermal vibrations of the atoms. Rule ii is based on the pressure effects eliminating gaps and voids around the central cation, which, in turn, favor even distributions of ligands and reduce the distortions of polyhedra in the compressed structures. Rule iii states that the reacting molecules or ions must be located in the vicinity of the cation. Most of pressure-induced reactions in coordination compounds reported so far conform to these rules (i–iii), as well as to the inverse p/T rule.

These coordination-compression rules complement the general knowledge on the microscopic changes of soft structural parameters in compressed compounds. It can be applied for employing the pressure techniques for obtaining new CPs by modifying specifically designed substrates.

■ EXPERIMENTAL SECTION

Synthesis. Single crystals of the coordination polymer $Cd(APP)_2NO_3{\cdot}NO_3$ were obtained using a diffusion method, similar to those described previously (Figure 7).[19,30,77−79] In our present study, the two layers containing the substrates, 0.075 g (1 mmol) of cadmium nitrate (Sigma-Aldrich) dissolved in 5 mL of MeCN and 0.1 mL (0.5 mmol) of 1,4-bis(3-aminopropyl)piperazine dissolved in 5 mL of xylene, were separated by the mixture of 1 mL of MeCN with 1 mL of xylene providing the diffusion environment. After 1 week, many transparent crystals appeared, a few of which were the desired product. Their block morphology was significantly distinct from other mainly needle-shaped crystals.

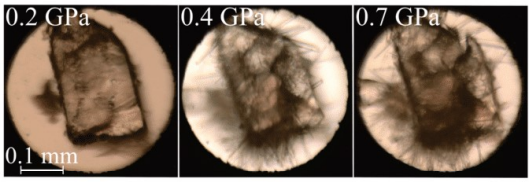

Figure 7. Single crystal of $Cd(APP)_2NO_3{\cdot}NO_3$ isothermally compressed in isopropyl alcohol in the DAC, as indicated at the top of the photographs. Several ruby chips for the pressure calibration lie by the left side of the crystal.

High-Pressure Measurements. High-pressure experiments on $Cd(APP)_2NO_3{\cdot}NO_3$ were performed in a Merrill-Bassett diamond-anvil cell (DAC),[80] modified by mounting the diamond anvils directly onto the steel supports with conical windows. The pressure in the DAC was calibrated by the ruby-fluorescence method with a photon control spectrometer, affording an accuracy of 0.03 GPa.[81,82] The gaskets were made of a 0.3-mm-thick tungsten foil with the spark-eroded holes 0.5 mm in diameter. Isopropyl alcohol was used as the hydrostatic medium. The X-ray diffraction data were measured on a KUMA4-CCD diffractometer with Mo Kα radiation (λ = 0.71073 Å). The DAC was centered by the gasket-shadow method.[83] The collected data were preliminarily reduced with the *CrysAlisPro* suite, version 171.38.46.[84] *OLEX2* was used.[85] The structure was solved by direct methods with *SHELXS* and least-squares refined with *SHELXL*.[86,87] The ambient-pressure structure was the starting model for the low-temperature and high-pressure structures below the reaction pressure. High-pressure absorption corrections were calculated by the program *REDSHABS*.[88,89] The final crystal data are summarized in Table 1 (cf. Tables S4 and S5) and have been deposited in the Cambridge Structural Database as supplementary publications CCDS 1549093, 1558178, 1558180, 1558181, 1558183, and 1830173−1830180. These deposits can be obtained free of

DOI: 10.1021/acs.inorgchem.8b00913
Inorg. Chem. 2018, 57, 8942−8950

charge from www.ccdc.cam.ac.uk and from the Crystallography Open Database (www.crystallography.net).

Low-Temperature X-ray Diffraction. The low-temperature data were measured on an Xcalibur EOS-CCD diffractometer equipped with a gas-flow Oxford Cryostream attachment, as a function of the temperature between 100 and 297 K in 40 K steps. All non-H atoms were refined with anisotropic thermal parameters. H atoms were located in the difference Fourier map and from the molecular geometry. Parameters U_{iso} of H atoms were set to 1.2 times U_{eq} of their carriers.

■ ASSOCIATED CONTENT

Supporting Information

The Supporting Information is available free of charge on the ACS Publications website at DOI: 10.1021/acs.inorgchem.8b00913.

> Exceptional reduction of the coordination number under pressure, schematically presented layers in Cd(APP)$_2$NO$_3$·NO$_3$, an overlay of structures before and after reaction, full X-ray diffraction images for 0.2, 0.4, and 0.7 GPa, CCSD database analysis of Cd−O/N distances, pressure dependence of all Cd−ligand distances and angles between them, schematically illustrated idealized coordination polyhedra formed in phases I and II, thermal expansion, compressibility analysis, and detailed crystallographic data including ambient- and high-pressure measurements (DOCX)

Accession Codes

CCDC 1549093, 1558178, 1558180−1558181, 1558183, and 1830173−1830180 contain the supplementary crystallographic data for this paper. These data can be obtained free of charge via www.ccdc.cam.ac.uk/data_request/cif, or by emailing data_request@ccdc.cam.ac.uk, or by contacting The Cambridge Crystallographic Data Centre, 12 Union Road, Cambridge CB2 1EZ, UK; fax: +44 1223 336033.

■ AUTHOR INFORMATION

Corresponding Author

*E-mail: katran@amu.edu.pl. Phone: 48 61 8291590.

ORCID

Szymon Sobczak: 0000-0001-8234-2503

Andrzej Katrusiak: 0000-0002-1439-7278

Author Contributions

†These authors contributed equally.

Notes

The authors declare no competing financial interest.

■ ACKNOWLEDGMENTS

The authors are grateful to Dr. Michał Andrzejewski of Department of Chemistry and Biochemistry, University of Bern, for his advice and encouragement. This research was supported by funding from the Polish National Science Centre (OPUS 10 No. UMO-2015/19/B/ST5/00262).

■ REFERENCES

(1) Boldyreva, E.; Dera, P. *High-Pressure Crystallography: From Fundamental Phenomena to Technological Applications*; Springer Science & Business Media, 2010.

(2) Katrusiak, A.; McMillan, P. *High-Pressure Crystallography*; Springer Science & Business Media, 2004; Vol. *140*.

(3) McMillan, P. F. New Materials from High-Pressure Experiments. *Nat. Mater.* **2002**, *1*, 19−25.

(4) Wang, Y.; Wang, L.; Zheng, H.; Li, K.; Andrzejewski, M.; Hattori, T.; Sano-Furukawa, A.; Katrusiak, A.; Meng, Y.; Liao, F.; Hong, F.; Mao, H. Phase Transitions and Polymerization of C_6H_6−C_6F_6 Cocrystal under Extreme Conditions. *J. Phys. Chem. C* **2016**, *120*, 29510−29519.

(5) Blank, V. D.; Buga, S. G. B.; Dubitsky, G. A.; Serebryanaya, N. R.; Popov, M. Y.; Sundqvist, B. High-Pressure Polymerized Phases of C60. *Carbon* **1998**, *36*, 319−343.

(6) Sakashita, M.; Yamawaki, H.; Aoki, K. FT-IR Study of the Solid State Polymerization of Acetylene under Pressure. *J. Phys. Chem.* **1996**, *100* (23), 9943−9947.

(7) Eremets, M. I.; Popov, M. Y.; Trojan, I. A.; Denisov, V. N.; Boehler, R.; Hemley, R. J. Polymerization of Nitrogen in Sodium Azide. *J. Chem. Phys.* **2004**, *120*, 10618−10623.

(8) Aoki, K.; Usuba, S.; Yoshida, M.; Kakudate, Y.; Tanaka, K.; Fujiwara, S. Raman Study of the Solid-State Polymerization of Acetylene at High Pressure. *J. Chem. Phys.* **1988**, *89*, 529−534.

(9) Badding, J. V.; Parker, L. J.; Nesting, D. C. High Pressure Synthesis of Metastable Materials. *J. Solid State Chem.* **1995**, *117*, 229−235.

(10) Chelazzi, D.; Ceppatelli, M.; Santoro, M.; Bini, R.; Schettino, V. Pressure-Induced Polymerization in Solid Ethylene. *J. Phys. Chem. B* **2005**, *109*, 21658−21663.

(11) Nicol, M.; Yin, G. Organic chemistry at high pressure: can unsaturated bonds survive 10 GPa ? *J. Phys. Colloq* **1984**, *45*, C8-163−C8−172.

(12) Bastron, V. C.; Drickamer, H. G. Solid State Reactions in Organic Crystals at Very High Pressure. *J. Solid State Chem.* **1971**, *3*, 550−563.

(13) Yoo, C. S.; Nicol, M. Kinetics of a Pressure-Induced Polymerization Reaction of Cyanogen. *J. Phys. Chem.* **1986**, *90*, 6732−6736.

(14) Allan, D. R.; Blake, A. J.; Huang, D.; Prior, T. J.; Schröder, M. High Pressure Co-Ordination Chemistry of a Palladium Thioether Complex: Pressure versus Electrons. *Chem. Commun.* **2006**, *2*, 4081−4083.

(15) Moggach, S. A.; Galloway, K. W.; Lennie, A. R.; Parois, P.; Rowantree, N.; Brechin, E. K.; Warren, J. E.; Murrie, M.; Parsons, S. Polymerisation of a Cu(II) Dimer into 1D Chains Using High Pressure. *CrystEngComm* **2009**, *11*, 2601.

(16) Moggach, S. A.; Parsons, S. High Pressure Crystallography of Inorganic and Organometallic Complexes. *Spectroscopic Properties of Inorganic and Organometallic Compounds*; The Royal Society of Chemistry, 2009; Vol. *40*, pp 324−354.

(17) Gould, J. A.; Rosseinsky, M. J.; Moggach, S. A. Tuning the Coordination Chemistry of a Cu(Ii) Complex at High-Pressure. *Dalt. Trans.* **2012**, *41*, 5464.

(18) Clegg, J. K.; Brock, A. J.; Jolliffe, K. A.; Lindoy, L. F.; Parsons, S.; Tasker, P. A.; White, F. J. Reversible Pressure-Controlled Depolymerization of a Copper(II)-Containing Coordination Polymer. *Chem. - Eur. J.* **2017**, *23*, 12480−12483.

(19) Andrzejewski, M.; Katrusiak, A. Piezochromic Topology Switch in a Coordination Polymer. *J. Phys. Chem. Lett.* **2017**, *8*, 929−935.

(20) Lanza, A.; Germann, L. S.; Fisch, M.; Casati, N.; Macchi, P. Solid-State Reversible Nucleophilic Addition in a Highly Flexible MOF. *J. Am. Chem. Soc.* **2015**, *137*, 13072−13078.

(21) Li, M.; Liu, B.; Wang, B.; Wang, Z.; Gao, S.; Kurmoo, M. Erbium-Formate Frameworks Templated by Diammonium Cations: Syntheses, Structures, Structural Transition and Magnetic Properties. *Dalt. Trans.* **2011**, *40*, 6038.

(22) Spencer, E. C.; Angel, R. J.; Ross, N. L.; Hanson, B. E.; Howard, J. A. K. Pressure-Induced Cooperative Bond Rearrangement in a Zinc Imidazolate Framework: A High-Pressure Single-Crystal X-Ray Diffraction Study. *J. Am. Chem. Soc.* **2009**, *131*, 4022−4026.

(23) Spencer, E. C.; Kiran, M. S. R. N.; Li, W.; Ramamurty, U.; Ross, N. L.; Cheetham, A. K. Pressure-Induced Bond Rearrangement and Reversible Phase Transformation in a Metal-Organic Framework. *Angew. Chem., Int. Ed.* **2014**, *53*, 5583−5586.

DOI: 10.1021/acs.inorgchem.8b00913
Inorg. Chem. 2018, 57, 8942−8950

(24) Ortiz, A. U.; Boutin, A.; Gagnon, K. J.; Clearfield, A.; Coudert, F. X. Remarkable Pressure Responses of Metal-Organic Frameworks: Proton Transfer and Linker Coiling in Zinc Alkyl Gates. *J. Am. Chem. Soc.* **2014**, *136*, 11540−11545.
(25) Im, J.; Seoung, D.; Hwang, G. C.; Jun, J. W.; Jhung, S. H.; Kao, C. C.; Vogt, T.; Lee, Y. Pressure-Dependent Structural and Chemical Changes in a Metal-Organic Framework with One-Dimensional Pore Structure. *Chem. Mater.* **2016**, *28*, 5336−5341.
(26) Coudert, F. X. Responsive Metal-Organic Frameworks and Framework Materials: Under Pressure, Taking the Heat, in the Spotlight, with Friends. *Chem. Mater.* **2015**, *27*, 1905−1916.
(27) McKellar, S. C.; Moggach, S. A. Structural Studies of Metal-Organic Frameworks under High Pressure. *Acta Crystallogr., Sect. B: Struct. Sci., Cryst. Eng. Mater.* **2015**, *71*, 587−607.
(28) Wang, Z.; Cohen, S. M. Postsynthetic Modification of Metal−organic Frameworks. *Chem. Soc. Rev.* **2009**, *38*, 1315.
(29) Su, Z.; Miao, Y.-R.; Zhang, G.; Miller, J. T.; Suslick, K. S. Bond Breakage under Pressure in a Metal Organic Framework. *Chem. Sci.* **2017**, *8*, 8004−8011.
(30) Andrzejewski, M.; Casati, N.; Katrusiak, A. Reversible Pressure-Preamorphization of a Piezochromic Metal-Organic Framework. *Dalt. Trans* **2017**, *46*, 14795−14803.
(31) Hu, Y. H.; Zhang, L. Amorphization of Metal-Organic Framework MOF-5 at Unusually Low Applied Pressure. *Phys. Rev. B: Condens. Matter Mater. Phys.* **2010**, *81*, 1−5.
(32) Bennett, T. D.; Simoncic, P.; Moggach, S. A.; Gozzo, F.; Macchi, P.; Keen, D. A.; Tan, J.-C.; Cheetham, A. K. Reversible Pressure-Induced Amorphization of a Zeolitic Imidazolate Framework (ZIF-4). *Chem. Commun.* **2011**, *47*, 7983.
(33) Cai, W.; Gladysiak, A.; Anioła, M.; Smith, V. J.; Barbour, L. J.; Katrusiak, A. Giant Negative Area Compressibility Tunable in a Soft Porous Framework Material. *J. Am. Chem. Soc.* **2015**, *137*, 9296−9301.
(34) Moggach, S. A.; Parsons, S. High Pressure Crystallography of Inorganic and Organometallic Complexes. *Spectroscopic Properties of Inorganic and Organometallic Compounds*; The Royal Society of Chemistry, 2009; Vol. *40*, pp 324−354.
(35) Patyk, E.; Jenczak, A.; Katrusiak, A. Giant Strain Geared to Transformable H-Bonded Network in Compressed *β*-*d*-Mannose. *Phys. Chem. Chem. Phys.* **2016**, *18*, 11474−11479.
(36) Katrusiak, A. High-Pressure X-Ray Diffraction Study on the Structure and Phase Transition of 1,3-Cyclohexanedione Crystals. *Acta Crystallogr., Sect. B: Struct. Sci.* **1990**, *46* (2), 246−256.
(37) Kleywegt, G. J.; Wiesmeijer, W. G. R.; Van Driel, G. J.; Driessen, W. L.; Reedijk, J.; Noordik, J. H. Unidentate versus Symmetrically and Unsymmetrically Bidentate Nitrate Co-Ordination in Pyrazole-Containing Chelates. The Crystal and Molecular Structures of (Nitrato-O)[tris(3,5-Dimethylpyrazol-1-Ylmethyl)-amine]copper(II) Nitrate, (Nitrato-O,O′)[tris(3,5-dimethylpyrazol-1-ylmethyl)amine]copper(II) nitrate, (nitrato-O,O′)[tris(3,5-dimethylpyrazol-1-ylmethyl)amine]nickel(II). *J. Chem. Soc., Dalton Trans.* **1985**, *10*, 2177−2184.
(38) Addison, C. C.; Logan, N.; Wallwork, S. C.; Garner, C. D. Structural Aspects of Co-Ordinated Nitrate Groups. *Q. Rev., Chem. Soc.* **1971**, *25*, 289.
(39) Parkin, G. Alkyl, Hydride, and Hydroxide Derivatives of the s- and p-Block Elements Supported by Poly(pyrazolyl)borato Ligation: Models for Carbonic Anhydrase, Receptors for Anions, and the Study of Controlled Crystallographic Disorder. In *Advances in Inorganic Chemistry*; Sykes, A. G., Ed.; Academic Press, 1995; Vol. *42*, pp 291−393.
(40) Papon, P.; Leblond, J.; Meijer, P. H. E. *The Physics of Phase Transition—Concepts and Applications*; Springer-Verlag: Berlin 2002; p 419.
(41) Groom, C. R.; Bruno, I. J.; Lightfoot, M. P.; Ward, S. C. The Cambridge Structural Database. *Acta Crystallogr., Sect. B: Struct. Sci., Cryst. Eng. Mater.* **2016**, *72*, 171−179.
(42) Glidewell, C. Metal-Ligand Coordinate Bond Energy Terms in Complexes of Ammonia and 1, 2-Diaminoethane. *J. Coord. Chem.* **1977**, *6*, 189−192.
(43) Nimmermark, A.; Öhrström, L.; Reedijk, J. Metal-Ligand Bond Lengths and Strengths: Are They Correlated? A Detailed CSD Analysis. *Z. Kristallogr. - Cryst. Mater.* **2013**, *228* (7), 311−317.
(44) Slichter, C. P.; Drickamer, H. G. Pressure-Induced Electronic Changes in Compounds of Iron. *J. Chem. Phys.* **1972**, *56*, 2142−2160.
(45) Drickamer, H. G.; Frank, C. W. *Electronic Structure, Electronic Transitions, and the High Pressure Chemistry and Physics of Solids*; Annual Reviews, 1972; Vol. *23*.
(46) Schettino, V.; Bini, R.; Ceppatelli, M.; Ciabini, L.; Citroni, M. Chemical Reactions at Very High Pressure. *Advances in Chemical Physics*; Wiley-Blackwell, 2005; Vol. *131*, pp 105−242.
(47) McKellar, S. C.; Graham, A. J.; Allan, D. R.; Mohideen, M. I. H.; Morris, R. E.; Moggach, S. A. The Effect of Pressure on the Post-Synthetic Modification of a Nanoporous Metal−organic Framework. *Nanoscale* **2014**, *6*, 4163−4173.
(48) Albarski, O.; Hillebrecht, H.; Rotter, H. W.; Thiele, G. Über Caesiumtrichloromercurat(II) CsHgCl3: Lösung Einer Komplexen Überstruktur Und Verhalten Unter Hohen Drücken. *Z. Anorg. Allg. Chem.* **2000**, *626*, 1296−1304.
(49) Schwarz, U.; Wagner, F.; Syassen, K.; Hillebrecht, H. Effect of Pressure on the Optical-Absorption Edges of And. *Phys. Rev. B: Condens. Matter Mater. Phys.* **1996**, *53*, 12545−12548.
(50) Heines, P.; Keller, H.-L.; Armbrüster, M.; Schwarz, U.; Tse, J. Pressure-Induced Internal Redox Reaction of $Cs_2[PdI_4]\cdot I_2$, $Cs_2[PdBr_4]\cdot I_2$, and $Cs_2[PdCl_4]\cdot I_2$. *Inorg. Chem.* **2006**, *45*, 9818−9825.
(51) Denner, W.; Schulz, H.; d'Amour, H. The Influence of High Hydrostatic Pressure on the Crystal Structure of Cesium Gold Chloride ($Cs_2Au^IAu^{III}Cl_6$) in the Pressure Range up to 52×10^8 Pa. *Acta Crystallogr., Sect. A: Cryst. Phys., Diffr., Theor. Gen. Crystallogr.* **1979**, *35*, 360−365.
(52) Tidey, J. P.; Wong, H. L. S.; McMaster, J.; Schroder, M.; Blake, A. J. High-Pressure Studies of Three Polymorphs of a Palladium(II) Oxathioether Macrocyclic Complex. *Acta Crystallogr., Sect. B: Struct. Sci., Cryst. Eng. Mater.* **2016**, *72*, 357−371.
(53) Bujak, M.; Angel, R. J. High-Pressure- and Low-Temperature-Induced Changes in $[(CH_3)_3NH(CH_3)_3NH_3][SbCl_5]$. *J. Phys. Chem. B* **2006**, *110*, 10322−10331.
(54) Prescimone, A.; Sanchez-Benitez, J.; Kamenev, K. K.; Moggach, S. A.; Warren, J. E.; Lennie, A. R.; Murrie, M.; Parsons, S.; Brechin, E. K. High Pressure Studies of Hydroxo-Bridged Cu(II) Dimers. *Dalt. Trans.* **2010**, *39*, 113−123.
(55) Batten, S. R.; Champness, N. R.; Chen, X.-M.; Garcia-Martinez, J.; Kitagawa, S.; Öhrström, L.; O'Keeffe, M.; Paik Suh, M.; Reedijk, J. Terminology of Metal−organic Frameworks and Coordination Polymers (IUPAC Recommendations 2013). *Pure Appl. Chem.* **2013**, *85*, 1715.
(56) Batten, S. R.; Champness, N. R.; Chen, X.-M.; Garcia-Martinez, J.; Kitagawa, S.; Öhrström, L.; O'Keeffe, M.; Suh, M. P.; Reedijk, J. Coordination Polymers, Metal−organic Frameworks and the Need for Terminology Guidelines. *CrystEngComm* **2012**, *14*, 3001.
(57) Zhang, J. P.; Chen, X. M. Exceptional Framework Flexibility and Sorption Behavior of a Multifunctional Porous Cuprous Triazolate Framework. *J. Am. Chem. Soc.* **2008**, *130*, 6010−6017.
(58) Mason, J. A.; Oktawiec, J.; Taylor, M. K.; Hudson, M. R.; Rodriguez, J.; Bachman, J. E.; Gonzalez, M. I.; Cervellino, A.; Guagliardi, A.; Brown, C. M.; Llewellyn, P. L.; Masciocchi, N.; Long, J. R. Methane Storage in Flexible Metal-Organic Frameworks with Intrinsic Thermal Management. *Nature* **2015**, *527*, 357−361.
(59) Zhang, J. P.; Lin, Y. Y.; Zhang, W. X.; Chen, X. M. Temperature- or Guest-Induced Drastic Single-Crystal-to-Single-Crystal Transformations of a Nanoporous Coordination Polymer. *J. Am. Chem. Soc.* **2005**, *127*, 14162−14163.
(60) Zhang, J.-P.; Zhou, H.-L.; Zhou, D.-D.; Liao, P.-Q.; Chen, X.-M. Controlling Flexibility of Metal−organic Frameworks. *Natl. Sci. Rev.* **2017**, *March*, 1−13.

DOI: 10.1021/acs.inorgchem.8b00913
Inorg. Chem. 2018, 57, 8942−8950

(61) Chapman, K. W.; Sava, D. F.; Halder, G. J.; Chupas, P. J.; Nenoff, T. M. Trapping Guests within a Nanoporous Metal-Organic Framework through Pressure-Induced Amorphization. *J. Am. Chem. Soc.* **2011**, *133*, 18583−18585.
(62) Hazen, R. M.; Finger, L. W. *Comparative Crystal Chemistry: Temperature, Pressure, Composition, and the Variation of Crystal Structure*; John Wiley, 1982.
(63) Katrusiak, A. High-Pressure x-Ray Diffraction Studies of Organic Crystals. *High Pressure Res.* **1990**, *4*, 496−498.
(64) Hu, C.; Englert, U. Crystal-to-Crystal Transformation from a Chain Polymer to a Two-Dimensional Network at Low Temperatures. *Angew. Chem., Int. Ed.* **2005**, *44*, 2281−2283.
(65) Xie, Z.; Mei, L.; Wu, Q.; Hu, K.; Xia, L.; Chai, Z.; Shi, W. Temperature-Induced Reversible Single-Crystal-to-Single-Crystal Isomerisation of Uranyl Polyrotaxanes: An Exquisite Case of Coordination Variability of the Uranyl Center. *Dalt. Trans* **2017**, *46*, 7392−7396.
(66) Zhu, M.; Song, X. Z.; Song, S. Y.; Zhao, S. N.; Meng, X.; Wu, L. L.; Wang, C.; Zhang, H. J. A Temperature-Responsive Smart Europium Metal-Organic Framework Switch for Reversible Capture and Release of Intrinsic Eu^{3+} Ions. *Adv. Sci.* **2015**, *2*, 1500012.
(67) Bernini, M. C.; Gandara, F.; Iglesias, M.; Snejko, N.; Gutierrez-Puebla, E.; Brusau, E. V.; Narda, G. E.; Monge, M. A. Reversible Breaking and Forming of Metal-Ligand Coordination Bonds: Temperature-Triggered Single-Crystal to Single-Crystal Transformation in a Metal-Organic Framework. *Chem. - Eur. J.* **2009**, *15*, 4896−4905.
(68) Mobin, S. M.; Srivastava, A. K.; Mathur, P.; Lahiri, G. K. Reversible Single-Crystal to Single-Crystal Transformations in a Hg(II) Derivative. 1D-Polymeric Chain ⇌ 2D-Networking as a Function of Temperature. *Dalt. Trans* **2010**, *39*, 8698.
(69) Slater, J. C. Atomic Radii in Crystals. *J. Chem. Phys.* **1964**, *41*, 3199−3204.
(70) Pauling, L. The Sizes of Ions and the Structure of Ionic Crystals. *J. Am. Chem. Soc.* **1927**, *49*, 765−790.
(71) Shannon, R. D. Revised Effective Ionic Radii and Systematic Studies of Interatomic Distances in Halides and Chalcogenides. *Acta Crystallogr., Sect. A: Cryst. Phys., Diffr., Theor. Gen. Crystallogr.* **1976**, *32*, 751−767.
(72) Pauling, L. Determination of Ionic Radii from Cation-Anion Distances in Crystal Structures; Discussion. *Am. Mineral.* **1987**, *72*, 1016.
(73) Shannon, R. D.; Prewitt, C. T. Effective Ionic Radii in Oxides and Fluorides. *Acta Crystallogr., Sect. B: Struct. Crystallogr. Cryst. Chem.* **1969**, *25*, 925−946.
(74) Miller, V. L.; Tidrow, S. C. Perovskites: Temperature and Coordination Dependent Ionic Radii. *Integr. Ferroelectr.* **2013**, *148*, 1−16.
(75) Kole, G. K.; Vittal, J. J. Solid-State Reactivity and Structural Transformations Involving Coordination Polymers. *Chem. Soc. Rev.* **2013**, *42*, 1755−1775.
(76) Vittal, J. J. Supramolecular Structural Transformations Involving Coordination Polymers in the Solid State. *Coord. Chem. Rev.* **2007**, *251*, 1781−1795.
(77) Sobczak, S.; Katrusiak, A. Zone-Collapse Amorphization Mimicking the Negative Compressibility of a Porous Compound. *Cryst. Growth Des.* **2018**, *18*, 1082−1089.
(78) Andrzejewski, M.; Katrusiak, A. Piezochromic Porous Metal−Organic Framework. *J. Phys. Chem. Lett.* **2017**, *8*, 279−284.
(79) Cai, W.; Katrusiak, A. Giant Negative Linear Compression Positively Coupled to Massive Thermal Expansion in a Metal-Organic Framework. *Nat. Commun.* **2014**, *5*, 4337.
(80) Merrill, L.; Bassett, W. A. Miniature Diamond Anvil Pressure Cell for Single Crystal X-Ray Diffraction Studies. *Rev. Sci. Instrum.* **1974**, *45*, 290−294.
(81) Mao, H. K.; Xu, J.; Bell, P. M. Calibration of the Ruby Pressure Gauge to 800 Kbar under Quasi-Hydrostatic Conditions. *J. Geophys. Res.* **1986**, *91*, 4673.
(82) Piermarini, G. J.; Block, S.; Barnett, J. D.; Forman, R. A. Calibration of the Pressure Dependence of the R1ruby Fluorescence Line to 195 Kbar. *J. Appl. Phys.* **1975**, *46*, 2774−2780.
(83) Budzianowski, A.; Katrusiak, A. High-Pressure Crystallographic Experiments With a CCD-Detector. *High Press. Crystallogr.* **2004**, *140*, 101−112.
(84) *Agilent CrysAlisPro Software System*; Technol. UK Ltd.: Yarnton, Oxford, U.K., 2014; Vol. *44*
(85) Dolomanov, O. V.; Bourhis, L. J.; Gildea, R. J.; Howard, J. A. K.; Puschmann, H. Olex2: A Complete Structure Solution, Refinement and Analysis Program. *J. Appl. Crystallogr.* **2009**, *42*, 339−341.
(86) Sheldrick, G. M. A Short History of SHELX. *Acta Crystallogr., Sect. A: Found. Crystallogr.* **2008**, *64*, 112−122.
(87) Sheldrick, G. M. Crystal Structure Refinement with SHELXL. *Acta Crystallogr., Sect. C: Struct. Chem.* **2015**, *71*, 3−8.
(88) Katrusiak, A. *REDSHABS—Program for Correcting Reflections Intensities for DAC Absorption, Gasket Shadowing and Sample Crystal Absorption*; Adam Mickiewicz University: Poznań, Poland, 2003.
(89) Katrusiak, A. Shadowing and Absorption Corrections of Single-Crystal High-Pressure Data. *Z. Kristallogr. - Cryst. Mater.* **2004**, *219*, 461−467.

DOI: 10.1021/acs.inorgchem.8b00913
Inorg. Chem. 2018, 57, 8942−8950

Author contribution

Poznań, 30 June 2023

Aleksandra Półrolniczak

Department of Materials Chemistry

Adam Mickiewicz University

Uniwersytetu Poznańskiego 8,

63-714 Poznań,

Poland

PhD candidate declaration

With reference to Aleksandra Półrolniczak's application for the Doctoral degree in Chemical Sciences at the Adam Mickiewicz University in Poznań, I declare that I am a co-author of the publication:

- S. Bhattacharyya, S. Sobczak, A. Polrolniczak, S. Roy, D. Samanta, A. Katrusiak, T. K. Maji, *"Dynamic Resolution of Piezosensitivity in Single Crystals of π-Conjugated Molecules"*, Chem. – Eur. J., 2019, 25, 6092–6097.
  My contribution to this paper concerns the performance of project conceptualization; designing and performing experiments; preparation of the sample in diamond anvil cell; data collection and analysis; taking photographs and preparing a movie; discussing the results, conducting structural analysis and its discussion, and providing relevant literature background to support the findings; writing the draft & editing the manuscript.

- S. Sobczak, A. Półrolniczak, P. Ratajczyk, W. Cai, A. Gładysiak, V. I. Nikolayenko, D. C. Castell, L. J. Barbour, A. Katrusiak; *„Large Negative Linear Compressibility of a Porous Molecular Co-Crystal"* Chem. Commun., 2020, 56, 4324–4327.
  My contribution to this paper concerns the performance of project conceptualization; designing and performing experiments; preparation of the sample in diamond anvil cell; data collection and analysis; discussing the results, conducting structural analysis and its discussion, and providing relevant literature background to support the findings; writing the draft & editing the manuscript.

- A. Półrolniczak, S. Sobczak, V.I. Nikolayenko, L.J. Barbour, A. Katrusiak; *„Solvent-controlled elongation and mechanochemical strain in a metal–organic framework"* Dalton Transactions 50 (47), 17478-17481.
  My contribution to this paper concerns the performance of project conceptualization; designing and performing experiments; preparation of the sample in diamond anvil cell; data collection and analysis; discussing the results, conducting structural analysis and its discussion, and providing relevant literature background to support the findings; writing the draft & editing the manuscript.

1/2

- A. Półrolniczak, A. Katrusiak; *"Self-healing ferroelastic metal–organic framework sensing guests, pressure and chemical environment"* Materials Advances 2 (14), 4677-4684.
My contribution to this paper concerns the performance of project conceptualization; sample synthesis; designing and performing experiments; preparation of the sample in diamond anvil cell; data collection and analysis; taking photographs and preparing a movie; discussing the results, conducting structural analysis and its discussion, and providing relevant literature background to support the findings; writing the draft & editing the manuscript.

- A. Półrolniczak, S. Sobczak, A. Katrusiak; *„Solid-state associative reactions and the coordination compression mechanism"* Inorganic Chemistry 57 (15), 8942-8950.
My contribution to this paper concerns the performance of project conceptualization; sample synthesis; designing and performing experiments; preparation of the sample in diamond anvil cell; data collection and analysis; discussing the results, conducting structural analysis and its discussion, and providing relevant literature background to support the findings; writing the draft & editing the manuscript.

A. Katrusiak Aleksandra Półrolniczak

2/2

Poznań, 30 June 2023

Prof. Andrzej Katrusiak

Department of Materials Chemistry

Adam Mickiewicz University

Uniwersytetu Poznańskiego 8,

63-714 Poznań,

Poland

Supervisor's declaration

With reference to Aleksandra Półrolniczak's application for the Doctoral degree in Chemical Sciences at the Adam Mickiewicz University in Poznań, I declare that I am a co-author of the publication:

- S. Bhattacharyya, S. Sobczak, A. Polrolniczak, S. Roy, D. Samanta, A. Katrusiak, T. K. Maji, *"Dynamic Resolution of Piezosensitivity in Single Crystals of π-Conjugated Molecules"*, Chem. – Eur. J., 2019, 25, 6092–6097. My contribution to this paper included discussing the design of the experiments and the obtained results; supervision of the project and reviewing of the manuscript.
- S. Sobczak, A. Półrolniczak, P. Ratajczyk, W. Cai, A. Gładysiak, V. I. Nikolayenko, D. C. Castell, L. J. Barbour, A. Katrusiak; *„Large Negative Linear Compressibility of a Porous Molecular Co-Crystal"* Chem. Commun., 2020, 56, 4324–4327. My contribution to this paper included discussing the design of the experiments and the obtained results; supervision of the project and reviewing of the manuscript.
- A. Półrolniczak, S. Sobczak, V.I. Nikolayenko, L.J. Barbour, A. Katrusiak; *„Solvent-controlled elongation and mechanochemical strain in a metal–organic framework"* Dalton Transactions 50 (47), 17478-17481. My contribution to this paper included discussing the design of the experiments and the obtained results; supervision of the project and reviewing of the manuscript.
- A. Półrolniczak, A. Katrusiak; *"Self-healing ferroelastic metal–organic framework sensing guests, pressure and chemical environment"* Materials Advances 2 (14), 4677-4684. My contribution to this paper included discussing the design of the experiments and the obtained results; supervision of the project and reviewing of the manuscript.
- A. Półrolniczak, S. Sobczak, A. Katrusiak; *„Solid-state associative reactions and the coordination compression mechanism"* Inorganic Chemistry 57 (15), 8942-8950. My contribution to this paper included discussing the design of the experiments and the obtained results; supervision of the project and reviewing of the manuscript.

Poznań, 30 June 2023

Dr. Szymon Sobczak

Department of Materials Chemistry

Adam Mickiewicz University

Uniwersytetu Poznańskiego 8,

63-714 Poznań,

Poland

Co-author declaration

With reference to Aleksandra Półrolniczak's application for the Doctoral degree in Chemical Sciences at the Adam Mickiewicz University in Poznań, I declare that I am a co-author of the publication:

- S. Bhattacharyya, S. Sobczak, A. Polrolniczak, S. Roy, D. Samanta, A. Katrusiak, T. K. Maji, *"Dynamic Resolution of Piezosensitivity in Single Crystals of π-Conjugated Molecules"*, Chem. – Eur. J., 2019, 25, 6092–6097. My contribution to this paper included project conceptualization, design of experiments, high-pressure X-ray diffraction data analysis, and writing and editing of the manuscript.
- S. Sobczak, A. Półrolniczak, P. Ratajczyk, W. Cai, A. Gładysiak, V. I. Nikolayenko, D. C. Castell, L. J. Barbour, A. Katrusiak; *„Large Negative Linear Compressibility of a Porous Molecular Co-Crystal"* Chem. Commun., 2020, 56, 4324–4327. My contribution to this paper included project conceptualization, design of experiments, high-pressure X-ray diffraction data analysis, and writing and editing of the manuscript.
- A. Półrolniczak, S. Sobczak, V.I. Nikolayenko, L.J. Barbour, A. Katrusiak; *„Solvent-controlled elongation and mechanochemical strain in a metal–organic framework"* Dalton Transactions 50 (47), 17478-17481. My contribution to this paper included project conceptualization, design of experiments, high-pressure X-ray diffraction data analysis, and writing and editing of the manuscript.
- A. Półrolniczak, S. Sobczak, A. Katrusiak; *„Solid-state associative reactions and the coordination compression mechanism"* Inorganic Chemistry 57 (15), 8942-8950. My contribution to this paper included project conceptualization, design of experiments, high-pressure X-ray diffraction data analysis, and writing and editing of the manuscript.

dr Szymon Sobczak

Limerick, 06 July 2023

Dr. Varvara I. Nikolayenko

Department of Chemical Sciences,

Bernal Institute,

University of Limerick

Limerick V94T9PX

Ireland

Co-author declaration

With reference to Aleksandra Półrolniczak's application for the Doctoral degree in Chemical Sciences at the Adam Mickiewicz University in Poznań, I declare that I am a co-author of the publication:

- S. Sobczak, A. Półrolniczak, P. Ratajczyk, W. Cai, A. Gładysiak, V. I. Nikolayenko, D. C. Castell, L. J. Barbour, A. Katrusiak; *„Large Negative Linear Compressibility of a Porous Molecular Co-Crystal"* Chem. Commun., 2020, 56, 4324–4327. My contribution to this paper concerns the initial idea development, performance of sample synthesis and editing of the manuscript. My percentage contribution is 20%
- A. Półrolniczak, S. Sobczak, V.I. Nikolayenko, L.J. Barbour, A. Katrusiak; *„Solvent-controlled elongation and mechanochemical strain in a metal–organic framework"* Dalton Transactions 50 (47), 17478-17481. My contribution to this paper concerns the initial idea development, performance of sample synthesis and editing of the manuscript. My percentage contribution is 20%

Varvara I. Nikolayenko

Bangalore, 5 July, 2023

Dr. Sohini Bhattacharyya

Molecular Materials Laboratory,

Chemistry and Physics of Materials Unit,

School of AdvancedMaterials (SAMat),

Jawaharlal Nehru Centre for Advanced Scientific Research,

Bangalore 560 064, India

Co-author declaration

With reference to Aleksandra Półrolniczak's application for the Doctoral degree in Chemical Sciences at the Adam Mickiewicz University in Poznań, I declare that I am a co-author of the publication:

S. Bhattacharyya, S. Sobczak, A. Polrolniczak, S. Roy, D. Samanta, A. Katrusiak, T. K. Maji, *"Dynamic Resolution of Piezosensitivity in Single Crystals of π-Conjugated Molecules"*, Chem. – Eur. J., 2019, 25, 6092–6097. My contribution to this paper concerns the synthesis and purification of the OPE-5 molecule, its structure determination by single crystal X-ray diffraction, experimental design, collecting and analysis of PXRD patterns of C5-PPB before and after grinding, taking photographs of the sample under a UV lamp before and after grinding, measuring and analysis of emission spectra of the sample before and after grinding, conductivity measurements and analysis, data interpretation, and writing and editing of the manuscript.

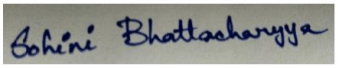

Sohini Bhattacharyya.

Date: 5th July, 2023.

Bangalore, 30 June 2023

Dr. Syamantak Roy

Molecular Materials Laboratory,

Chemistry and Physics of Materials Unit,

School of AdvancedMaterials (SAMat),

Jawaharlal Nehru Centre for Advanced Scientific Research,

Bangalore 560 064, India

Co-author declaration

With reference to Aleksandra Półrolniczak's application for the Doctoral degree in Chemical Sciences at the Adam Mickiewicz University in Poznań, I declare that I am a co-author of the publication:

S. Bhattacharyya, S. Sobczak, A. Polrolniczak, S. Roy, D. Samanta, A. Katrusiak, T. K. Maji, *"Dynamic Resolution of Piezosensitivity in Single Crystals of π-Conjugated Molecules"*, Chem. – Eur. J., 2019, 25, 6092–6097. My contribution to this paper concerns the performance of sample synthesis, experimental design, ambient conditions X-ray diffraction analysis, collecting and analysis of PXRD patterns of C5-PPB before and after grinding, taking photographs of the sample under a UV lamp before and after grinding, measuring and analysis of emission spectra of the sample before and after grinding, conductivity measurements and analysis, data interpretation, and writing and editing of the manuscript.

Yours Sincerely,

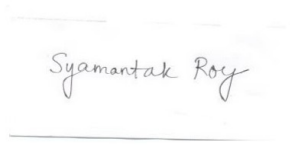

(SYAMANTAK ROY)

Bangalore, 30 June 2023

Dr. Debabrata Samanta

Molecular Materials Laboratory,

Chemistry and Physics of Materials Unit,

School of AdvancedMaterials (SAMat),

Jawaharlal Nehru Centre for Advanced Scientific Research,

Bangalore 560 064, India

Co-author declaration

With reference to Aleksandra Półrolniczak's application for the Doctoral degree in Chemical Sciences at the Adam Mickiewicz University in Poznań, I declare that I am a co-author of the publication:

S. Bhattacharyya, S. Sobczak, A. Polrolniczak, S. Roy, D. Samanta, A. Katrusiak, T. K. Maji, *"Dynamic Resolution of Piezosensitivity in Single Crystals of π-Conjugated Molecules"*, Chem. – Eur. J., 2019, 25, 6092–6097. My contribution to this paper concerns to get a deeper insight into the structural changes associated with the mechanochromic behaviour with the help of time-dependent density functional theory (TD-DFT) computations.

Debabrata Samanta
04/07/2023

Poznań, 30 June 2023

Paulina Ratajczyk

Department of Materials Chemistry

Adam Mickiewicz University

Uniwersytetu Poznańskiego 8,

63-714 Poznań,

Poland

Co-author declaration

With reference to Aleksandra Półrolniczak's application for the Doctoral degree in Chemical Sciences at the Adam Mickiewicz University in Poznań, I declare that I am a co-author of the publication:

S. Sobczak, A. Półrolniczak, P. Ratajczyk, W. Cai, A. Gładysiak, V. I. Nikolayenko, D. C. Castell, L. J. Barbour, A. Katrusiak; *„Large Negative Linear Compressibility of a Porous Molecular Co-Crystal"* Chem. Commun., 2020, 56, 4324–4327. My contribution to this paper concerns a comprehensive review of relevant literature.

Paulina Ratajczyk

Materials Discovery Laboratory
Department of Chemistry
Oregon State University
153 Gilbert Hall
Corvallis, Oregon 97331

P 541-905-1671

7/4/2023

Co-author declaration

With reference to Aleksandra Półrolniczak's application for the Doctoral degree in Chemical Sciences at the Adam Mickiewicz University in Poznań, I declare that I am a co-author of the publication:

- S. Sobczak, A. Półrolniczak, P. Ratajczyk, W. Cai, A. Gładysiak, V. I. Nikolayenko, D. C. Castell, L. J. Barbour, A. Katrusiak; *„Large Negative Linear Compressibility of a Porous Molecular Co-Crystal"* Chem. Commun., 2020, 56, 4324–4327. My contribution to this paper concerns the performance of editing of the manuscript.

Andrzej Gładysiak
Postdoctoral Scholar
Oregon State University

Chengdu, 30 June 2023

Prof. Weizhao Cai

School of Materials and Energy,

University of Electronic Science and Technology of China,

Chengdu, Sichuan 611731,

People's Republic of China

Co-author declaration

With reference to Aleksandra Półrolniczak's application for the Doctoral degree in Chemical Sciences at the Adam Mickiewicz University in Poznań, I declare that I am a co-author of the publication:

- S. Sobczak, A. Półrolniczak, P. Ratajczyk, W. Cai, A. Gładysiak, V. I. Nikolayenko, D. C. Castell, L. J. Barbour, A. Katrusiak; *„Large Negative Linear Compressibility of a Porous Molecular Co-Crystal"* Chem. Commun., 2020, 56, 4324–4327.

My contribution to this paper concerns the performance of editing of the manuscript.

Weizhao Cai

07.04.2023.

Scientific achievements

The list of published articles

1) S. Bhattacharyya*, S. Sobczak*, **A. Półrolniczak***, S. Roy, D. Samanta, A. Katrusiak, T. K.Maji
Dynamic Resolution of Piezosensitivity in Single Crystals of π-Conjugated Molecules
Chemistry–A European Journal 25 (24), 6092-6097 2019 IF_{2019}= 4.857
DOI: 10.1002/chem.201900054

2) S. Sobczak, **A. Półrolniczak**, P. Ratajczyk, W. Cai, A. Gładysiak, V. I Nikolayenko, D. C Castell, L. J Barbour, A. Katrusiak
Large negative linear compressibility of a porous molecular co-crystal
Chemical Communications 56 (31), 4324-4327 2020 IF_{2020}= 6.222
DOI: 10.1039/D0CC00461H

3) **A. Półrolniczak**, S. Sobczak, V. Nikolayenko, L. Barbour, A. Katrusiak
Solvent-controlled elongation and mechanochemical strain in a metal-organic framework
Dalton Transactions 50, 17478-17481 2021 IF_{2021}= 4.569
DOI: 10.1039/D1DT01937F

4) **A. Półrolniczak**, A. Katrusiak
Self-healing ferroelastic metal-organic framework sensing guests, pressure and chemical environment
Materials Advances 2, 4677-4684 2021 IF_{2022}= 5.0
DOI: 10.1039/D1MA00111F

5) **A. Półrolniczak***, S. Sobczak*, A. Katrusiak
Solid-state associative reactions and the coordination compression mechanism
Inorganic chemistry 57 (15), 8942-8950 16 2018 IF_{2018}= 4.85
DOI: 10.1021/acs.inorgchem.8b00913

6) HY Wong, XL Zhou, CT Yeung, WL Man, P. Woźny, **A. Półrolniczak**, A. Katrusiak, M. Runowski, GL Law
Stress to distress: Triboluminescence and pressure luminescence of lanthanide diketonates
Chemical Engineering Journal Advances 11, 100326 2022 IF_{2022}= 0.13
DOI: 10.1016/j.ceja.2022.100326

7) **A. Półrolniczak**, S. Sobczak, A. Katrusiak
Engineering anomalous elastic properties of metal-organic polymers and their amorphization by employing flexible linkers
Just Accepted in Journal of Materials Chemistry C IF_{2022}=6.4

** These authors contributed equally.*

The list of conferences

International

1) **Poster** - Aleksandra Półrolniczak, Szymon Sobczak, Andrzej Katrusiak; "Flexible amines – a new route for designing advanced, porous materials."; ECS4 - 4th European Crystallography School; 2-7 July 2017; Warszawa, Poland

2) **Poster** - Aleksandra Półrolniczak, Szymon Sobczak, Andrzej Katrusiak; "Flexible amines – a new route for designing advanced, porous materials."; 55th European High Pressure Research Group Meeting; 3-8 September 2017; Poznań, Poland

3) **Poster** - Półrolniczak Aleksandra, Sobczak Szymon, Andrzej Katrusiak, "Pressure-induced solid-state reactions of coordination polymers", The 31st European Crystallographic Meeting, ECM31, 22-27 August 2018, Oviedo, Spain

4) **Poster** - Półrolniczak Aleksandra, Sobczak Szymon, Andrzej Katrusiak, "Pressure-induced solid-state reactions of coordination polymers", 12 HIGH-PRESSURE DIFFRACTION WORKSHOP IN POZNAŃ · FROLIC GOATS, 14-16 April 2019, Poznań, Poland

5) **Poster** - Aleksandra Półrolniczak, Szymon Sobczak and Andrzej Katrusiak; "Kinetically driven frowning of the crystal phase"; 57th European High Pressure Research Group Meeting on High Pressure Science and Technology (EHPRG2019); 1-6 September 2019; Prague, Czech Republic

6) **Oral presentation** - Aleksandra Półrolniczak, Szymon Sobczak, Andrzej Katrusiak; "Structural diversity, phase transition and pores activation of Cd(II)-metal organic frameworks based on 4,4"-azopyridine and terephthalic acid"; Joint Polish-German Crystallographic Meeting 2020 (JPGCM-2020); 24–27 February 2020,Wrocław, Poland

7) **Oral presentation** - Aleksandra Półrolniczak, Szymon Sobczak and Andrzej Katrusiak; "Kinetically driven frowning of the crystal phase"; 13th Frolic Goats High-Pressure Workshop, 4-5 May, 2020 Poznań, Poland (online)

8) **Oral presentation** - Aleksandra Półrolniczak, Andrzej Katrusiak; "SELF-HEALING METAL-ORGANIC FRAMEWORK"; IUCr High-Pressure Commission Workshop HPW-21; 1-6 February 2021; Novosibirsk, Russian Federation (Online)

9) **Poster** - Aleksandra Półrolniczak, Andrzej Katrusiak; "Highly sensitive, self-healing metal-organic framework"; 33rd European Crystallographic Meeting; 23-27 August 2022, Versailles, France

10) **Poster** - Aleksandra Półrolniczak, Szymon Sobczak and Andrzej Katrusiak; "INFLUENCE OF THE PRESSURE TRANSMITTING MEDIUM ON THE PRESSURE EFFECT IN METAL-ORGANIC FRAMEWORK"; 25th International Conference on the Chemistry of the Organic Solid State 3-8 July 2022, Ohrid, Macedonia

Domestic

1) **Poster** - Aleksandra Półrolniczak, Szymon Sobczak, Andrzej Katrusiak; "Two similar cadmium coordination polymers and their different behaviour under high pressure" 11th HIGH- PRESSURE DIFFRACTION WORKSHOP FROLIC GOATS; 13-15 May 2018; Poznań, Poland

2) **Poster** - Aleksandra Półrolniczak, Szymon Sobczak, Andrzej Katrusiak; „Indukowana ciśnieniem reakcja polimeru koordynacyjnego, zwiększająca liczbę koordynacyjną centrum metalicznego"; 60 Konwersatorium Krystalograficzne; 28-29 June 2018; Wrocław, Poland

3) **Poster** - Półrolniczak Aleksandra, Sobczak Szymon, Andrzej Katrusiak, "Negative linear compressibility of a chiral metal-organic framework", 61. Konwersatorium Krystalograficzne, 27-28 June 2019, Wrocław, Poland

4) **Poster** - Aleksandra Półrolniczak, Andrzej Katrusiak; "ENVIRONMENT SENSITIVE SELF-HEALING FERROELASTIC METAL-ORGANIC FRAMEWORK"; 62 Konwersatorium (Online)

Scientific internships

1) European Synchrotron Radiation Facility, Grenoble, France; 05.11.2021-16.11.2021

2) Departamento de Física Fundamental y Experimental, Electrónica y Sistemas; Facultad de Físicas. Universidad de La Laguna, La Laguna, Spain; 05.01.2022 – 19.04.2022

Research projects

1) 07/2020-10/2023 Principal Investigator
Project Manager and principal investigator in the National Science Center PRELUDIUM 18 No. UMO-2019/35/N/ST5/01838 project 'Examination of sorption abilities and pressure induced effects on 4,4'-azo(bis)pyridine based metal-organic frameworks' at the Department of Materials Chemistry, Adam Mickiewicz University in Poznań, Poland

2) 10/2016-10/2020 Co-investigator
Co-investigator in the NCN grant OPUS 10 No. UMO-2015/19/B/ST5/00262 'Porous materials under extreme conditions' at the Department of Materials Chemistry, Adam Mickiewicz University in Poznań, Poland

3) 10/2017-10/2023 Participant
Participant of POWR.03.02.00-00-I026/16 grant co-financed by the EU European Social Fund under the Operational Program Knowledge Education Development at Adam Mickiewicz University in Poznań, Poland

4) 07/2022-07/2023 Co-investigator
Co-investigator in the NCN grant OPUS 21 No. UMO- 2021/41/B/ST8/03758 'Development of new high entropy nitrides composites synthesized at high pressure and temperature' at the Department of Materials Chemistry, Adam Mickiewicz University in Poznań, Poland